

## ABSTRACT

KIZEWSKI, FIONA RAO. Phosphate Binding and Fe(III) Reduction as Affected by Fe(III) and Organic Matter Interactions. (Under the direction of Dr. James D. Martin and Dr. Dean L. Hesterberg).

Being a vital element for life, phosphorus (P) is usually added to soils in the forms of P fertilizer and animal waste (manure) to enhance plant growth. However, due to the imbalance between P input and uptake by plant produce, excess P accumulates in soils. This surplus P will post an environmental threat if P runs off soils to an aquatic system because the elevated P could deteriorate the ecosystem in the aquatic system. As important soil components, organic matter (OM) and Fe-oxide minerals both play critical roles in nutrient retention and release for plant growth. Understanding the interactions between OM and Fe-oxides is crucial for soil remediation or effective P fertilizer application. The goal of this research is to determine at a mechanistic level how interactions between soil iron minerals and organic matter affect phosphate ( $\text{PO}_4$ ) binding and reductive dissolution. The specific objectives are: (1) determine whether simple organic acids (OA) compete or cooperate with phosphate to bind with Fe and the conditions in which a ternary OA-Fe- $\text{PO}_4$  compound forms; (2) synthesize an organo-Fe(III)- $\text{PO}_4$  ternary compound and determine its XAS (X-ray absorption spectroscopy) spectral features that can be applied to characterize  $\text{PO}_4$  binding to Fe-OM complexes; (3) determine how interactions between organic matter and ferrihydrite with time affects  $\text{PO}_4$  sorption and elucidate the underlying mechanism; (4) determine the redox properties of particulate organic matter, Pahokee peat; (5) determine the influence of Pahokee peat on ferrihydrite chemical and microbial reduction. Coordination between Fe and  $\text{PO}_4$  dominates the reactions of Fe(III),  $\text{PO}_4$ , and each of the six organic acids, including

oxalate, citrate, malonate, succinate, tartrate, and benzoate at pH 5.5. With a structural directing template, 1,3-diaminopropane, a new mixed anion Fe(III) phosphate/oxalate ternary compound,  $[\text{C}_3\text{H}_{12}\text{N}_2]_2[\text{Fe}_5(\text{C}_2\text{O}_4)_2(\text{H}_x\text{PO}_4)_8]$  (**I**), was synthesized. EXAFS (extended X-ray absorption fine structure spectroscopy) analysis of **I** illustrates that Fe-phosphate bonding is unambiguously differentiated from Fe-oxalate bonding, which confirms the feasibility of deciphering the coordination structure of Fe in complex matrices by EXAFS spectroscopy. Ferrihydrite (FH) was mixed with various amount of organic matter and the mixtures were let age for 55 days. All OM/FH mixtures show decreased  $\text{PO}_4$  sorption upon aging. With controlled constant total Fe and peat, a peat/ $\text{FeCl}_3$ /FH mixture is more effective for  $\text{PO}_4$  sorption than a peat/FH mixture. Fe-peat complexation illustrates characteristic EXAFS spectral features which are missing in the EXAFS spectra of aged peat/FH mixtures. The decreased  $\text{PO}_4$  sorption in the aged OM/FH mixtures and the lack of EXAFS spectral features for Fe-peat complexation confirm no Fe migration from the mineral to organic matter. We conclude that the sorption interaction between OM and ferrihydrite during aging increases OM stability so that it possesses stronger ability to resist the competition with  $\text{PO}_4$  for sorption sites. Pahokee peat, was reduced chemically and tested for its reducing capacity with respective to ferrihydrite, Fe-citrate (Fe-Cit), and  $\text{FeCl}_3$ . The amount of electron transferred from  $\text{H}_2$  reduced peat to Fe(III) compounds follows the order of  $\text{FeCl}_3 > \text{Fe-Cit} > \text{FH}$ . The kinetics of peat chemical reduction is well fit by a diffusion limited rate law proceeding in spherical particles. Two distinct redox reservoirs exist in peat: one assigned to quinone functional groups and the other to reducible acid and neutral carbonyl functional groups. Chemical reduction of peat/FH mixtures clearly demonstrates that ferrihydrite and peat are

reduced independently and peat does not act as an active shuttle between  $H_2$ , the electron source and ferrihydrite. Moreover, peat inhibits ferrihydrite chemical reduction. Kinetic modeling of all chemical reduction data reveals that the interactions between peat and ferrihydrite regulate the mechanism by which peat influences ferrihydrite chemical reduction. By contrast, peat acts as an electron shuttle in ferrihydrite microbial reduction and enhances the reduction. However, data of dissolved Fe(II) and organic carbon suggest that organic matter also act as an Fe(II) complexation agent which facilitates biogenic Fe(II) transport and eliminates the formation of mixed valence secondary Fe mineral.

## **DEDICATION**

I would like to dedicate all the good coming out of this work to my hard working parents. My parents were born to poor families in a poor area during the chaotic era in China. They didn't have the chance to have good education. Although working hard the whole life, they cannot provide much more than shelter and food to us. However, they always know the importance of education and a proper attitude towards life. They made sure I had good education although girls were not always preferred in a family at that time. They imparted a hardworking habit and good life ethics to me so that I became a proud citizen in the society.

## BIOGRAPHY

Fiona Rao Kizewski was born on Sep 8<sup>th</sup>, 1974 with the maiden name of Rao Jieling (饶洁玲) in a small town named Shiqiao outside Guangzhou, south China, P.R.C. Before college, Fiona spent her whole childhood and teenage in that small town. Instead of playing with toys or video games, she spent most of her childhood chasing her playmates in the alleys, climbing up trees, or riding a bicycle to the countryside when off school. During her teenage Fiona read a lot of literary books, including ancient and contemporary Chinese books, translated contemporary works from Russia, Britain, France, etc. On the meantime school education instilled the philosophy of Confucianism into her. From reading and school education she gradually established her view of the world, life, and her role in the society. Ever since teenage Fiona has always been sure that she wants to be an independent human being in the society. At the age of 18, Fiona left home for her first college experience.

Ever since high school Fiona had always wanted to study chemistry in college. However, the chance of taking a chemistry major slipped by her when she first attended college in South China Agricultural University (SCAU), Guangzhou, P.R.C. Nevertheless the 4-year higher education in SCAU taught her social skills and self-educating skills, which have been proven to be very critical in her future life. After graduating from SCAU with a bachelor degree, Fiona worked in several companies for seven years.

In Feb 2003, Fiona travelled across the Pacific Ocean to start a new life in the United States. There she grasped the second chance to pursue her dream in chemistry. Only that, instead of a bachelor degree, this time she wanted to earn a Ph.D. in chemistry.

Starting from Aug 2005, Fiona has been in the Ph.D. program in the Department of Chemistry of North Carolina State University under the direction of Dr. James Martin and Dr. Dean Hesterberg. During the past five years, along with the responsibilities of being a wife and a mom, experiments, science conferences, seminars, and publication writing filled her life. She enjoys doing experiments and seeing the outcomes; she savors the precious moments of intellectual conversations with her fellows or her advisers. Being a wife and the mom of her lovely son, Fiona always treasures her family life. Her life has been busy but happy and complete.

By Feb 2011 Fiona will have been living in the United States for eight years. Life in America has changed her a lot in many respects, e.g. her view of human rights or participation in political issues. Fiona has been exposed to many things that were hidden from her. She has realized that the world has many facets.

Upon finishing her graduate study, in the near future Fiona wishes to continue conducting research on the subjects that interest her. She would like to pursue a career in the academic field or in a research institute.

## ACKNOWLEDGEMENTS

The biggest skill I have gained during the 5-year graduate study is the skill to locate a scientific problem and work out a research scheme to solve it. I am indebted to my two advisers, Dr. James Martin and Dr. Dean Hesterberg for my progress.

I have learned many things concerning science and life from Dr. Martin. He has taught me analytical skills, the pursuit of science rigor, etc. Most importantly, he has taught me the perseverant spirit towards science. The experience of working with him on publications made me realize what merits a real scientist should possess. His passion towards science, human rights, and education has shaped up the way I look at many issues about human beings.

Dr. Hesterberg is the very professor who instilled the importance of research design into me. Because of that, I have become more and more rigorous about experimental procedures. I had many conversations or discussion with Dr. Hesterberg about science or life in general. All these conversations have great intellectual values. Dr. Hesterberg has also provided invaluable input to my research so that my work can offer interdisciplinary scope to both the inorganic chemistry and soil chemistry community.

I owe lot of people for their help with my research. Dr. Linda Martin provided valuable inputs to my dissertation document although she was so busily occupied by many things. Dr. Folmer is always the person who I turn to whenever I am puzzled by my research. My groupmates, Lusia Liu, Amanda Morris, Eric Dill, and other past graduate students are my research allies. Whenever I feel frustrated or tired, a joke from them or a short

conversation always refuels my spirit. Their insight on various scientific issues also helps me achieve my research goal.

Outside the academic field, the very person who has given me the biggest support is my husband, Wayne. Wayne is a very kind and funny gentleman, a loving dad also. When I first attempted to attend a Ph. D. program in chemistry, he gave me encouragement so that I became sure about the choice. During the past five years, he has been very supportive and helpful in my family and academic life. Without him, I wouldn't have been where I am.

My parents always tell me that there are always many more nice and kind people than evil ones. My life experience has proven to me that is true. I sincerely thank all people who have helped me achieve my goal. I wish them all the best.

# TABLES OF CONTENTS

<b>LIST OF TABLES.....</b>	<b>ix</b>
<b>LIST OF FIGURES.....</b>	<b>x</b>
<b>LIST OF ABBREVIATIONS.....</b>	<b>xiv</b>
<b>Chapter 1: General Introduction.....</b>	<b>1</b>
1.1. Soil phosphorus accumulation and the environmental hazard.....	2
1.2. Phosphate sorption/desorption in soils.....	4
1.3. A model predicting PO <sub>4</sub> sorption-desorption path .....	10
1.4. Goal and objectives.....	11
1.5. References.....	13
<b>Chapter 2: Competition between Phosphate and Organic Acids to Bind with Iron.....</b>	<b>19</b>
2.1. Introduction.....	21
2.2. Materials and methods.....	24
2.3. Results.....	25
2.4. Discussion.....	30
2.5. Conclusions.....	33
2.6. References.....	34
<b>Chapter 3: Mixed Anion (Phosphate/Oxalate) Bonding to Iron(III) Materials.....</b>	<b>39</b>
Introduction.....	41
Results.....	44
Discussion.....	54
Conclusions.....	61
Experimental Section.....	62
REFERENCES.....	66
<b>Chapter 4: Phosphate Sorption to Organic Matter/Ferrihydrite Mixtures as Affected by Aging Time.....</b>	<b>69</b>
4.1. Introduction.....	71
4.2. Materials and methods.....	74

4.3. Results.....	80
4.4. Discussion.....	86
4.5. Conclusions.....	91
4.6. References.....	92
<b>Chapter 5: Determining the Redox Capacity of Pahokee Peat and the Mechanism of Its Chemical Reduction.....</b>	<b>96</b>
5.1. Introduction.....	96
5.2. Materials and methods.....	100
5.3. Results and discussion.....	102
5.4. Conclusions.....	122
5.5. References.....	124
<b>Chapter 6: Influence of Pahokee Peat on Ferrihydrite Chemical and Microbial Reduction.....</b>	<b>128</b>
6.1. Introduction.....	130
6.2. Materials and methods.....	133
6.3. Results.....	135
6.4. Discussion.....	142
6.5. Conclusions.....	149
6.6. References.....	150
<b>Chapter 7: Conclusions.....</b>	<b>156</b>
7.1. Ternary complexation between organic matter, iron, and phosphate.....	157
7.2. Organic matter/Fe-oxide interactions.....	133
7.3. Multiple mechanisms contribute to the enhancement of organic matter in Fe(III)-oxide microbial reduction.....	135
7.4. References.....	142

## LIST OF TABLES

<b>Table 2-1.</b> Molecular formula, pKa and $\text{Log}K_{\text{Fe(III)}}$ values for the six organic acids.....	<b>24</b>
<b>Table 2-2.</b> Solid species formed in all $\text{PO}_4$ , Fe(III), and organic acid reactions as identified by X-ray diffraction.....	<b>25</b>
<b>Table 3-1.</b> Crystal data and structure refinement parameters of <b>I</b> .....	<b>46</b>
<b>Table 3-2.</b> P-O bond lengths in <b>I</b> .....	<b>48</b>
<b>Table 3-3.</b> Fe-O bond lengths of <b>I</b> .....	<b>49</b>
<b>Table 3-4.</b> Fitting results of <b>I</b> , including coordination number (CN, fixed), interatomic distance (R), and Debye-Waller Factors ( $S^2$ ). Amplitude reduction factor ( $S_0^2$ ) and $\text{DELE}^\circ$ apply to all paths. $S_0^2$ is fixed at 0.84.....	<b>60</b>
<b>Table 4-1.</b> Fitting parameters for the EXAFS data of the peat/ $\text{FeCl}_3$ /FH mixtures and three peat/FH mixtures (0% $\text{FeCl}_3$ ) that have aged for 1, 7, and 55 days. All systems were controlled for a constant total Fe to peat input which is equal to 1200 mmol Fe/kg peat. The interatomic distances of all paths for the three peat/FH (0% $\text{FeCl}_3$ ) systems are the same. FH=ferrihydrite.....	<b>85</b>
<b>Table 5-1.</b> Summary of Pahokee peat reduction data. $\text{PP}_1$ , $\text{PP}_2$ , and $\text{PP}_3$ represent the redox domains probed by different oxidation agents. $\text{PP}_Q$ = quinone functional groups; $\text{PP}_A$ = carboxyl acid groups. $\text{PP}_C$ = neutral carbonyl groups; natFe = Fe native to peat. PB refers to phase boundary limited model. All kinetic data were fit to a diffusion controlled model unless specified.....	<b>104</b>
<b>Table 5-2.</b> Post-reduction reducing capacity of a PP/FH mixture with peat input of 1.55 g $\text{g}^{-1}$ FH.....	<b>119</b>
<b>Table 6-1.</b> Fitting results for the extent of diffusion controlled reaction, rate constant of the phase boundary controlled reaction for the chemical reduction of peat/ferrihydrite mixtures with peat input ranging from 0 to 2.2 g $\text{g}^{-1}$ FH at pH 6. All reduction was conducted with 1.7% $\text{H}_2$ .....	<b>140</b>

## LIST OF FIGURES

- Figure 1-1.** Soil phosphorus runoff pathways (adopted from the report of Agricultural Phosphorus and Eutrophication by U.S. Department of Agriculture.<sup>1</sup>).....**2**
- Figure 1-2.** Schematic drawing showing organic matter shuttles electrons from the electron source, hydrogen to Fe(III). OM<sub>ox</sub>=oxidized organic matter, OM<sub>re</sub>=reduced organic matter.....**9**
- Figure 1-3.** Schematic drawing showing PO<sub>4</sub> adsorbed to organic matter via Al or Fe bridges and to the surface of goethite. (Courtesy of Dr. Dean Hesterberg, North Carolina State University).....**10**
- Figure 2-1.** X-ray diffraction patterns of the two solid species from reactions of Fe(III), H<sub>3</sub>PO<sub>4</sub>, and various organic acids at pH 5.5 under hydrothermal conditions.....**26**
- Figure 2-2.** Normalized Fe K-edge XANES spectra of the solid products of reactions of PO<sub>4</sub>, Fe(III), and oxalate at various molar ratios at pH 5.5.....**27**
- Figure 2-3.** Normalized Fe K-XANES spectra of the solid products of reaction of PO<sub>4</sub>, Fe(III), and citrate at various molar ratios at pH 5.5.....**28**
- Figure 2-4.** Normalized Fe K-XANES spectra of the solid products from reactions of PO<sub>4</sub>, Fe(III), and tartrate at various molar ratios at pH 5.5.....**28**
- Figure 2-5.** Calculated amounts of phosphorus retained in the solid products from all reactions of PO<sub>4</sub>, Fe(III), and organic acid at pH 5.5.....**30**
- Figure 3-1.** ORTEP drawing of the asymmetric unit of **1** which describes the atom labeling scheme.....**47**
- Figure 3-2.** (a) Crystal packing view of the structure of **1** oriented to emphasize the phosphate/oxalate chains that run along the <-1, -1, 3> direction (vertical in figure). Green and purple brackets emphasize the (0,0,2) alternating iron phosphate and iron oxalate layers of the structure. (b) View of the phosphate/oxalate cage templated by two DAP cations. View of the (c) iron phosphate and (d) iron oxalate layers as viewed looking down the <-1,-1,3>. The alkylammonium cations reside within the oxalate layers.....**51**
- Figure 3-3.** Normalized Fe K-edge XANES spectrum of **I** (blue), compared with the spectra of the Fe(III) standard strengite (FePO<sub>4</sub>·2H<sub>2</sub>O) (red), the Fe (II) standard Fe<sub>3</sub>(PO<sub>4</sub>)<sub>2</sub>·8H<sub>2</sub>O (black) and iron foil (green).....**53**

- Figure 3-4.** First derivative spectra of the Fe K-edge XANES of **I** (black) and strengite ( $\text{FePO}_4 \cdot 2\text{H}_2\text{O}$ ) (red)..... **54**
- Figure 3-5.** Fourier-transform magnitude of the Fe EXAFS spectrum of (a) strengite ( $\text{FePO}_4 \cdot 2\text{H}_2\text{O}$ ), (b) **I** and (c)  $\text{Fe}_2(\text{C}_2\text{O}_4)_3 \cdot 6\text{H}_2\text{O}$ . For (b) the solid line represents the experimental data, and the dotted line represents the calculated best fit using the single crystal structure as a model. Arrows highlight the Fe--P and Fe--C second nearest neighbor peaks in strengite and  $\text{Fe}_2(\text{C}_2\text{O}_4)_3 \cdot 6\text{H}_2\text{O}$ , respectively. (Distances are not corrected for phase shift.)..... **58**
- Figure 3-6.** Fourier transform of the real part of the  $k^3$ -weighted Fe EXAFS spectrum of **I** (black) along with the best fit (red). The contributions of the signals from single-scattering paths (left) and multiple-scattering paths (right) calculated from the crystal structure of **I** (plotted in the lower portion of the figure with a different color assigned to each path) demonstrate the differential contribution of the iron to oxygen, phosphorus and carbon neighbors. (Distances are not corrected for phase shift.)..... **59**
- Figure 4-1.** Change of  $\text{PO}_4$  sorption to ferrihydrite and organic matter/ferrihydrite mixtures as a function of aging time at pH 6.0. All mixtures are described by the mass of organic matter per gram of ferrihydrite. FH=ferrihydrite.....**80**
- Figure 4-2.**  $\text{PO}_4$  sorption to peat/ $\text{FeCl}_3$ /ferrihydrite mixtures as a function of  $\text{FeCl}_3$  input at pH 6.0. Total Fe and peat in these systems were controlled to be constant.....**81**
- Figure 4-3.** Fourier transform filtered ( $R+\Delta R=1-3.5 \text{ \AA}$ ) Fe K-edge EXAFS spectra of fresh peat/ $\text{FeCl}_3$ /FH mixtures and peat/FH mixtures that have aged for 7 and 55 days. \*FH=ferrihydrite.....**83**
- Figure 4-4.** X-ray diffraction patterns of ferrihydrite that has aged for various time periods showing the transformation of ferrihydrite to hematite.....**86**
- Figure 4-5.** Phosphate sorption capacity as a function of 0.4 M HCl extractable Fe from three organic matter/ferrihydrite mixtures during aging for 55 days.....**87**
- Figure 4-6.** Dissolved organic carbon concentration before (hollow symbols) and after (solid symbols)  $\text{PO}_4$  addition to three organic matter/ferrihydrite mixtures during the aging of 55 days. HA=Pahokee peat humic acid.....**89**
- Figure 5-1.** Comparison of the rate of reduction of iron(III) native to Pahokee peat under 1.7%  $\text{H}_2$  and the rate of ferrihydrite reduction by  $\text{H}_2$  reduced peat (24 h). The ferrihydrite data were obtained from reactions of ferrihydrite and reduced peat for 15 min, 1, 4, and 24 h, respectively.....**105**

- Figure 5-2.** Reducing capacity of Pahokee peat after 24 h reduction by 1.7% H<sub>2</sub> as probed by different Fe(III) compounds and sequential mixtures of Fe(III) compounds. Error bars show standard deviation of three replicates.....106
- Figure 5-3.** Reduction kinetics of samples of Pahokee peat (PP) for which the Pt/C catalyst was added immediately preceding reduction by 1.7% H<sub>2</sub>, Exp. 2, and 0.5% H<sub>2</sub>, Exp. 3. Reduction of Fe(III) native to peat (rust circles); the reduction of peat as probed by subsequent oxidation by FH (green squares, PP<sub>1</sub>), by Fe-Cit (blue triangles, PP<sub>1</sub>+PP<sub>2</sub>) and FeCl<sub>3</sub> (red diamonds, PP<sub>1</sub>+PP<sub>2</sub>+PP<sub>3</sub>), the acid consumed to maintain constant pH = 6 (pink circles, PP<sub>A</sub>); and Fe-Cit - FH (open blue triangles, PP<sub>2</sub>) and FeCl<sub>3</sub> - Fe-Cit (open red diamonds, PP<sub>3</sub>). The solid lines represent fits to the kinetic model. See Table 1 caption for denotations.....108
- Figure 5-4.** Schematic drawing showing the estimated reduction potentials in peat based on the redox state, continuum and two-reservoir models in relation to the reduction potentials of FeCl<sub>3</sub>, Fe-citrate, ferrihydrite, and hydrogen at pH 6. PP<sub>CA</sub> denotes the sum of neutral carbonyl groups (PP<sub>C</sub>) and acid groups (PP<sub>A</sub>). See Table 5-1 caption for denotations.....113
- Figure 5-5.** Kinetics of H<sub>2</sub> reduction of a sample of PP that had been pre-treated with the Pt/C catalyst for 24 h, Exp. 4. Reduction of Fe(III) native to PP (rust circles, PP<sub>nat Fe</sub>); the reduction of PP as probed by subsequent oxidation by FH (green squares, PP<sub>1</sub> = PP<sub>Q</sub>), by Fe-Cit (blue triangles, PP<sub>1</sub> + PP<sub>2</sub>) and FeCl<sub>3</sub> (red diamonds, PP<sub>1</sub> + PP<sub>2</sub> + PP<sub>3</sub>), the acid consumed to maintain constant pH = 6 (pink circles, equals PP<sub>A</sub>); and calculated neutral carbonyl group, PP<sub>C</sub> (purple diamonds, PP<sub>C</sub> = (PP<sub>2</sub>+PP<sub>3</sub>)/2-H<sup>+</sup>). The solid lines represent fits to respective kinetic models; the fit of the Fe-Cit curve is based on an estimated ratio of PP<sub>2</sub>/PP<sub>3</sub> and thus represented as a dotted line. See Table 5-1 caption for denotations.....115
- Figure 6-1.** Production of 0.5 M HCl extractable Fe(II) during ferrihydrite reduction by 1.7% and 0.5% H<sub>2</sub> with a Pt/C catalyst at pH 6. Each suspension contained 0.5 g FH kg<sup>-1</sup>. Symbols represent experimental data, solid lines are the fits.....135
- Figure 6-2.** Production of 0.5 M HCl extractable Fe(II) during the chemical reduction (1.7% H<sub>2</sub>) of peat/ferrihydrite mixtures at pH 6. Each suspension contained 0.5 g FH kg<sup>-1</sup>. Symbols represent experimental data, solid lines are the fits to the sum of the diffusion controlled and phase boundary controlled kinetic model.....138
- Figure 6-3.** The extent of diffusion controlled reaction in the chemical reduction (1.7% H<sub>2</sub>) of ferrihydrite and peat/ferrihydrite mixtures as a function of peat input. The extent of diffusion is presented as the percentage of total Fe.....139

- Figure 6-4.** The calculated rate constants of the phase boundary controlled reaction in the chemical reduction (1.7% H<sub>2</sub>) of ferrihydrite and peat/ferrihydrite mixtures as a function of peat input.....**139**
- Figure 6-5.** Production of 0.5 M HCl extractable Fe(II) during the microbial reduction (1.7% H<sub>2</sub> with CN32) of ferrihydrite or peat/ferrihydrite mixtures. The inset figure shows the kinetic data of ferrihydrite microbial reduction data follow a non-linear pattern.....**141**
- Figure 6-6.** 0.5 M HCl extractable and dissolved Fe(II) from the chemical (1.7% H<sub>2</sub> + Pt/C) and microbial (1.7% H<sub>2</sub> + CN32) reduction of the peat/FH mixture of 0.5 g g<sup>-1</sup> FH at pH 6.0. Solid symbols are acid extractable Fe(II), hollow symbols are dissolved Fe(II).....**148**
- Figure 7-1.** Schematic drawing showing the interactions between ferrihydrite and peat and the impact on ferrihydrite chemical reduction. All systems were reduced with hydrogen in the presence of a Pt/C catalyst. FH=ferrihydrite.....**160**
- Figure 7-2.** Schematic drawing showing the interactions between ferrihydrite and peat and the impact on ferrihydrite microbial reduction. The reduction was conducted with hydrogen gas. FH=ferrihydrite.....**161**

## LIST OF ABBREVIATIONS

OM	organic matter
DOC	dissolved organic carbon
HA	humic acid
HS	humic substances
IHSS	International Humic Substances Society
PP	Pahokee peat
PO <sub>4</sub>	phosphate
OA	organic acid
XAS	X-ray absorption spectroscopy
EXAFS	extended X-ray absorption fine structure spectroscopy
XANES	X-ray absorption near edge structure spectroscopy
FT	Fourier transforms
FH	ferrihydrate

# **Chapter 1: General introduction**

## 1.1. Soil phosphorus accumulation and the environmental hazard

Phosphorus (P) is one of the key elements for life because it participates in many metabolic processes of all living organisms. Soils are the principal reservoirs of biologically accessible P in terrestrial systems.<sup>1</sup> However, soil P is easily fixated in relatively insoluble forms limiting phyto-available P. Converting stable soil P to labile P to meet crop growth requirement normally takes a longer time than a crop production cycle. Hence, application of P fertilizer to soil is a common practice to enhance crop growth, which accounts for one major external source of soil P. Another external source for soil P is animal manure (waste) which has a significant content of phosphorus.<sup>3</sup> Manure application to soils is an economical way for animal waste disposal; it can also improve soil structure and reduce erosion.

The positive benefits of manure application to soils are widely accepted, however, manure application becomes problematic when soil P accumulation from animal waste

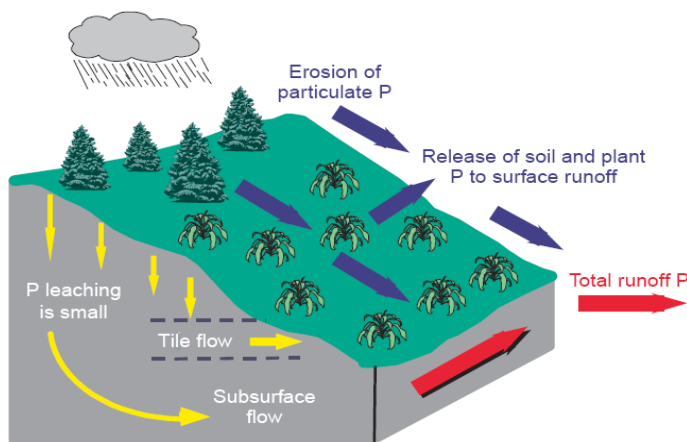


**Figure 1-1.** Soil phosphorus runoff pathways (adopted from the report of Agricultural Phosphorus and Eutrophication by U.S. Department of Agriculture.<sup>2</sup>)

exceeds plant uptake. According to a report about agricultural phosphorus from the U.S. Department of Agriculture (USDA),<sup>2</sup> only 30 percent of soil P from fertilizer and animal waste is converted to crop and animal produce. This low conversion rate has caused the imbalance between P inputs and

outputs. The direct consequence is that surplus soil P is subject to runoff to low lying aquatic systems as illustrated in Figure 1-1. Eighty percent of surface runoff P from cultivated land occurs through erosion of soil particulates and organic matter.<sup>4</sup> Interactions between surface soil and rainfall or irrigation water lead to further loss of dissolved P in surface runoff.<sup>4</sup> Once the runoff P reaches an aquatic system, it poses a pollution threat because accumulation of P in an aquatic system greatly accelerates eutrophication, a process wherein accumulated nutrients, e.g. P or N, boosts the growth of undesired algae that would kill other aquatic lives by depleting oxygen. Eutrophication greatly impairs water quality and restricts water use for fisheries, recreation, and drinking.

Decrease of soil P runoff is crucial to reducing the risk of eutrophication in aquatic systems. However, fundamental mechanisms controlling P release from soils are still not well understood. Gaining such fundamental knowledge is challenged by the fact that soils are very complex and thus mechanistic questions must be multi-faceted. For example, what soil components are P retention media? What are the P retention mechanisms? Why can soils lose P through dissolution but dissolved P in soil solution tends to be not sufficient in some soils for plant growth?

Essentially, effective P fertilizer application and soil management schemes require an accurate prediction of the fate of soil P which mandates a thorough understanding of the mechanisms that control the P sorption-desorption cycle. To achieve this goal, both macroscopic (field scale) and molecular studies are needed. The study presented in this dissertation seeks to provide mechanistic explanations at a molecular level for the observed factors that impact soil P sorption-desorption cycle in macroscopic studies. It is anticipated

that findings from this study will ultimately be useful in guiding the design of studies that examine the soil P sorption-desorption cycle on a macroscopic scale.

## **1.2. Phosphate sorption/desorption in soils**

Soil P is normally divided into organic and inorganic P. Organic P is contained in undecomposed soil biomass and organic matter (OM). Inorganic P, in the form of phosphate ( $\text{PO}_4$ ), is usually associated with metals, e.g. aluminum (Al) or iron (Fe) in the form of phosphate minerals or adsorbed species.<sup>2</sup> Although numerous phosphate minerals have been discovered in soils, the majority of inorganic soil P exists as adsorbed species in acid soils. In calcareous soils, calcium associated phosphate is the dominant species.<sup>5</sup> The discussion in this dissertation will only focus on inorganic P, phosphate, hereafter.

***Phosphate sorption to oxide minerals*** Studies have shown that Fe- or Al-(hydr)oxide minerals, especially non- or poorly crystalline ones, are major sinks for soil  $\text{PO}_4$ . Khare et al.<sup>6</sup> reported that ferrihydrite (FH), a poorly crystalline Fe(III) oxide, can sorb up to 1860 mmol P  $\text{kg}^{-1}$  FH. For non-crystalline Al-(hydr)oxide, a  $\text{PO}_4$  sorption maximum of ~4000 mmol P  $\text{kg}^{-1}$  was reported by Liu and Hesterberg (publication in preparation).<sup>7</sup> Violante and Pigna<sup>8</sup> reported that poorly crystalline Al- and Fe-oxides can sorb 30- to 90-fold more  $\text{PO}_4$  than phyllosilicates, 20- to 40-fold greater than Mn-oxides, and 3- to 6-fold greater than crystalline Fe- and Al-oxides.

Spectroscopic techniques have been applied to determine the molecular configuration of  $\text{PO}_4$  adsorption on Al- or Fe-oxide mineral surface. Based on FT-IR spectroscopy, Tejedor-Tejedor and Anderson<sup>9</sup> proposed that  $\text{PO}_4$  forms three types of inner sphere

complexes on goethite ( $\alpha$ -FeOOH) surface: protonated bidentate binuclear, non-protonated bidentate binuclear, and non-protonated monodentate complex. Again based on FT-IR spectroscopy, however, Persson et al.<sup>10</sup> argued that only monodentate complexation takes place for PO<sub>4</sub> adsorption on goethite surface. Phosphate sorption to ferrihydrite<sup>11</sup> and boehmite ( $\gamma$ -AlOOH)<sup>12,13</sup> via the formation of inner sphere bidentate bridging complexes has been supported by theoretical molecular orbital calculation and various spectroscopic techniques. Although it is not yet certain whether PO<sub>4</sub> forms monodentate or bidentate complex on oxide mineral surface, it is clear that adsorbed PO<sub>4</sub> does form FePO<sub>4</sub>-or AlPO<sub>4</sub>-like surface precipitates as PO<sub>4</sub> loading approaches the maximum sorption capacity of the mineral.<sup>14-16</sup>

***Organic matter impact on phosphate sorption*** Because of its vicinity to minerals in soils, organic matter has been widely studied with respect to its impact on PO<sub>4</sub> sorption. Soil organic matter (OM) is the product of biomass decomposition. The content of OM in a soil ranges from trace amounts in sandy soils to >90% in organic soils.<sup>17</sup> Even that trace amount of organic matter is very important because it is a nutrient retention medium for soil living organisms and it is involved in many soil chemical processes, e.g. water and nutrient retention, or buffering action. Carbon is the main element in organic matter which normally accounts for ~50% of the bulk mass. Although the structure of organic matter is ill-defined, it is believed that the major chemical functional groups are carboxyls, phenols OH, enols, quinones, alcohols OH, ethers, etc.<sup>18</sup> It is widely recognized that OM inhibits PO<sub>4</sub> sorption to oxides or in soils.<sup>19-24</sup> Organic matter exhibits high Al or Fe complexation ability<sup>25,26</sup> and sorption affinity to oxide minerals.<sup>27,28</sup> Our sorption experiment with dissolved organic

matter (DOM) from Pahokee peat humic acid showed that ferrihydrite can sorb up to 400 mg DOM g<sup>-1</sup> FH. Competition between OM and PO<sub>4</sub> for sorption sites on mineral surface is proposed to account for the observed inhibitory effect from OM on PO<sub>4</sub> sorption. Nevertheless, some investigations found that the studied organic matter exerted no significant impact on PO<sub>4</sub> sorption.<sup>29,30</sup>

Organic matter itself retains little or no PO<sub>4</sub>. By contrast, OM with added Fe or Al can sorb a significant amount of PO<sub>4</sub><sup>31-33</sup> although the molecular details of the binding mechanism is not yet well understood. The amount of Al or Fe complexed with OM can be measured by pyrophosphate (Na<sub>4</sub>P<sub>2</sub>O<sub>5</sub>) extraction. Several investigators have established a positive correlation between pyrophosphate extractable Al and Fe and the system's PO<sub>4</sub> sorption capacity.<sup>34,35</sup> Therefore, PO<sub>4</sub> sorption to Fe or Al laden OM has been attributed to Al/Fe-OM complexes. It has been postulated that PO<sub>4</sub> binds to Al/Fe-OM complexes via the formation of OM-Al/Fe-PO<sub>4</sub> ternary complexes.<sup>32,36</sup> However, such postulation is mainly based on observations from macroscopic studies. Direct and conclusive evidence for such ternary complexes is still lacking.

Although OM has been shown to impose an instantaneous inhibitory effect on PO<sub>4</sub> sorption to oxides, OM seems to enhance PO<sub>4</sub> sorption to OM/oxide mixtures as the mixtures age.<sup>37,38</sup> The increased PO<sub>4</sub> sorption is parallel with increased pyrophosphate extractable Al or Fe, suggesting that more Al/Fe is complexed by OM during aging. The increased OM-Al/Fe complexes are believed to be responsible for the system's greater PO<sub>4</sub> sorption capacity as new sorption sites for PO<sub>4</sub> are provided via the formation of OM-Al/Fe-PO<sub>4</sub> ternary complexes. In the past decades, few studies have been conducted to delve into this

ternary complexation mechanism; and how aging transforms the structure of an oxide mineral as it ages with OM remains unclear. Thus, there is currently little understanding of such mechanism and more conclusive and direct evidence is needed to validate the hypothesis of OM-Al/Fe-PO<sub>4</sub> ternary complexation.

### ***Iron(III)-oxide reduction as affected by organic matter***

The redox potential in a soil can vary significantly as the water table fluctuates.<sup>39</sup> Generally, dissolved P increases as the soil's redox potential drops. Classically, the lowered potential is thought to cause Fe(III) reduction and dissolution which then releases P. Lab scale studies on reduction of Fe(III) minerals or soil samples have shown that Fe(III) reduction releases PO<sub>4</sub> concomitantly.<sup>40-43</sup> The close relation between Fe(III) reduction and PO<sub>4</sub> release suggests it is important to understand the factors that affect Fe(III) oxide reductions, as it is these factors that control the rate and extent of reductive dissolution of phosphate in soils. Particularly, knowledge of the impact from other soil components on Fe-oxide mineral reduction is critical for controlling the dynamics of phosphorus reductive dissolution.

Organic matter (OM) is an integral component in soils for it participates in many soil chemical and physical processes.<sup>17,18</sup> Besides its impact on PO<sub>4</sub> sorption to Fe(III) oxides, organic matter has been studied with respect to its role on ferric oxide microbial reduction. Research has shown that OM is able to store and transfer electrons from heterotrophic microorganisms to an electron acceptor, e.g. Fe(III).<sup>44-46</sup> In other words, OM can act as an electron shuttle between microorganisms and the electron acceptor. Such ability has been attributed to the one electron processes interconverting quinones to semiquinones to

hydroquinones.<sup>47,48</sup> Lovley et al.<sup>44</sup> first demonstrated that ferric oxide (ferric oxides include Fe(III) oxide, hydroxide, and oxyhydroxide minerals hereafter) microbial reduction was enhanced by OM and the enhancement was ascribed to an electron shuttling ability of OM. In the following decades, ample studies confirmed that OM enhances Fe(III) oxide microbial reduction. Most of these studies reiterate the proposed electron shuttle mechanism by OM.<sup>49-</sup>  
<sup>54</sup> The classic model describing the role of OM in microbial Fe(III) oxide reduction is presented in Figure 1-2.

It has been observed that microbial reduction of various ferric oxides ceases after only a small fraction, normally ~10%, of total Fe is reduced in a non-flow condition.<sup>55,56</sup> Biogenic Fe(II) deposition, either in the form of surface precipitates or secondary mix-valence Fe minerals, has been found in ferric oxide microbial reduction.<sup>57-59</sup> By contrast, Fe(II) removal during reduction significantly enhances ferric oxide microbial reduction.<sup>56,60,61</sup> Thus, biogenic Fe(II) accumulation on microbes or mineral surfaces is believed to be responsible for the cessation of reduction.<sup>56,62,63</sup> In addition to the model (Fig. 1-2) which suggests that OM acts as an active electron shuttle between microorganisms and Fe(III), Royer et al.<sup>49</sup> have suggested that OM may also act as an Fe(II) complexing agent facilitating Fe(II) transport away from the microbes so that Fe(II) accumulation is moderated. Direct proof for OM acting as an active electron shuttle in Fe(III) oxide bio-reduction has yet to be presented. Thus there is a need for well controlled studies of the reduction reaction mechanism(s) to delineate the relation between bio-reduction enhancement by OM, electron shuttling, and Fe(II)-OM complexation.

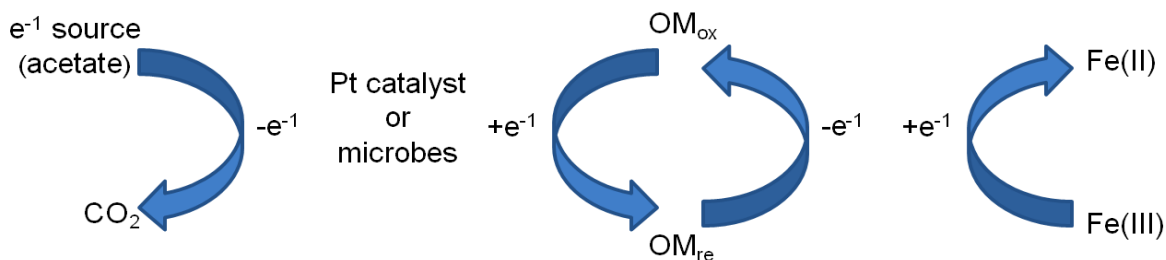


**Figure 1-2.** Schematic drawing showing organic matter shuttles electrons from the electron source (acetate is chosen in this schematic drawing) to Fe(III).  $\text{OM}_{\text{ox}}$ =oxidized organic matter,  $\text{OM}_{\text{re}}$ =reduced organic matter

Chemically reduced organic matter, e.g. by  $\text{H}_2$  gas in the presence of a Pt catalyst, also exhibits the ability to transfer electrons to Fe(III) sources.<sup>45,64,65</sup> Thus, chemically reduced OM can also shuttle electrons between the electron source and Fe(III) (See Fig. 1-2 where a Pt catalyst replaces microorganisms). Microbial and chemical reduction of OM appear to reduce the same functional groups, since the same amount of electrons is transferred from microbially-reduced OM to Fe(III) sources as from chemically-reduced OM. Thus OM is expected to enhance Fe(III) oxide chemical reduction. However, it is largely unclear whether OM exerts the same impact on Fe(III) oxide chemical reduction. Although microorganism mediation is the main driving force for reduction of ferric species in soils, ferric iron can be chemically reduced by Fe(III) reducing species, e.g. sulfide in anoxic soils. Therefore it is also important to pursue a thorough understanding of how OM impacts ferric oxide chemical reduction. In addition, chemical reduction systems can be more carefully controlled so that these systems are well suited for studies for the redox properties of OM and its impact on the reduction of iron oxides.

### 1.3. A model predicting PO<sub>4</sub> sorption-desorption path and questions to be answered

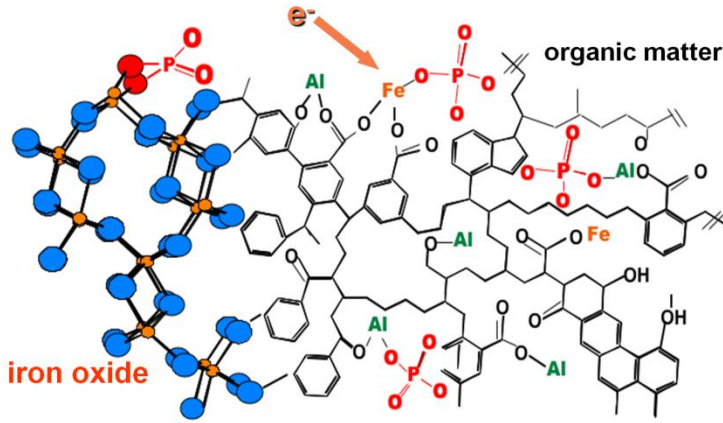


**Figure 1-3.** Schematic drawing showing PO<sub>4</sub> adsorbed to organic matter via Al or Fe bridges and to the surface of goethite. (Courtesy of Dr. Dean Hesterberg, North Carolina State University)

Although molecular-level mechanisms remain to be determined, the roles of Al- or Fe-oxides and organic matter on PO<sub>4</sub> retention and mobilization have been extensively discussed in the literature. Based on the discussion, a PO<sub>4</sub> sorption-desorption model using the structure of goethite to represent

Fe(III) oxide has been created as illustrated in Figure 1-3. This model depicts the interactions between organic matter and Fe-oxide as follows: (1) PO<sub>4</sub> adsorbs to Al or Fe containing organic matter via the formation of OM-Al/Fe-PO<sub>4</sub> ternary complexes; (2) organic matter initially decreases PO<sub>4</sub> to oxide minerals because it competes with PO<sub>4</sub> for sorption sites on mineral surface; (3) as the oxide mineral interacts (ages) with OM, Fe atoms migrate to OM to form organometallic complexes which provide new sorption sites for PO<sub>4</sub> so that PO<sub>4</sub> sorption capacity of the entire system increases; (4) as the system goes through, either chemical or microbial reduction, reductive dissolution of PO<sub>4</sub> is enhanced because OM facilitates Fe(III) reduction

In order to verify the validity of the model discussed above, the following questions need to be answered: (1) Do  $\text{PO}_4\text{-Al/Fe-OM}$  ternary complexes exist? (2) To what extent is an oxide mineral incorporated into organic matter with aging? (3) Does organic matter enhance Fe(III)-oxide chemical reduction? (4) If so, does organic matter act as an active electron shuttle? The answers to these questions will not only verify the validity of the model described in Fig.1-3, but also pertain to authentication of many additional hypotheses in the literature.

## 1.4. Goal and objectives

With increasing global population and food shortage, only sustainable agriculture can lead to a brighter future for human beings. One requirement of sustainable agriculture is to develop strategies to effectively use fertilizer so that nutrient runoff from soils to aquatic systems is reduced. In this regard, research to elucidate the mechanisms that control soil P retention and mobilization is extremely important. The goal of this dissertation research is to determine at a molecular mechanistic level how the interactions between Fe minerals and soil organic matter regulate phosphate binding and Fe(III) reduction.

In order to make the research findings relevant to soil systems, representative Fe(III) oxide and organic matter were chosen to create the research systems. Ferrihydrite is a poorly crystalline ferric oxide that widely spreads on the Earth's surface.<sup>66</sup> It is usually described as  $\text{Fe}(\text{OH})_3$  simply based on charge balance. A few more precise empirical molecular formulas have been proposed:  $5\text{Fe}_2\text{O}_3 \cdot 9\text{H}_2\text{O}$ ,<sup>67</sup>  $\text{Fe}_5\text{O}_7(\text{OH}) \cdot 4\text{H}_2\text{O}$  or  $\text{Fe}_5\text{O}_3(\text{OH})_9$ ,<sup>68</sup> and  $\text{Fe}_4\text{O}_5(\text{OH})_2 \cdot 2.6\text{H}_2\text{O}$ .<sup>69</sup> Lab synthesized 2-line ferrihydrite exhibits two broad peaks in its X-ray diffraction pattern indicating its short range structural order. Because of its natural

abundance and its high  $\text{PO}_4$  sorption capacity, ferrihydrite was chosen to represent a soil Fe(III) oxide in this study. Dissolved humic substances have been commonly used in studies for the impact of organic matter on  $\text{PO}_4$  sorption and Fe(III) microbial reduction. However, solid particulate organic matter should be a closer representative of OM in soils. Therefore, solid Pahokee peat was chosen as the organic matter.

As mentioned above, carboxyl groups are believed to be one of the major chemically active functional groups in organic matter. Spectroscopic data have confirmed that carboxyl groups are responsible for metal-OM complexation.<sup>25,26</sup> Therefore, small molecule carboxylic organic acids (OA) can be treated as models of organic matter. In order to determine whether organic matter competes or cooperates with  $\text{PO}_4$ , simple organic acids with different Fe(III) complexation affinities were reacted with Fe and  $\text{PO}_4$  and the solid products were characterized. In addition, an OA-Fe- $\text{PO}_4$  was to be synthesized and its X-ray absorption spectral features studied. X-ray diffraction and X-ray absorption spectroscopy were the major techniques for solid species characterization (Chapter 2 and 3). The interaction between OM and oxide minerals with time is expected to exert a significant impact on  $\text{PO}_4$  sorption. Ferrihydrite/OM mixtures were let age for a period of 55 days during which the mixtures'  $\text{PO}_4$  sorption capacity, ferrihydrite crystallinity, and dissolved organic carbon concentration were monitored. Moreover, the technique of EXAFS (extended X-ray absorption fine structure spectroscopy) was applied to detect any structural transformation of Fe in ferrihydrite as it aged with OM (Chapter 4). Another major component of the study presented in this dissertation is the redox properties of a particulate

organic matter, Pahokee peat (Chapter 5) and its impact on ferrihydrite chemical reduction (Chapter 6).

The findings of this study are expected to bridge the current gap between research observations regarding PO<sub>4</sub> and a final PO<sub>4</sub> sorption/desorption mechanistic understanding which will build upon this work.

## 1.5. References

- (1) Paul, E. A.; Clark, F. E. *Soil Microbiology and biochemistry*; Academic Press: San Diego, CA. USA, 1996.
- (2) Sharpley, A. N.; Daniel, T.; Simes, T.; Lemunyon, J.; Stevens, R.; Parry, R. *Agricultural Phosphorus and Eutrophication*, United States Department of Agriculture Agricultural Research Service, 2003.
- (3) Toor, G. S.; S.Hunger; J.D.Peak; J.T.Sims; Sparks, D. L. *Advances in agronomy* **2006**, 89, 1.
- (4) Sharpley, A. N.; Smith, S. J.; Jones, O. R.; Berg, W. A.; Coleman, G. A. *Journal of Environmental Quality* **1992**, 21, 30.
- (5) Hesterberg, D. *Macroscale chemical properties and X-ray absorption spectroscopy of soil phosphorus*; Elsevier B.V.: The Netherlands, 2010.
- (6) Khare, N.; Hesterberg, D.; Beauchemin, S.; Wang, S. L. *Soil Science Society of America Journal* **2004**, 68, 460.
- (7) Liu, Y.; Hesterberg, D. *Environmetal Science & Technology* **2010**. (publication in preparation)
- (8) Violante, A.; Pigna, M. *Soil Science Society of America Journal* **2002**, 66, 1788.
- (9) Tejedor-tejedor, M. I.; Anderson, M. A. *Langmuir* **1990**, 6, 602.

- (10) Persson, P.; Nilsson, N.; Sjoberg, S. *Journal of Colloid and Interface Science* **1996**, *177*, 263.
- (11) Khare, N.; Martin, J. D.; Hesterberg, D. *Geochimica Et Cosmochimica Acta* **2007**, *71*, 4405.
- (12) Bleam, W. F.; Pfeffer, P. E.; Goldberg, S.; Taylor, R. W.; Dudley, R. *Langmuir* **1991**, *7*, 1702.
- (13) Li, W.; Feng, J.; Kwon, K. D.; Kubicki, J. D.; Phillips, B. L. *Langmuir* **2010**, *26*, 4753.
- (14) Lookman, R.; Grobet, P.; Merckx, R.; Vlassak, K. *European Journal of Soil Science* **1994**, *45*, 37.
- (15) Nanzyo, M. *Journal of Soil Science* **1984**, *35*, 63.
- (16) Nanzyo, M.; Watanabe, Y. *Soil Science and Plant Nutrition* **1982**, *28*, 359.
- (17) Bot, A.; Benites, J. *The importance of soil organic matter*; Food and Agriculture Organization of the United Nations: Rome Italy, 2005.
- (18) Stevenson, F. J. *Humus chemistry: genesis, composition, reactions*; Wiley & Sons, Inc.: New York NY USA, 1982.
- (19) Hunt, J. F.; Ohno, T.; He, Z. Q.; Honeycutt, C. W.; Dail, D. B. *Biology and Fertility of Soils* **2007**, *44*, 277.
- (20) Ohno, T.; Hoskins, B. R.; Erich, M. S. *Biology and Fertility of Soils* **2007**, *43*, 683.
- (21) Ohno, T.; Erich, M. S. *Journal of Environmental Quality* **1997**, *26*, 889.
- (22) Ohno, T.; Crannell, B. S. *Journal of Environmental Quality* **1996**, *25*, 1137.

- (23) Wang, S. R.; Jin, X. C.; Bu, Q. Y.; Zhou, X. N.; Wu, F. C. *Journal of Hazardous Materials* **2006**, *128*, 95.
- (24) Guan, X. H.; Shang, C.; Chen, G. H. *Journal of Colloid and Interface Science* **2006**, *296*, 51.
- (25) Boyd, S. A.; Sommers, L. E.; Nelson, D. W. *Soil Science Society of America Journal* **1981**, *45*, 1241.
- (26) Rose, A. L.; Waite, T. D. *Marine Chemistry* **2003**, *84*, 85.
- (27) Luider, C.; Peticrew, E.; Curtis, P. J. *Hydrobiologia* **2003**, *494*, 37.
- (28) Kaiser, K.; Guggenberger, G.; Haumaier, L.; Zech, W. *European Journal of Soil Science* **1997**, *48*, 301.
- (29) Guppy, C. N.; Menzies, N. W.; Blamey, F. P. C.; Moody, P. W. *Soil Science Society of America Journal* **2005**, *69*, 1405.
- (30) Borggaard, O. K.; Jorgensen, S. S.; Moberg, J. P.; Rabenlange, B. *Journal of Soil Science* **1990**, *41*, 443.
- (31) Bloom, P. R. *Soil Science Society of America Journal* **1981**, *45*, 267.
- (32) Gerke, J.; Hermann, R. *Zeitschrift Fur Pflanzenernahrung Und Bodenkunde* **1992**, *155*, 233.
- (33) James, B. R.; Rabenhorst, M. C.; Frigon, G. A. *Water Environment Research* **1992**, *64*, 699.
- (34) Gunjigake, N.; Wada, K. *Soil Science* **1981**, *132*, 347.
- (35) Vijayachandran, P. K.; Harter, R. D. *Soil Science* **1975**, *119*, 119.

- (36) Riggle, J.; von Wandruszka, R. *Talanta* **2005**, *66*, 372.
- (37) Gerke, J. *Geoderma* **1993**, *59*, 279.
- (38) Borggaard, O. K.; Raben-Lange, B.; Gimsing, A. L.; Strobel, B. W. *Geoderma* **2005**, *127*, 270.
- (39) Fiedler, S.; Vepraskas, M. J.; Richardson, J. L. In *Advances in Agronomy, Vol 94* 2007; Vol. 94, p 1.
- (40) Peretyazhko, T.; Sposito, G. *Geochimica Et Cosmochimica Acta* **2005**, *69*, 3643.
- (41) Hutchison, K. J.; Hesterberg, D. *Journal of Environmental Quality* **2004**, *33*, 1793.
- (42) Murray, G. C.; Hesterberg, D. *Soil Science Society of America Journal* **2006**, *70*, 1318.
- (43) Roden, E. E.; Edmonds, J. W. *Archiv Fur Hydrobiologie* **1997**, *139*, 347.
- (44) Lovley, D. R.; Coates, J. D.; Blunt-Harris, E. L.; Phillips, E. J. P.; Woodward, J. C. *Nature* **1996**, *382*, 445.
- (45) Jiang, J.; Kappler, A. *Environmental Science & Technology* **2008**, *42*, 3563.
- (46) Struyk, Z.; Sposito, G. *Geoderma* **2001**, *102*, 329.
- (47) Scott, D. T.; McKnight, D. M.; Blunt-Harris, E. L.; Kolesar, S. E.; Lovley, D. R. *Environmental Science & Technology* **1998**, *32*, 2984.
- (48) Klapper, L.; McKnight, D. M.; Fulton, J. R.; Blunt-Harris, E. L.; Nevin, K. P.; Lovley, D. R.; Hatcher, P. G. *Environmental Science & Technology* **2002**, *36*, 3170.
- (49) Royer, R. A.; Burgos, W. D.; Fisher, A. S.; Unz, R. F.; Dempsey, B. A. *Environmental Science & Technology* **2002**, *36*, 1939.

- (50) Chen, J.; Gu, B. H.; Royer, R. A.; Burgos, W. D. *Science of the Total Environment* **2003**, *307*, 167.
- (51) Wolf, M.; Kappler, A.; Jiang, J.; Meckenstock, R. U. *Environmental Science & Technology* **2009**, *43*, 5679.
- (52) Roden, E. E.; Kappler, A.; Bauer, I.; Jiang, J.; Paul, A.; Stoesser, R.; Konishi, H.; Xu, H. F. *Nature Geoscience* **2010**, *3*, 417.
- (53) Roden, E. E.; Wetzell, R. G. *Abstracts of the General Meeting of the American Society for Microbiology* **1999**, *99*, 452.
- (54) Rakshit, S.; Uchimiya, M.; Sposito, G. *Soil Science Society of America Journal* **2009**, *73*, 65.
- (55) Roden, E. E.; Urrutia, M. M. *Geomicrobiology Journal* **2002**, *19*, 209.
- (56) Roden, E. E.; Urrutia, M. M.; Mann, C. J. *Applied and Environmental Microbiology* **2000**, *66*, 1062.
- (57) Hansel, C. M.; Benner, S. G.; Neiss, J.; Dohnalkova, A.; Kukkadapu, R. K.; Fendorf, S. *Geochimica Et Cosmochimica Acta* **2003**, *67*, 2977.
- (58) O'Loughlin, E. J.; Gorski, C. A.; Scherer, M. M.; Boyanov, M. I.; Kemner, K. M. *Environmental Science & Technology* **2010**, *44*, 4570.
- (59) Borch, T.; Masue, Y.; Kukkadapu, R. K.; Fendorf, S. *Environmental Science & Technology* **2007**, *41*, 166.
- (60) Urrutia, M. M.; Roden, E. E.; Zachara, J. M. *Environmental Science & Technology* **1999**, *33*, 4022.
- (61) Roden, E. E.; Urrutia, M. M. *Environmental Science & Technology* **1999**, *33*, 1847.

- (62) Roden, E. E.; Zachara, J. M. *Environmental Science & Technology* **1996**, *30*, 1618.
- (63) Urrutia, M. M.; Roden, E. E.; Fredrickson, J. K.; Zachara, J. M. *Geomicrobiology Journal* **1998**, *15*, 269.
- (64) Peretyazhko, T.; Sposito, G. *Geoderma* **2006**, *137*, 140.
- (65) Bauer, I.; Kappler, A. *Environmental Science & Technology* **2009**, *43*, 4902.
- (66) Cornell, R. M.; Schwertmann, U. *The Iron Oxides: Structure, Properties, Reactions, Occurrences and Uses*; Wiley-VCH: Weinheim, Germany, 2003.
- (67) Loan, M.; Parkinson, G. M.; Richmond, W. R. *American Mineralogist* **2005**, *90*, 258.
- (68) Schwertmann, U.; Friedl, J.; Stanjek, H. *Journal of Colloid and Interface Science* **1999**, *209*, 215.
- (69) Bakardjieva, S.; Stengl, V.; Subrt, J.; Vecernikova, E. *Solid State Sciences* **2005**, *7*, 367.

## **Chapter 2: The Competition between Phosphate and Organic Acids to Bind with Iron**

## **Abstract**

It has been hypothesized that phosphate ( $\text{PO}_4$ ) adsorbs to Al or Fe laden organic matter (OM) via the formation  $\text{PO}_4$ -Al/Fe-OM ternary complexes. Organic matter has been found to inhibit  $\text{PO}_4$  sorption to oxide minerals due to the competition between OM and  $\text{PO}_4$  for sorption sites. Therefore, OM may either compete or cooperate with  $\text{PO}_4$  to bind to a metal center. To date, however, direct evidence for the  $\text{PO}_4$ -Al/Fe-OM ternary complexation and the competition between  $\text{PO}_4$  and OM is lacking. Six organic acids (OA), serving as analogues of reactive functional groups in OM, were reacted with Fe and  $\text{PO}_4$  at different molar ratios at pH 5.5 under hydrothermal conditions. The goal of this study is to determine whether the studied organic acids compete or cooperate with  $\text{PO}_4$  in relation to the Fe(III) affinity of each OA. X-ray diffraction and Fe K-edge XANES (X-ray absorption near edge structure) spectroscopy were utilized to characterize the solid products. Only Na-Fe- $\text{PO}_4$  compounds are produced regardless of the type and amount of OA input. None of the studied organic acids is able to compete or cooperate with  $\text{PO}_4$  to bind with Fe. Oxalate, citrate, and tartrate exhibits Fe(III) reducing capacity in the order of tartrate>citrate>oxalate. Fe(III) reduction by organic acids decreases  $\text{PO}_4$  retention in solid phase.

## 2.1. Introduction

Soil phosphorus (P) export in watershed runoff to an aquatic system can destroy the aquatic ecosystem because P accumulation in the aquatic system greatly accelerates eutrophication. Hence, mechanistic studies on soil P retention and mobilization have been research attention. Poorly or non-crystalline Al- or Fe-(hydr)oxides are considered major sinks for soil inorganic P (orthophosphate,  $\text{PO}_4$ ) because of their ubiquity and large  $\text{PO}_4$  sorption capacity.<sup>2-4</sup> It has been widely observed that soil organic matter (OM) inhibits  $\text{PO}_4$  sorption to oxide minerals or soils. Organic matter has a high affinity to oxide mineral.<sup>5,6</sup> Therefore, the inhibitory effect of OM on  $\text{PO}_4$  sorption has been explained by the competition between OM and  $\text{PO}_4$  for sorption sites.<sup>7-11</sup> Nonetheless, some investigations have found that OM has no or limited impact on  $\text{PO}_4$  sorption.<sup>13-16</sup>

Organic matter itself retains little or no  $\text{PO}_4$ . But Al or Fe laden OM can sorb a significant amount of  $\text{PO}_4$ .<sup>17-20</sup> Pyrophosphate extractable Al and Fe, which are indices of organic matter complexed Al and Fe, were found to have a positive correlation with a soil's  $\text{PO}_4$  sorption capacity.<sup>21-23</sup> It has been proposed that Fe/Al-OM complexes are directly responsible for  $\text{PO}_4$  sorption to organic matter via the formation of OM-Al/Fe- $\text{PO}_4$  ternary complexes.<sup>24</sup>

If the theory of OM-Al/Fe- $\text{PO}_4$  ternary complexation holds, given that some OM was found to compete with  $\text{PO}_4$  while some OM showed no impact, possible interaction between OM and  $\text{PO}_4$  with the same metal center is: no interaction, competition, and cooperation (coordinate to the same metal center). Soil organic matter itself is a complex entity, not to mention the complexity of a soil matrix. Direct characterization of the interaction between OM

and  $\text{PO}_4$  on mineral surface remains challenging. Although the structure of organic matter is not well defined, it is believed that the major functional groups in OM are carboxyls, phenols OH, quinones, alcohols OH, etc. Spectroscopic data have confirmed that carboxyl groups are responsible for metal-OM complexation.<sup>25,26</sup> Therefore, carboxylic organic acids (OA) can be treated as simplified models for OM. A thorough understanding of the interaction between OA and  $\text{PO}_4$  will aid delineating the role of organic matter on  $\text{PO}_4$  retention and mobilization.

A variety of organic acids was shown to mobilize P from oxide minerals or soils.<sup>27-31</sup> The presence of  $\text{PO}_4$  also decreases organic acid sorption to oxides.<sup>3,32</sup> Citrate and oxalate were found to be more effective in mobilizing P than other organic acids, e.g. malonate or acetate.<sup>27,29,31</sup> Regarding how organic acids mobilize  $\text{PO}_4$ , two mechanisms have been proposed: ligand exchange dissolution<sup>32-34</sup> and ligand promoted dissolution.<sup>30,35,36</sup> The ligand exchange dissolution mechanism refers to sorption site competition between OA and  $\text{PO}_4$  on mineral surface. The ligand promoted dissolution mechanism means that an OA solubilizes Fe or Al by forming soluble Fe/Al-OA complexes concomitantly releasing the sorbed  $\text{PO}_4$ . According to Stumm<sup>37</sup> and Duckworth and Martin<sup>38</sup>, organic acids that form bidentate mononuclear surface complexes facilitate Fe dissolution from Fe-oxides, while those that form monodentate or bidentate binuclear surface complexes inhibit Fe dissolution. Thus, whether an OA induces  $\text{PO}_4$  desorption via the ligand exchange or ligand promoted dissolution mechanism depends on the type of surface complex the OA forms on mineral surface, which may vary depending on OA concentration and pH.<sup>39-41</sup> Nevertheless, either mechanism, ligand exchange or ligand promoted dissolution, ultimately results in the competition between OA and  $\text{PO}_4$ . Although the binding configuration of certain organic acids or  $\text{PO}_4$  on

Al- or Fe-oxide surface has been proposed by spectroscopic evidence,<sup>42-45</sup> molecular evidence for the competition between organic acids and phosphate when they encounter each other on mineral surface is still lacking. After all, most of the mechanistic conclusions were based on experimental observations and mass balance calculation.

In light of the hypothesized OM-Al/Fe-PO<sub>4</sub> ternary complexes, both carboxyl and phosphate groups should be able to coordinate to the same metal center. However, such ternary compounds are not common. A search of the Cambridge Crystallographic Database for mixed anion iron compounds reveals few OA-Fe-PO<sub>4</sub> or OA-Al-PO<sub>4</sub> ternary compounds, with the majority known crystal structures being oxalate-Fe/Al-phosphate compounds.<sup>46-50</sup> Among these mixed anion (oxalate/phosphate) materials, virtually all of the syntheses require an amine, even in the reported structure in which no amine remains in the hybrid framework.<sup>51</sup> The fact that so few pure ternary crystalline structures exist raises additional questions as to the compatibility of organic matter, or even organic acid and phosphate binding to the same metal center.

Instead of focusing on the surface chemistry of organic acid and phosphate on oxide mineral, this study focuses on structural characterization of the resultant solid products from the reactions of various organic acids, phosphate, and Fe(III) at pH 5.5, a pH that is relevant to soils. Aiming at elucidating the interaction between organic matter and phosphate to the same metal center, the objectives of this study are: (1) determine whether the studied organic acids compete with PO<sub>4</sub> to bind to Fe and the mechanism of competition; (2) determine the conditions in which a ternary OA-Fe-PO<sub>4</sub> compound forms.

## 2.2. Materials and methods

### *Reactions of H<sub>3</sub>PO<sub>4</sub>, organic acids, and Fe(III)*

The organic acids chosen for this study are oxalate (Ox), citrate (Ci), tartrate (Ta), succinate (Si), malonate (Ma), and Benzoate (Be) in the form of sodium compounds.

All chemicals were used as purchased from Sigma-Aldrich without further purification. In order to establish the coordination motif of the resultant species, each of these organic acids was reacted with FeCl<sub>3</sub>·6H<sub>2</sub>O and H<sub>3</sub>PO<sub>4</sub> solution (0.5M) at different molar ratios at pH 5.5 under hydrothermal conditions. The molar ratio of PO<sub>4</sub>:Fe:OA

**Table 2-1.** Molecular formula, pKa and LogK<sub>Fe(III)</sub> values for the six organic acids.

organic acid	Chemical	pK <sub>1</sub> *	pK <sub>2</sub> *	*LogK <sub>Fe(III)</sub> **
Oxalate	Na <sub>2</sub> C <sub>2</sub> O <sub>4</sub>	1.25	4.27	8.8
Citrate	Na <sub>3</sub> C <sub>6</sub> H <sub>5</sub> O <sub>7</sub> ·2H <sub>2</sub> O	3.13	4.76	13.12
Tartrate	Na <sub>2</sub> C <sub>4</sub> H <sub>4</sub> O <sub>6</sub> ·2H <sub>2</sub> O	3.04	4.37	6.95
Succinate	C <sub>2</sub> H <sub>4</sub> (CO <sub>2</sub> H) <sub>2</sub>	4.21	5.64	8.49
Malonate	CH <sub>2</sub> (CO <sub>2</sub> Na) <sub>2</sub> ·H <sub>2</sub> O	2.85	5.7	9.13
Benzoate	C <sub>6</sub> H <sub>5</sub> CO <sub>2</sub> Na	4.2		1.83***

\* NIST (1997) <sup>1</sup>

\*\* The complexes represented by these log K<sub>Fe(III)</sub> values are described by the following equation: M<sup>3+</sup> + L<sup>n-</sup> → ML<sup>(3-n)+</sup>.

\*\*\* Basaran *et al.* 1994<sup>12</sup>

varies from 6:2:1 to 6:2:6. In a typical reaction, 12 mL of H<sub>3</sub>PO<sub>4</sub> solution (6 mmole PO<sub>4</sub> equivalent) was mixed with 540 mg FeCl<sub>3</sub>·6H<sub>2</sub>O (2 mmole Fe(III) equivalent) in a beaker while being stirred. Designated amount of one of the studied organic acids was added to the Fe/PO<sub>4</sub> mixture. The mixture pH was slowly raised to 5.5 with NaOH (2M). After the reaction mixture had been stirred for ~30 minutes, it was transferred to an acid digestion bomb (Parr Instrument Company, Moline IL U.S.A.) which was then placed in an oven set at

170°C for five days. Once the reaction was completed, the solid and solution products were separated by filtration and collected for further analyses.

### ***Analyses following reactions***

Powder X-ray diffraction (XRD) data were collected with an INEL XRG 3000 diffractometer with Co K $\alpha$  radiation ( $\lambda=1.789007 \text{ \AA}$ ). The aqueous solutions collected from all PO<sub>4</sub>/Fe/OA reactions were analyzed for total P and Fe using a ICP-OES spectrometer. Selected solid products were analyzed for their total carbon concentration by combustion. Representative solid products were acid digested (3M HCl) to form solutions for total Na, Fe, and P analysis. Infrared spectroscopy analysis was applied to selected solid products with a FT-IR-410 spectrometer. Iron K-edge XAS (X-ray absorption spectroscopy) data were collected for selected samples at Beamline X-11B at the National Synchrotron Light Source (NSLS) of Brookhaven National Lab, Upton NY.

## **2.3. Results**

### ***Solid species identified by X-ray diffraction***

A total of 37 solid products were collected from the reactions of H<sub>3</sub>PO<sub>4</sub>, Fe(III), and organic acids at different molar ratios.

**Table 2-2.** Solid species formed in all PO<sub>4</sub>, Fe(III), and organic acid reactions as identified by X-ray diffraction.

Organic Acid	Molar input of OA						
	0	1	2	3	4	5	6
Blank	A*						
Oxalate		A	A	A	A	A + B <sup>#</sup>	B
Citrate		A	A	A	A +	A +	B
Tartrate		B	B	B	B	B	B
Succinate		A	A	A	A	A	A
Malonate		A	A	A	A	A	A
Benzoate		A	A	A	A	A	A

\*A=Na<sub>3</sub>Fe<sub>3</sub>(PO<sub>4</sub>)<sub>4</sub> #B= Na<sub>2.4</sub>Fe<sub>3</sub>(PO<sub>4</sub>)<sub>4</sub>

However, only two species were identified through X-ray diffraction as presented in Figure 2-1. Most reactions produced one species while a mixture of the two species formed in some oxalate and citrate reactions. One species was identified to be  $\text{Na}_3\text{Fe}_3(\text{PO}_4)_4$ <sup>52</sup> which formed in most of oxalate or citrate reactions and all malonate, succinate, and benzoate reactions. With oxalate input being  $\geq 5$  mmole, citrate input  $\geq 4$  mmole, or tartrate input  $\geq 1$  mmole, another species formed. The diffraction pattern of this unknown species is very similar to the calculated pattern of  $\text{Na}_{1.702}\text{Fe}_3(\text{PO}_4)_3$ <sup>53</sup> which belongs to a series of compounds that has a general formula of  $\text{Na}_x\text{Fe}_3(\text{PO}_4)_3$ . In these compounds iron has a mixed valance of +2 and +3 and the stoichiometry of Na depends on Fe(III)/Fe(II) ratio. The peaks in the diffraction pattern of the unknown species can be indexed to those in the calculated pattern of  $\text{Na}_{1.702}\text{Fe}_3(\text{PO}_4)_3$ ; and the unit cell parameters were refined to be: space group of 15, monoclinic,  $a=12.017$  (Å),  $b=12.534$  (Å),  $c=6.543$  (Å),  $\beta=115.65^\circ$ . X-ray diffraction analysis and unit cell refinement confirm that the second species is isostructural to  $\text{Na}_{1.702}\text{Fe}_3(\text{PO}_4)_3$ . A few solid products that solely generated the diffraction pattern of the unknown species were acid digested to form solutions. The solutions were analyzed for their total Fe, P, and Na concentrations. The average

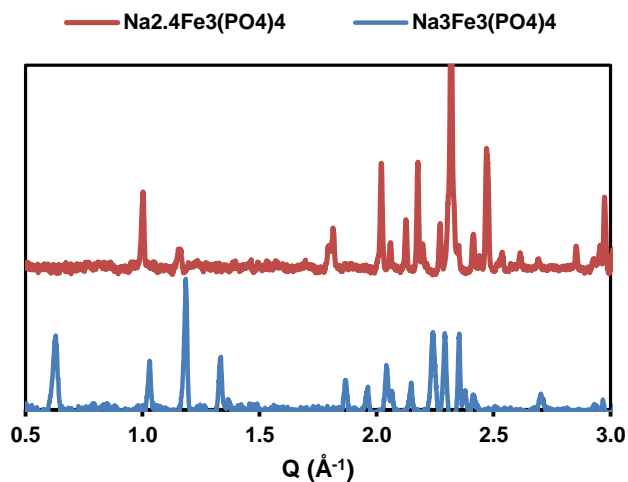


**Figure 2-1.** X-ray diffraction patterns of the two solid species from reactions of Fe(III),  $\text{H}_3\text{PO}_4$ , and various organic acids at pH 5.5 under hydrothermal conditions

Na:Fe:P molar ratio was 2.4:3.0:3.1. Thus the second species formed in some oxalate, citrate, and all tartrate reactions is determined to be  $\text{Na}_{2.4}\text{Fe}_3(\text{PO}_4)_3$ . With Na to Fe ratio being 2.4:3.0, the calculated Fe(III):Fe(II) ratio in  $\text{Na}_{2.4}\text{Fe}_3(\text{PO}_4)_3$  is 0.6:2.4. Clearly, the ferric Fe as starting material was partially reduced by oxalate, citrate, or tartrate at certain Fe/OA ratios. Products as identified by XRD from all  $\text{PO}_4/\text{Fe}/\text{OA}$  reactions are listed in Table 2-2. The fact that only Na-Fe- $\text{PO}_4$  compounds were identified by XRD confirms that none of the studied organic acids was able to form any crystalline Fe species in the presence of phosphate.

Iron(III) was also reacted with each organic acid with Fe:OA molar ratio being 2:6. In the absence of  $\text{PO}_4$ , hematite ( $\text{Fe}_2\text{O}_3$ ) is the only XRD identified solid species from the reactions of Fe(III) with malonate, succinate, or benzoate, respectively. When oxalate or citrate was reacted with Fe(III), siderite ( $\text{FeCO}_3$ ) and magnetite ( $\text{Fe}_3\text{O}_4$ ) were produced. Magnetite is the only XRD identified product in all Fe(III)/tartrate reactions. Again no crystalline Fe-OA species formed in all Fe/OA reactions even without phosphate.

***Iron(III) reduction by organic acids***

X-ray diffraction analyses on the solid products from  $\text{PO}_4/\text{Fe(III)}/\text{OA}$  reactions indicated partial Fe(III)

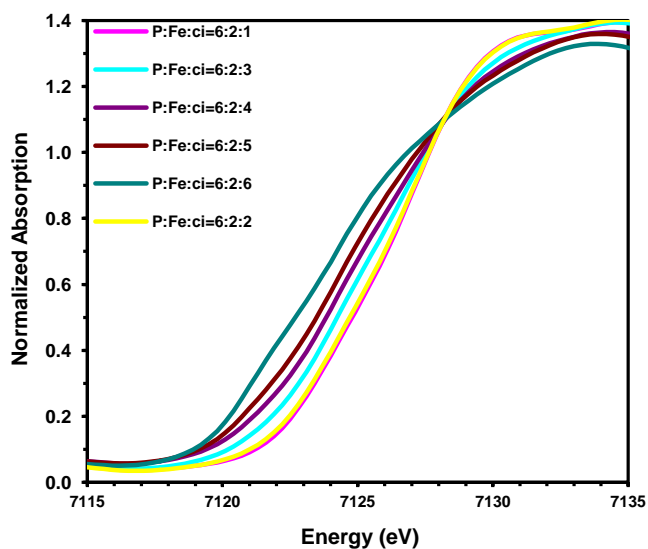


**Figure 2-2.** Normalized Fe K-edge XANES spectra of the solid products of reactions of  $\text{PO}_4$ , Fe(III), and oxalate at various molar ratios at pH 5.5.

reduction by oxalate, citrate, and tartrate. Iron(III) reduction was further confirmed by Fe XANES analyses on the solid products from oxalate, citrate, and tartrate reactions. The

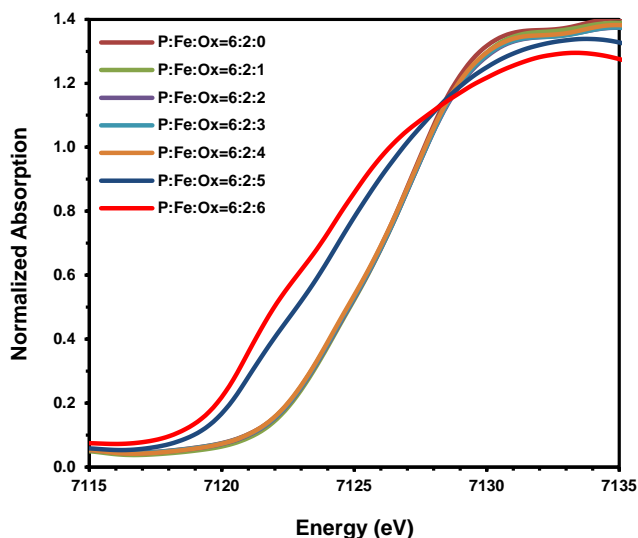


**Figure 2-3.** Normalized Fe K-XANES spectra of the solid products of reaction of PO<sub>4</sub>, Fe(III), and citrate at various molar ratios at pH 5.5.

oxidation state of Fe. In oxalate reactions when oxalate input was 5 mmole, XRD analysis confirmed the formation of Na<sub>2.4</sub>Fe<sub>3</sub>(PO<sub>4</sub>)<sub>3</sub> which resulted in a shift of the absorption edge to 7124.5 eV in its XANES spectrum as seen in Fig. 2-2A. More

Fe(III) was reduced by 6 mmole oxalate for the absorption edge shifted to 7123.5 in the spectrum of

normalized Fe K-edge XANES spectra of these solid products are presented in Figure 2-2, 2-3, and 2-4. For Na<sub>3</sub>Fe<sub>3</sub>(PO<sub>4</sub>)<sub>4</sub>, the product of the control reaction between Fe(III) and PO<sub>4</sub>, and most other reactions, the absorption edge of its XANES spectrum is at ~7127.0 eV (Fig. 2-2, labeled at

P:Fe:Ox=6:2:0) confirming a +3

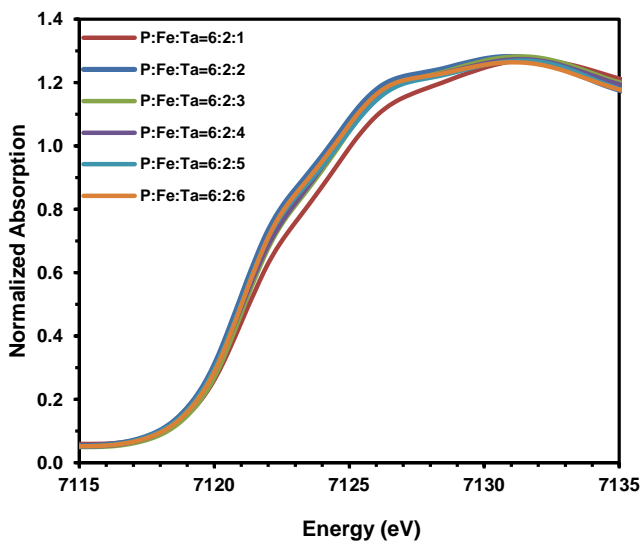


**Figure 2-4.** Normalized Fe K-XANES spectra of the solid products from reactions of PO<sub>4</sub>, Fe(III), and tartrate at various molar ratios at pH 5.5.

the solid product. The spectra in Fig. 2-2 were analyzed by linear combination fitting with Fe(II) and Fe(III) standards ( $\text{Fe}_3(\text{PO}_4)_2 \cdot 8\text{H}_2\text{O}$  and  $\text{FePO}_4 \cdot 2\text{H}_2\text{O}$ ). The fitting results show that 48.7% and 74.5% of the total Fe was reduced by oxalate when oxalate input was 5 and 6 mmole, respectively. Lesser amounts of oxalate addition show no evidence of Fe(III) reduction. For citrate reactions,  $\text{Na}_{2.4}\text{Fe}_3(\text{PO}_4)_3$  was not identified until citrate input was  $\geq 4$  mmole. Revealed by the graduate shift of the absorption edge towards 7123.8 eV (Fig. 2-3), Fe(III) reduction occurred as citrate input was  $>1$  mmole. All absorption edges of the XANES spectra of the solid products from the tartrate reactions are  $\sim 7121$  eV (Fig. 2-4). The results of linear combination fitting to these spectra show that Fe(II) accounts for  $\sim 85\%$  of total Fe in all solid products. This Fe(II) percentage is consistent with the stoichiometry of  $\text{Na}_{2.4}\text{Fe}_3(\text{PO}_4)_3$  in which 80% of total Fe is divalent Fe. Both XRD and XANES analyses have confirmed that tartrate is a stronger Fe(III) reducing agent than oxalate and citrate.

### ***Phosphorus distribution between solid and solution phase***

In order to determine the influence of organic acids on P retention in solid phase, all solutions collected from  $\text{PO}_4/\text{Fe(III)}/\text{OA}$  reactions were analyzed for total Fe and P concentrations. No or trace amounts of Fe was found in all reaction solutions indicating that all Fe as the starting material precipitated in the solid products. The amounts of P retained in the solid products were determined by the difference between added P and P remaining in the solutions as presented in Figure 2-5.

For the control reaction in which no organic acid was reacted, the calculated amount of P retained in solid phase is 2.68 mmole. As mentioned above that all of the 2 mmole Fe added as a starting material was incorporated in the solid products, the calculated P to Fe ratio is 1.34, which is consistent with the stoichiometry of Fe and P in  $\text{Na}_3\text{Fe}_3(\text{PO}_4)_4$ . For the

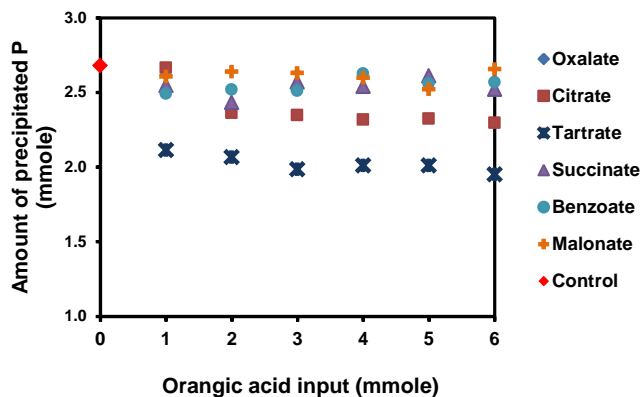


**Figure 2-5.** Calculated amounts of phosphorus retained in the solid products from all reactions of  $\text{PO}_4$ , Fe(III), and organic acid at pH 5.5.

reactions of malonate, succinate, and benzoate, and oxalate, the calculated amounts of P precipitated in solid

phase are ~ 2.6 mmole. Lesser amounts of P precipitated in citrate and tartrate reactions. For example, with citrate input being 6 mmole the amount of P retained in solid phase is 2.3 mmole. The P:Fe ratio in the solid product is 1.15. For tartrate reactions the calculated P:Fe ratios in all solid products are ~1 which is in accordance with the theoretical P:Fe ratio in  $\text{Na}_{2.4}\text{Fe}_3(\text{PO}_4)_3$  that was formed in all tartrate reactions.

## 2.4. Discussion

### *No competition or cooperation between phosphate and the organic acids*

According to the literature, phosphate desorption induced by organic acids has been attributed to either ligand exchange or ligand promoted dissolution mechanism. Either mechanism requires that an organic acid is able to coordinate to the metal atoms in the mineral. Based on XRD analyses, however, only Na-Fe- $\text{PO}_4$  compounds were formed in all

reactions between  $\text{PO}_4$ , Fe(III), and the studied organic acids regardless of the organic acid species and the molar input. Sodium is incorporated in the solid phase most likely because NaOH solution was employed to raise the pH of the reaction systems. Separate experiments for the reactions of  $\text{PO}_4$ , Fe(III), and succinate were conducted at pH lower than 5.5. Less NaOH was required for pH adjustment in these reactions and  $\text{Fe}_4(\text{OH})_3(\text{PO}_4)_3$  was produced. Obviously  $\text{Na}^+$  is a spectator ion filling the voids left from Fe; it does not affect the affinity between Fe and  $\text{PO}_4$ . X-ray diffraction analyses did not identify any crystalline organic acid species in all solid products. Total carbon analyses only detected trace amounts of carbon remaining in all solid products. Furthermore, FT-IR analyses found no evidence to support that the studied organic acids were incorporated in the solid products. All these analyses are indicating that Fe- $\text{PO}_4$  bonding dictates the interaction among Fe,  $\text{PO}_4$ , and the organic acids. None of the studied organic acids was able to compete with  $\text{PO}_4$  to coordinate to Fe. The results of this study show that organic acids do not always compete with  $\text{PO}_4$  to bind with Fe as suggested by the ligand exchange or ligand promoted dissolution mechanisms.

The fact that all of the studied organic acids are excluded from the solid products means that no  $\text{PO}_4$ -Fe-OA ternary compound formed under the experimental conditions. As mentioned above, the compatibility between phosphate and small molecule organic acid is questionable because the majority reported ternary compounds contain oxalate as the organic component. That raises a question about whether the formation of a  $\text{PO}_4$ -Fe-OA ternary compound requires the special geometry that only an oxalate ligand can provide. However, even oxalate failed to bind to Fe in this study, which may be due to the set pH of 5.5. But additional oxalate reactions conducted at lower pH did not produce any oxalate containing

solid products either. Virtually all syntheses of the reported PO<sub>4</sub>-Fe-Ox compounds require an organic amine to be the structure directing template. The lack of a structure directing template in this study may partially explain why no PO<sub>4</sub>-Fe-OA ternary compound formed in all reactions. To date, the proposal of the OM-Fe-PO<sub>4</sub> ternary complexation is fully based on the observations from macroscopic studies. In depth studies for molecular evidence are needed to support this binding mechanism for PO<sub>4</sub> sorption to OM.

### ***PO<sub>4</sub> mobilization as affected by Fe(III) reduction***

As seen in Fig. 2-4, the amount of phosphate retained in the solid products from malonate, succinate, and benzoate reactions remains constant, which is the same as the amount of PO<sub>4</sub> precipitated in the solid product from the blank reaction. In these reactions Fe(III) was not reduced. Less PO<sub>4</sub> was detected in the solid products from citrate or tartrate reactions in which partial Fe(III) reduction led to the formation of Na<sub>2.4</sub>Fe<sub>3</sub>(PO<sub>4</sub>)<sub>3</sub>. Therefore, decreased PO<sub>4</sub> retention in solid phase is not caused by the competition between OA and PO<sub>4</sub> but Fe(III) reduction by an organic acid under the experimental conditions in this study. Increased dissolved P is normally observed when redox potential drops in soils. The general explanation is that reduction of Fe(III) releases Fe(II) and P. Such explanation is supported by ample lab scale studies that have established the relation between Fe(III) oxide reduction and dissolution of Fe(II) and P.<sup>54-57</sup> However, the decrease of P retention in solid phase observed in this study is not supported by the reductive dissolution mechanism because no Fe dissolution was observed in all cases. For all malonate, succinate, benzoate, and most oxalate reactions, Fe(III) reduction did not occur. The resultant product was Na<sub>3</sub>Fe<sub>3</sub>(PO<sub>4</sub>)<sub>4</sub> in which P:Fe ratio is 1.33:1. Iron(III) was partially reduced by oxalate, citrate, or tartrate leading to

the formation of  $\text{Na}_{2.4}\text{Fe}_3(\text{PO}_4)$  in which P:Fe ratio is 1:1. Therefore, Fe(III) reduction affects P retention by forming different Fe- $\text{PO}_4$  species so that the stoichiometry of Fe and P changes. This mechanism has its significance in the environment. As an Fe(III)- $\text{PO}_4$  mineral goes through reduction, some Fe(II) is dissolved and some Fe(II) will be mineralized with  $\text{PO}_4$  forming ferrous phosphates, e.g. vivianite ( $\text{Fe}_3(\text{PO}_4)_2 \cdot 8\text{H}_2\text{O}$ ), in which P to Fe ratio decreases to 0.67:1. So P mobilization by Fe(III) reduction in soils should not only be attributed to Fe(II) dissolution, but also to the change of Fe to P ratio in solid phase due to the valence change of iron. While competition between organic acids and  $\text{PO}_4$  is not supported by the results in this study, the findings of this study suggest that Fe(III) reducing organic acids induce  $\text{PO}_4$  desorption by Fe(III) reduction.

## 2.5. Conclusions

Aiming at understanding the interactions between organic matter and phosphate in soils, the study presented in this chapter focuses on characterizing the solid products from reactions of phosphate, Fe(III), and six organic acids under hydrothermal conditions. Surprisingly Fe- $\text{PO}_4$  coordination dominated all reactions. No solid organic acid species was identified by analyses of X-ray diffraction, total carbon analysis, and FT-IR spectroscopy. The studied organic acids failed to compete with  $\text{PO}_4$  to bind to Fe so that various molar inputs of the non-Fe(III) reducing organic acids (malonate, succinate, and benzoate) did not affect the  $\text{PO}_4$  retention in solid phase. Oxalate, citrate, and tartrate exhibited Fe(III) reducing capacity in the order of tartrate>citrate>oxalate. Iron(III) reduction by these organic acids resulted in less phosphate retained in the solid products. The fact that no  $\text{PO}_4$ -Fe-OA ternary compound formed in this study makes the compatibility between organic matter and

phosphate questionable. In depth investigation is required to support the hypothesized PO<sub>4</sub>-Fe/Al-OM ternary complexation.

## 2.6. References

- (1) NIST; National Institute of Standards, U.S. Dep. of Commerce, Gaithersburg, MD: 1997.
- (2) Khare, N.; Hesterberg, D.; Beauchemin, S.; Wang, S. L. *Soil Science Society of America Journal* **2004**, *68*, 460.
- (3) Violante, A.; Colombo, C.; Buondonno, A. *Soil Science Society of America Journal* **1991**, *55*, 65.
- (4) Violante, A.; Pigna, M. *Soil Science Society of America Journal* **2002**, *66*, 1788.
- (5) Kaiser, K.; Guggenberger, G.; Haumaier, L.; Zech, W. *European Journal of Soil Science* **1997**, *48*, 301.
- (6) Luider, C.; Peticrew, E.; Curtis, P. J. *Hydrobiologia* **2003**, *494*, 37.
- (7) Hunt, J. F.; Ohno, T.; He, Z. Q.; Honeycutt, C. W.; Dail, D. B. *Biology and Fertility of Soils* **2007**, *44*, 277.
- (8) Ohno, T.; Crannell, B. S. *Journal of Environmental Quality* **1996**, *25*, 1137.
- (9) Ohno, T.; Erich, M. S. *Journal of Environmental Quality* **1997**, *26*, 889.
- (10) Ohno, T.; Hoskins, B. R.; Erich, M. S. *Biology and Fertility of Soils* **2007**, *43*, 683.
- (11) Guan, X. H.; Shang, C.; Chen, G. H. *Journal of Colloid and Interface Science* **2006**, *296*, 51.
- (12) Basaran, B.; Avsar, E.; Gocmen, A.; Erim, F. B. *Thermochimica Acta* **1994**, *247*, 407.

- (13) Borggaard, O. K.; Jorgensen, S. S.; Moberg, J. P.; Rabenlange, B.; *Journal of Soil Science* **1990**, *41*, 443.
- (14) Borggaard, O. K.; Raben-Lange, B.; Gimsing, A. L.; Strobel, B. W.; *Geoderma* **2005**, *127*, 270.
- (15) Guppy, C. N.; Menzies, N. W.; Blamey, F. P. C.; Moody, P. W.; *Py Soil Science Society of America Journal* **2005**, *69*, 1405.
- (16) Guppy, C. N.; Menzies, N. W.; Moody, P. W.; Blamey, F. P. C. *Australian Journal of Soil Research* **2005**, *43*, 189.
- (17) Bloom, P. R.; *Soil Science Society of America Journal* **1981**, *45*, 267.
- (18) Gerke, J.; Hermann, R. *Zeitschrift Fur Pflanzenernahrung Und Bodenkunde* **1992**, *155*, 233.
- (19) James, B. R.; Rabenhorst, M. C.; Frigon, G. A. *Water Environment Research* **1992**, *64*, 699.
- (20) Gerke, J. *Geoderma* **1993**, *59*, 279.
- (21) Burt, R.; Mays, M. D.; Benham, E. C.; Wilson, M. A. *Communications in Soil Science and Plant Analysis* **2002**, *33*, 117.
- (22) Vijayachandran, P. K.; Harter, R. D. *Soil Science* **1975**, *119*, 119.
- (23) Gunjigake, N.; Wada, K. *Soil Science* **1981**, *132*, 347.
- (24) Riggle, J.; von Wandruszka, R. *Talanta* **2005**, *66*, 372.
- (25) Boyd, S. A.; Sommers, L. E.; Nelson, D. W. *Soil Science Society of America Journal* **1981**, *45*, 1241.

- (26) Rose, A. L.; Waite, T. D. *Marine Chemistry* **2003**, *84*, 85.
- (27) Hu, H. Q.; He, J. Z.; Li, X. Y.; Liu, F. *Environment International* **2001**, *26*, 353.
- (28) Bhatti, J. S.; Comerford, N. B.; Johnston, C. T. *Soil Science Society of America Journal* **1998**, *62*, 1089.
- (29) W, L.; F., Z.; Y, C. *Plant nutrition-Food security and sustainability of agro-ecosystems* **2001**, 554.
- (30) Johnson, S. E.; Loeppert, R. H. *Soil Science Society of America Journal* **2006**, *70*, 222.
- (31) Hu, H. Q.; Tang, C. X.; Rengel, Z. *Journal of Plant Nutrition* **2005**, *28*, 1427.
- (32) Geelhoed, J. S.; Hiemstra, T.; Van Riemsdijk, W. H. *Environmental Science & Technology* **1998**, *32*, 2119.
- (33) Hue, N. V. *Soil Science* **1991**, *152*, 463.
- (34) He, Z. L.; Yang, X.; Yuan, K. N.; Zhu, Z. X. *Plant and Soil* **1994**, *162*, 89.
- (35) Jones, D. L.; Darrah, P. R.; Kochian, L. V. *Plant and Soil* **1996**, *180*, 57.
- (36) Kirk, G. J. D.; Santos, E. E.; Findenegg, G. R. *Plant and Soil* **1999**, *211*, 11.
- (37) Stumm, W. *Aquatic Sciences* **1993**, *55*, 273.
- (38) Duckworth, O. W.; Martin, S. T. *Geochimica Et Cosmochimica Acta* **2001**, *65*, 4289.
- (39) Timberlake, C. F. *Journal of the Chemical Society* **1964**, 5078.
- (40) Francis, A. J.; Dodge, C. J.; Gillow, J. B. *Nature* **1992**, *356*, 140.

- (41) Hamm, R. E.; Shull, C. M.; Grant, D. M. *Journal of the American Chemical Society* **1954**, *76*, 2111.
- (42) Tejedortejedor, M. I.; Yost, E. C.; Anderson, M. A. *Langmuir* **1990**, *6*, 979.
- (43) Tejedortejedor, M. I.; Anderson, M. A. *Langmuir* **1990**, *6*, 602.
- (44) Persson, P.; Nordin, J.; Rosenqvist, J.; Lovgren, L.; Ohman, L. O.; Sjoberg, S. *Journal of Colloid and Interface Science* **1998**, *206*, 252.
- (45) Persson, P.; Nilsson, N.; Sjoberg, S. *Journal of Colloid and Interface Science* **1996**, *177*, 263.
- (46) Choudhury, A.; Natarajan, S.; Rao, C. N. R. *Chemistry of Materials* **1999**, *11*, 2316.
- (47) Choudhury, A.; Natarajan, S. *Journal of Materials Chemistry* **1999**, *9*, 3113.
- (48) Lin, H. M.; Lii, K. H.; Jiang, Y. C.; Wang, S. L. *Chemistry of Materials* **1999**, *11*, 519.
- (49) Chang, W. J.; Lin, H. M.; Lii, K. W. *Journal of Solid State Chemistry* **2001**, *157*, 233.
- (50) Jiang, Y. C.; Wang, S. L.; Lii, K. H.; Nguyen, N.; Ducouret, A. *Chemistry of Materials* **2003**, *15*, 1633.
- (51) Choudhury, A.; Natarajan, S.; Rao, C. N. R. *Chemistry-a European Journal* **2000**, *6*, 1168.
- (52) Lajmi, B.; Hidouri, M.; Rzeigui, M.; Ben Amara, M. *Materials Research Bulletin* **2002**, *37*, 2407.
- (53) Hatert, F.; Rebbouh, L.; Hermann, R. P.; Fransolet, A. M.; Long, G. J.; Grandjean, F. *American Mineralogist* **2005**, *90*, 653.

- (54) Peretyazhko, T.; Sposito, G. *Geochimica Et Cosmochimica Acta* **2005**, *69*, 3643.
- (55) Hutchison, K. J.; Hesterberg, D. *Journal of Environmental Quality* **2004**, *33*, 1793.
- (56) Murray, G. C.; Hesterberg, D. *Soil Science Society of America Journal* **2006**, *70*, 1318.
- (57) Roden, E. E.; Edmonds, J. W. *Archiv Fur Hydrobiologie* **1997**, *139*, 347.

## **Chapter 3: Mixed Anion (Phosphate/Oxalate) Bonding to Iron(III) Materials**

Kizewski, F. R.; Boyle, P.; Hesterberg, D.; Martin, J. D. *Journal of the American Chemical Society* **2010**, *132*, 2301.

## Abstract

A novel phosphate/oxalate inorganic-organic hybrid material has been prepared to elucidate synthesis and bonding characteristics of iron(III) with both phosphate and organic matter (OM). Such mixed anion bonding of inorganic oxyanions and OM to iron(III) and aluminum(III) in environmental systems has been proposed but not proven, mainly because of the complexity of natural geochemical matrices. The compound reported here with the molecular formula of  $[\text{C}_3\text{H}_{12}\text{N}_2]_2[\text{Fe}_5(\text{C}_2\text{O}_4)_2(\text{H}_x\text{PO}_4)_8]$  (**I**) was hydrothermally synthesized and characterized by single crystal X-ray diffraction and X-ray absorption spectroscopy (XAS). In this new structure, Fe-O octahedra and P-O tetrahedra are connected by corner-sharing to form a 2-D network in the a-b plane. Oxalate anions cross link these Fe-P layers constructing a 3-D anionic framework. A diprotonated structure-directing template, DAP (1,3-diaminopropane), resides in the oxalate layer of the structure and offsets the negative charge of the anionic framework. Iron K-edge XANES spectra confirmed that the iron in **I** is Fe(III). The crystal structure of **I** is used to successfully fit its Fe K-edge EXAFS spectrum, which exhibits spectral signatures that unambiguously identify iron-phosphate and iron-OM bonding. Such molecular spectroscopic features will be invaluable for the evaluation of complex environmental systems. Furthermore, syntheses demonstrated the critical role of the templating amine to mediate whether or not the iron(III) is reduced by the organic acid.

## KEYWORDS

Iron Phosphate, organic-inorganic hybrid, X-ray Absorption Spectroscopy, XANES, EXAFS

## Introduction

Chemical speciation (chemical form) of contaminants largely control their mobility and potential toxicity in environmental systems including the soil-subsurface continuum, groundwater aquifers, freshwater and marine sediments. However, characterization of contaminant speciation is hindered by the extreme complexity of these systems. Contaminants like phosphate, arsenate, and metal cations can be bonded to multiple matrix components that include various oxide, hydroxide, and silicate minerals and structurally heterogeneous organic matter (humics), as well as ternary adducts of these components.<sup>1</sup> Moreover, adsorbed, mineral, and co-precipitated forms of contaminants can co-exist in nature, presenting an analytical challenge for characterizing chemical speciation.

Although phosphorus is an essential macronutrient for life, excessive P inputs from agricultural systems is a major environmental concern because P transfer to surface waters causes eutrophication. Understanding mechanisms for P binding in soils, sediment or other natural geochemical systems is extremely important to predict P distribution and mobility. Phosphate concentration, matrix composition (e.g. mineralogy and OM content), pH, and redox properties are considered primary determining factors in controlling phosphate binding and mobility both in soils and sediments.<sup>2-3</sup> These matrices are complex, multi-component materials, with sorbed or mineral precipitated inorganic phosphate being a relatively minor component. Thus, characterizing the fundamental characteristics of phosphate binding to minerals is challenging, particularly in the presence of OM. Iron- and aluminum-oxide minerals are considered important sorbents for phosphate in acid soils.<sup>4,5</sup> Moreover, it has been hypothesized that natural organic matter significantly impacts phosphate sorption via

the formation of OM-Fe(III)-PO<sub>4</sub> or OM-Al(III)-PO<sub>4</sub> ternary complexes, though direct evidence for such ternary complexation is lacking.<sup>6-7</sup>

Spectroscopic methods for directly characterizing molecular bonding in environmental systems are usually compromised by interfering elements or the extreme complexity of the matrix. For example, nuclear magnetic resonance (NMR) spectroscopy suffers from interference by the magnetism of Fe, one of the more abundant elements in earth-surface systems. Fourier-transform infrared (FT-IR) spectroscopy analysis of minor components like phosphate in environmental samples is often hindered by stronger, overlapping absorption bands of more dominant matrix components. X-ray absorption spectroscopy is an element-specific technique that is less subject to matrix interferences than other spectroscopies. But the resulting spectrum reflects the average local molecular coordination environment around atoms of the absorber element. Hence, in complex matrices, XAS does not directly distinguish, for example, between ternary coordination structures involving an inorganic oxyanion and an organic ligand bonded to the same metal center versus binary complexes of each of these ligands to different metal centers. It is therefore necessary to obtain structurally well defined systems that can be used as models for spectroscopically interrogating more complex systems.

A search of the Cambridge Crystallographic Database for structures containing small-molecule organic acids that would serve as OM analogues reveals very few phosphate-Fe(III)-organic-acid ternary complexes, with the majority of known crystal structures being phosphate-Fe-oxalate complexes.<sup>8-10</sup> Among these phosphate/oxalate containing materials, virtually all of the syntheses require the presence of an amine, even in the reported structure

in which no amine is found in the hybrid framework.<sup>11</sup> The fact that few pure ternary crystalline structures exist raises additional questions as to the compatibility of organic acid and phosphate anions binding to the same metal center.

X-ray absorption near edge structure (XANES) spectroscopy at the phosphorus K-edge has recently been exploited to probe phosphate binding in environmental matrices.<sup>12-13</sup> By comparing spectra from these systems with minerals of known structure, it was shown that P K-edge XANES can effectively differentiate phosphate bound to iron and aluminum oxide minerals based on the characteristics of pre-white line features.<sup>14,15</sup> In addition, researchers have applied iron K-edge EXAFS (extended x-ray absorption fine structure) to investigate the Fe coordination environment in soil organic matter.<sup>16-17</sup> Using Fe EXAFS, Karlsson et al.<sup>18</sup> proposed that Fe either exists as mononuclear Fe(III)-OM complexes or precipitated as Fe(III) (hydr)oxides. However, no literature to date provides conclusive experimental evidence for the hypothesized PO<sub>4</sub>-Fe-OM ternary complexation. Thus the aim of this research was to synthesize and characterize a crystalline ternary compound, specifically involving phosphate and a carboxylic acid bound to a common iron(III) center, that would serve as a model system for XAS spectroscopic interrogation of ternary complexation in natural systems.

From a series of syntheses attempting to reproduce bulk quantities of template free iron phosphate/oxalate materials that were reported in the literature,<sup>11</sup> a new templated iron phosphate/oxalate material was discovered. We here report the synthesis, single crystal structural, and XAS characterization of [DAP]<sub>2</sub>[Fe<sub>5</sub>(C<sub>2</sub>O<sub>4</sub>)<sub>2</sub>(H<sub>x</sub>PO<sub>4</sub>)<sub>8</sub>] (**I**) (DAP = C<sub>3</sub>H<sub>12</sub>N<sub>2</sub>H<sub>2</sub>). While the gross framework bonding is similar among all of the reported

iron(III) phosphate/oxalate materials,<sup>11-16</sup> **I** represents the most phosphate rich (P/Fe = 1.6) and the second most oxalate poor (Ox/Fe = 0.4) of these materials. In this study, a combination of the precise structural detail from the single crystal structure with thorough XAS spectroscopic characterization that is amenable to bulk and trace material analysis, demonstrates an important application of fundamental structural chemistry for the development of a molecular understanding of complex environmental systems.

## Results

**Synthesis of [DAP]<sub>2</sub>[Fe<sub>5</sub>(C<sub>2</sub>O<sub>4</sub>)<sub>2</sub>(H<sub>x</sub>PO<sub>4</sub>)<sub>8</sub>, **I**.** In keeping with literature reports of mixed anion (phosphate/organic acid) materials,<sup>11</sup> reactions were explored both with and without the addition of a potentially structure directing amines as templates. Hydrothermal treatment of an aqueous solution of H<sub>3</sub>PO<sub>4</sub>, 1,3-diaminopropane (DAP), FeCl<sub>3</sub>·6H<sub>2</sub>O and H<sub>2</sub>C<sub>2</sub>O<sub>4</sub> (see experimental) yielded a pale pink crystalline product. Single crystals were harvested for X-ray diffraction analysis, and X-ray powder diffraction confirmed that the bulk product was the same material as the single crystal. Thermogravimetric analysis of **I** from room temperature to 800 °C under a N<sub>2</sub> atmosphere exhibited a sharp weight loss of 23% starting approximately at 300 °C followed by two more gradual weight loss steps of an additional 6% (See supplementary information Figure S1). This result is consistent with an initial decomposition resulting in the loss of the templating ammonium cation and the carboxylate ligands, calculated to be 23.8 % based on the chemical formula determined from the single crystal structure. The subsequent 6% weight loss is consistent with the loss of 4.5 equiv of water (calculated = 5.9%) from decomposition of the

$\text{HPO}_4^{2-}$  and  $\text{H}_2\text{PO}_4^-$  ligands, for which there are 9 protons per formula unit, likely forming pyrophosphate ligands upon loss of water.

Interestingly, the order of addition of the reactants is critical in obtaining a significant yield of **I**. To obtain the highest yield of **I**, the amine, DAP, is added to the phosphoric acid solution, followed by the iron chloride and finally the oxalic acid. By contrast, when DAP is added as the final reactant, a pale green solution is achieved after addition of the  $\text{H}_3\text{PO}_4$ ,  $\text{FeCl}_3 \cdot 6\text{H}_2\text{O}$  and  $\text{H}_2\text{C}_2\text{O}_4$ . Subsequent addition of the amine yields a colorless precipitate resulting in a slurry that does not redissolve after 30 min of stirring at room temperature. After hydrothermal treatment of this slurry, the major product is a black crystalline material. This material was identified as  $\text{Fe}_3(\text{PO}_4)_2(\text{OH})_2$  by powder X-ray diffraction. Reactions performed in the absence of the added amine similarly formed  $\text{Fe}(\text{PO}_4)_2(\text{OH})_2$ .

**Single Crystal Structure.** The crystal structure of **I** was determined by single crystal X-ray diffraction; a summary of the crystallographic data is given in Table 1. Full details of the structure solution are available in the Supporting Information. An ORTEP drawing of the asymmetric unit of **I** is given in Figure 1. The P-O and Fe-O distances are given in Tables 2 and 3. In the structure solution, only the heavy atom positions could be located in the difference maps. While the hydrogen atoms associated with the DAP cation can be reasonably placed in calculated positions, the number of protons associated with the phosphate anions, let alone their positions, cannot be assigned without further analysis of the oxidation state of iron. The assignment of hydrogen phosphate protons can be accounted by consideration of the O-P and O-Fe bonding, as will be described below. Symmetry independent iron atoms Fe2 and Fe3, which amount to 4/5 of the total iron atoms, are ligated

to both oxalate and phosphate anions, whereas Fe1 is only ligated to phosphate. In all cases the phosphate anions are bound in an  $\eta^1$ -fashion to the metal centers, with P1, P2 and P4 each bound to three distinct iron atoms, and P3 bridging only two kinds of iron atoms. The corresponding terminal P-O bonds are the most likely locations of H atoms of the hydrogen- or dihydrogen-phosphate ligands.

**Table 3-1.** Crystal data and structure refinement parameters of **I**.

Empirical formula	[C <sub>6</sub> H <sub>24</sub> N <sub>4</sub> ][C <sub>4</sub> H <sub>9</sub> O <sub>40</sub> P <sub>8</sub> Fe <sub>5</sub> ]
Formula weight	1376
Crystal Dimensions ( <i>mm</i> )	0.10 × 0.08 × 0.05
Crystal Color and Habit	colorless prism
Crystal System	triclinic
Space Group	P - 1
Temperature, K	173
<i>a</i> , Å	9.7851(3)
<i>b</i> , Å	9.8986(3)
<i>c</i> , Å	10.7420(3)
α, °	73.7900(15)
β, °	71.6838(14)
γ, °	79.3001(13)
<i>V</i> , Å <sup>3</sup>	942.99(5)
<i>Z</i>	1
<i>R</i> <sup>a</sup>	0.037
<i>R</i> <sub>w</sub> <sup>b</sup>	0.051
GOF	1.48

a.  $R = \sum ||F_o| - |F_c|| / \sum |F_o|$ . b.  $R_w = \sum (|F_o| - |F_c|)^2 / \sum |F_o|^2$ .

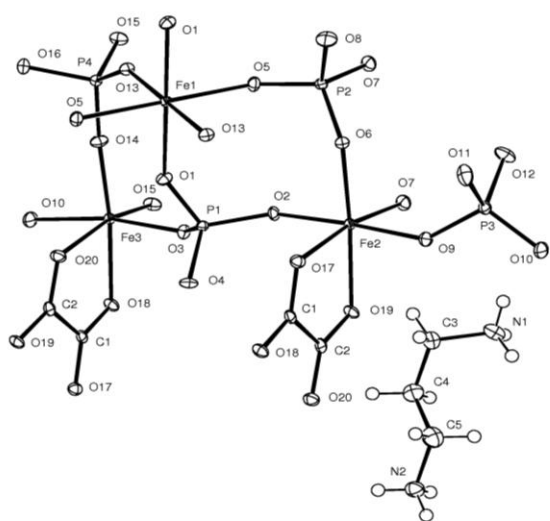


**Figure 3-1.** ORTEP drawing of the asymmetric unit of 1 which describes the atom labeling scheme.

**Table 3-2** P-O bond lengths in **I**.

P	O	Length (Å)	Bound to
P1	O1	1.5219	Fe1
	O2	1.53528	Fe2
	O3	1.53348	Fe3
	O4	1.54377	terminal
P2	O5	1.51975	Fe1
	O6	1.53207	Fe2
	O7	1.50117	Fe2
	O8	1.58369	terminal
P3	O9	1.49645	Fe2
	O10	1.49858	Fe3
	O11	1.56341	terminal
	O12	1.56654	terminal
P4	O13	1.51511	Fe1
	O14	1.50056	Fe3
	O15	1.51395	Fe3
	O16	1.59245	terminal

**Table 3-3.** Fe-O bond lengths of **I**.

Fe	O	Distance	Bound to	Bond Valence Sum
Fe1	O1	1.932	P1	2.99
	O1	1.932	P1	
	O5	2.072	P2	
	O5	2.072	P2	
	O13	2.011	P4	
	O13	2.011	P4	
Fe2	O2	1.929	P1	3.04
	O6	1.997	P2	
	O7	1.922	P2	
	O9	1.972	P3	
	O17	2.097	C	
	O19	2.088	C	
Fe3	O3	1.937	P1	3.07
	O10	1.987	P3	
	O14	1.919	P4	
	O15	1.917	P4	
	O18	2.132	C	
	O20	2.113	C	

In this structure, moieties of  $\text{FeO}_6$ ,  $\text{PO}_4$ , and  $\text{C}_2\text{O}_4$  are assembled into a 3-D anionic framework, which is charge balanced and templated by the DAP alkylammonium cations. A series of views of the crystal packing are given in Figure 2. A distinguishing feature to help visualize this structure is the chains running along the  $\langle -1, -1, 3 \rangle$  direction consisting of iron octahedra (Fe2 and Fe3) for which opposite edges are alternately bridged by either a pair of phosphates (a pair of P2 or a pair of P4) or a single oxalate ligand. These chains are distributed in approximately a square grid, most clearly seen in the projections of Figure 2c and d, and are pair-wise connected along the  $\langle 1, -1, 0 \rangle$  direction by another phosphate bridge (P1 or P3). In three-dimensions the Fe2 and Fe3 octahedra are distributed in a distorted CsCl-type packing with one quarter of the distorted CsCl-type cubes centered by an Fe1 octahedron, one quarter of the distorted cubes are empty, and half are centered by DAP cations. Stacked together, these result in the large cation filled cage shown in Figure 2b.

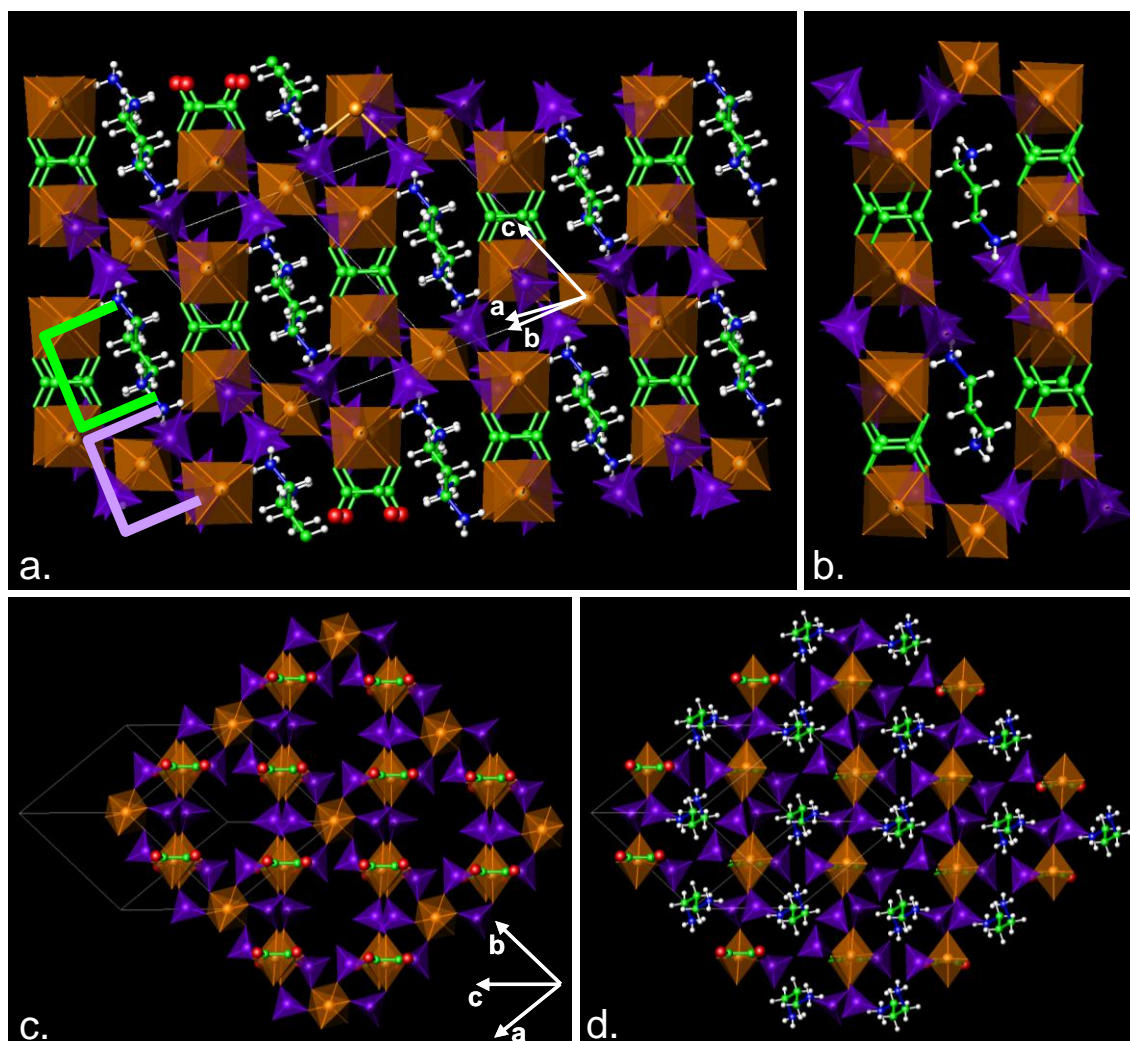


**Figure 3-2.**

(a) Crystal packing view of the structure of 1 oriented to emphasize the phosphate/oxalate chains that run along the  $\langle -1, -1, 3 \rangle$  direction (vertical in figure). Green and purple brackets emphasize the (0,0,2) alternating iron phosphate and iron oxalate layers of the structure. (b) View of the phosphate/oxalate cage templated by two DAP cations. View of the (c) iron phosphate and (d) iron oxalate layers as viewed looking down the  $\langle -1, -1, 3 \rangle$ . The alkylammonium cations reside within the oxalate layers.

Alternatively, it can be useful to view the structure of **I** as being composed of alternating organic and inorganic layers, parallel to the (001), as highlighted with green and purple brackets, respectively in Figure 2a. The organic layers contain the  $C_2O_4^{2-}$  ligands and DAP cations, whereas the inorganic layers exclusively contain iron phosphate. These respective inorganic and organic layers are shown in Figures 2c and d, as projected onto the (-1-13) plane, the direction which is approximately perpendicular to the iron phosphate/oxalate chains described above. Again it can be seen that the Fe1 octahedra and the DAP cations fill comparative sites, the former bridged by phosphates and the latter sitting in an oxalate cage with the ammonium head groups hydrogen bonded to the phosphates above and below the organic layer.

**X-ray Absorption Spectroscopy.** The X-ray absorption spectrum of **I** was collected at the Fe K-edge; and the XANES portion was compared with that of  $FePO_4 \cdot 2H_2O$  (strengite), an Fe(III) standard;  $Fe_3(PO_4)_2 \cdot 8H_2O$ , an Fe(II) standard; and iron foil, an Fe(0) standard. The EXAFS portion of these spectra is discussed in a later section. XANES spectra are given in Figure 3 for **I** and the comparative standards, and the derivative XANES spectra for **I** and strengite are given in Figure 4. The pre-edge peak observed in the spectrum at about 7113 eV has been assigned to the electronic transition from the Fe-1s core orbital to Fe-3d based M-L  $\sigma^*$  antibonding molecular orbital.<sup>19</sup> The more prominent features of the absorption edge at about 7125 and 7128 eV can be assigned to the electronic transition from the Fe-1s core to the Fe4p-O2p  $\sigma^*$  and the P3p-O2p  $\sigma^*$  antibonding molecular orbitals.<sup>5</sup> The energy of these transitions, noted by the inflection points of the pre-edge and edge features

(most easily seen as peaks in the derivative spectra in Fig. 4) is highly sensitive to the oxidation state of Fe; the stronger Fe-O bonding in an Fe(III) environment shifts this transition to higher energy. The XANES spectra show little difference between that of **I** and strengite, both of which exhibit transitions at significantly higher energy than is observed for the Fe(II) and Fe(0) standards. Therefore, it can be reasonably inferred that all Fe atoms in **I** have the same oxidation state of those in strengite, i.e. Fe(III). This is also consistent with the oxidation state assignment based on bond valence sums calculated from the Fe-O distances, Table 3.

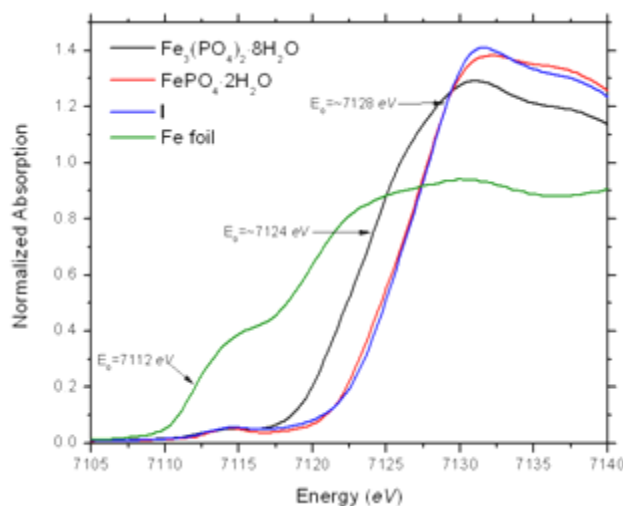


**Figure 3-3.**

Normalized Fe K-edge XANES spectrum of **I** (blue), compared with the spectra of the Fe(III) standard strengite ( $\text{FePO}_4 \cdot 2\text{H}_2\text{O}$ ) (red), the Fe (II) standard  $\text{Fe}_3(\text{PO}_4)_2 \cdot 8\text{H}_2\text{O}$  (black) and iron foil (green).

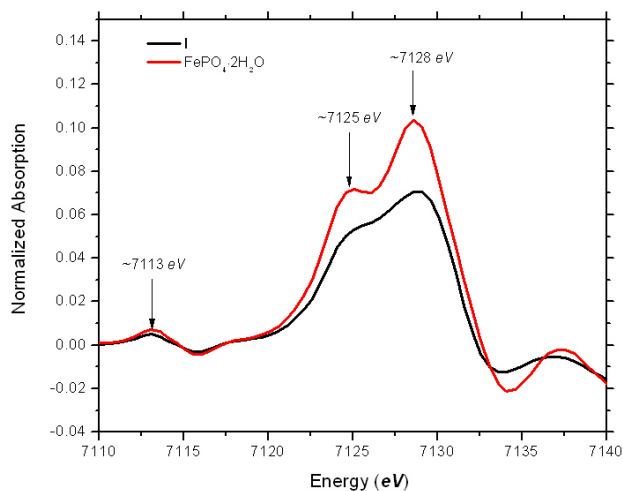


**Figure 3-4.**

First derivative spectra of the Fe K-edge XANES of **I** (black) and strengite ( $\text{FePO}_4 \cdot 2\text{H}_2\text{O}$ ) (red).

## Discussion

**Synthesis of mixed anion materials.** We have successfully prepared a new iron(III) phosphate/oxalate material that, in addition to being a novel inorganic/organic hybrid framework, can serve as a useful model for analysing structural details of possible phosphate/organic matter binding to iron in complex environmental matrices. A search of the Cambridge Crystallographic Database finds a relatively small number of iron(III) mixed phosphate/organic acid materials, with those reported being exclusively with oxalate as the organic acid anion. Furthermore, almost all of the mixed anion compounds reported exhibit a framework structure that is templated by an organic ammonium cation. This in part is likely due to the fact that many organic acids can reduce the Fe(III) to Fe(II). The standard reduction potentials for Fe(III)/Fe(II) exhibit considerable variation depending on the anionic species present. For example, the CRC Handbook of Chemistry and Physics reports the

standard Fe(III)/Fe(II) reduction potential to be 0.77 V in 1f HCl, but 0.44 V in 1f H<sub>3</sub>PO<sub>4</sub>. Given the standard reduction potential of oxalic acid is -0.49 V, it is not surprising that the extent of iron reduction in the presence of an organic acid will be very dependent on synthesis conditions. Because the reduction of Fe(III) by oxalate is known to be photosensitive,<sup>20,21</sup> reactions were carried out in the dark. However, the synthetic variable found to have the greatest impact on the respective formation of the ternary compound **I** vs. the reduction of iron and the resultant formation of Fe<sub>3</sub>(PO<sub>4</sub>)<sub>2</sub>(OH)<sub>2</sub> was the sequential order in which the reactants were added. Reduction occurred when oxalic acid was added to a solution of H<sub>3</sub>PO<sub>4</sub> and FeCl<sub>3</sub>. By contrast, if the amine (DAP) was added to the reaction mixture prior to the addition of the oxalic acid, no iron reduction was observed. These synthetic results suggest that the amine plays a significant role in preventing iron reduction by oxalate.

**PO<sub>4</sub><sup>3-</sup>, HPO<sub>4</sub><sup>2-</sup> or H<sub>2</sub>PO<sub>4</sub><sup>-</sup>.** The Fe K-edge XANES spectra provide strong evidence that all of the iron in **I** exists in the +3 oxidation state. Given the heavy atom structure, discernable from the single crystal X-ray diffraction, for which the empirical formula includes two DAP cations, five iron atoms, two oxalate and eight phosphate ligands, the phosphates must exist as some combination of non-protonated phosphate, hydrogen phosphate and/or dihydrogen phosphate ligands. To achieve charge neutrality a total of nine protons must be distributed among the eight phosphate ligands. An analysis of the P-O and Fe-O bond lengths, listed in Tables 2 and 3, affords a reasonable basis for P-O vs. P-OH assignments. Clearly a terminal P = O double bond should exhibit the shortest distance. Given that H has a slightly greater electronegativity than Fe, the P-O distance is expected to

be lengthened slightly when bridged to an H compared to when it is bridged to Fe. A bridging hydroxyl (P-OH-Fe) would be expected to also exhibit P-O elongation. Such a bridging hydroxyl would also be anticipated to exhibit a longer Fe-O distance than a non-protonated Fe-O-P bridge. Known crystal structures bear out these expected trends.<sup>22,23,24</sup> By way of reference, the structure of  $\text{Fe}(\text{H}_2\text{PO}_4)_3$  demonstrates that the bridging P-O<sub>Fe</sub> distance is 1.48 Å, while P-O<sub>H</sub> distances as long as 1.63 Å are observed,<sup>24</sup> whereas in  $\text{FePO}_4 \cdot 2\text{H}_2\text{O}$  all the P-O bonds are bridged between Fe and P and exhibit distances within the narrow range of 1.52 Å to 1.54 Å.<sup>22</sup>

In **I**, P-O bond lengths are observed to range between 1.50 Å to 1.59 Å. With the exception of the terminal P1-O4 bond, the terminal P-O bonds are significantly longer (>0.06 Å) than the bridging P-O bonds suggesting that the terminal oxygen atoms bound to P2, P3, and P4 each have protons bonded. Such P-O bond distance arguments account for a total of eight protons, one associated with each of the two P2 and P4 phosphates (hydrogen phosphate), and two associated with each of the two P3 phosphates (dihydrogen phosphate). Assignment of the 9<sup>th</sup> proton is less clear. While the terminal P1-O4 is the longest bond to P1, it is only 0.008 Å longer than the next longest bridging contact. Furthermore, O4 forms the closest contact to the alkylammonium cation. Thus hydrogen bonding to the ammonium template rather than being a hydrogen phosphate is the likely cause for the slight lengthening of the P1-O4 bond. Phosphate P1 therefore is assigned as a non-protonated  $\text{PO}_4^{3-}$  ligand. Consideration of the Fe-O bonding finds that Fe1-O5 bonds (2.07 Å) are the longest Fe-O<sub>p</sub> bonds by more than 0.07 Å. Their neighbor Fe2-O6 is the next longest at 2.00 Å. Both O5 and O6 are bound to P2. It therefore is proposed that the ninth proton is associated with the

P2 phosphate ligand. However, since each of the phosphate ligands exist as symmetry equivalent pairs because of a crystallographic inversion center, we suggest that P2 represents a mixed hydrogen phosphate/dihydrogen phosphate ligand. Overall then, these account for the empirical molecular formula of **I** to be  $[\text{C}_3\text{N}_2\text{H}_{12}]_2[\text{Fe}_5(\text{C}_2\text{O}_4)_2(\text{H}_2\text{PO}_4)_2(\text{H}_{1.5}\text{PO}_4)_2(\text{HPO}_4)_2(\text{PO}_4)_2]$ .

### **Differentiation of Phosphate vs. Organic Matter Binding by EXAFS.**

Examination of the structure of **I** as well as the structures of other Fe(III) materials with phosphate or organic acid (primarily oxalate or acetate) ligation demonstrates that while the metal-oxygen distances of these two ligand systems are reasonably similar ( $\sim 2.0 \pm 0.1 \text{ \AA}$ ), the second nearest neighbour distances between the iron and the phosphorous or carbon differ considerably ( $\text{Fe--P} \approx 3.3 \pm 0.1 \text{ \AA}$  and  $\text{Fe--C} \approx 2.9 \pm 0.1 \text{ \AA}$ ). This difference should be well resolvable by EXAFS, a technique that is also amenable to characterization of complex environmental systems. The Fourier-transform magnitude of the  $k^3$ -weighted, Fe K-edge EXAFS spectrum of **I** along with the spectra of strengite ( $\text{FePO}_4 \cdot 2\text{H}_2\text{O}$ ) and  $\text{Fe}_2(\text{C}_2\text{O}_4)_3 \cdot 6\text{H}_2\text{O}$ , and a fitting model based on the crystal structure of **I** are presented in Figure 5. Using the crystal structure of **I**, the contributions of signals from single- and multiple-scattering paths used to fit the spectrum can be evaluated as shown in Figure 6 with fitting parameters given in Table 4. The spectra of the strengite and iron oxalate controls (Figure 5a and c) clearly show the distinction between the phosphorous and carbon second nearest neighbors with a respective peak or lack of a peak in the R-space EXAFS spectrum corresponding to the respective Fe--C and Fe--P distances. In the R-space EXAFS spectrum of **I**, evidence of iron coordination to both oxalate and the phosphate is clearly present with

the Fe--C and Fe-P signals between 2.2 and 3.0 Å (phase shift uncorrected), as shown in Figure 6. Clearly, the structural characteristics of **I** are well reflected in its EXAFS spectrum which thus provides an important fingerprint to differentiate phosphate from organic matter binding in complex natural systems.

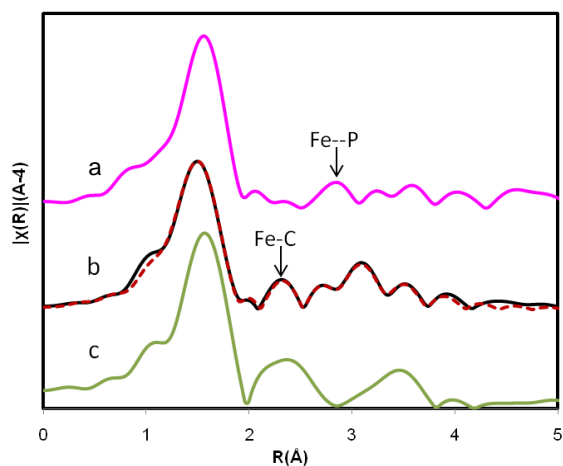


**Figure 3-5.**

Fourier-transform magnitude of the Fe EXAFS spectrum of (a) strengite ( $\text{FePO}_4 \cdot 2\text{H}_2\text{O}$ ), (b) **I** and (c)  $\text{Fe}_2(\text{C}_2\text{O}_4)_3 \cdot 6\text{H}_2\text{O}$ . For (b) the solid line represents the experimental data, and the dotted line represents the calculated best fit using the single crystal structure as a model. Arrows highlight the Fe--P and Fe--C second nearest neighbor peaks in strengite and  $\text{Fe}_2(\text{C}_2\text{O}_4)_3 \cdot 6\text{H}_2\text{O}$ , respectively. (Distances are not corrected for phase shift.)

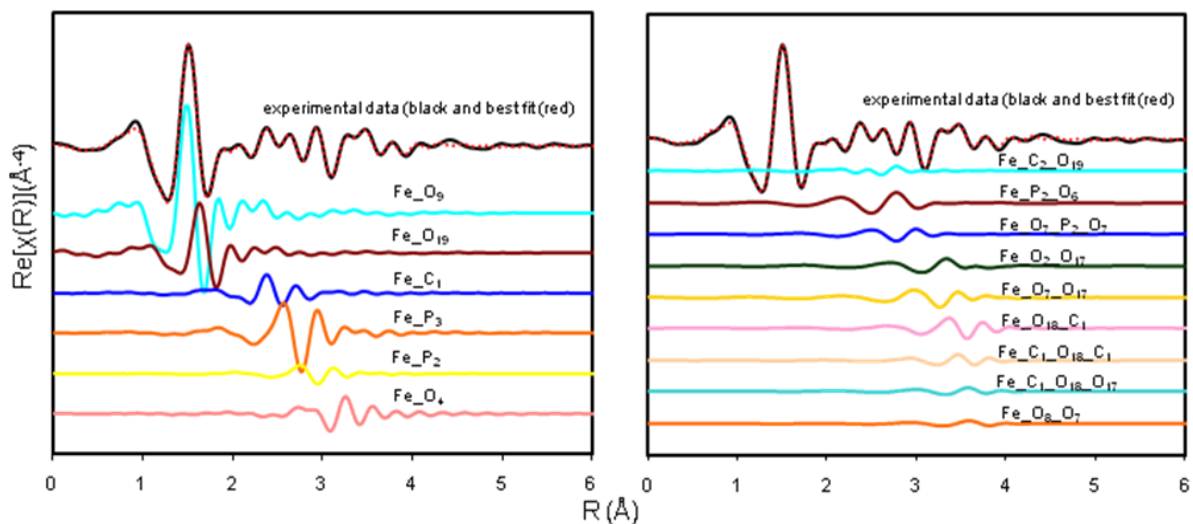


**Figure 3-6.**

Fourier transform of the real part of the  $k^3$ -weighted Fe EXAFS spectrum of **I** (black) along with the best fit (red). The contributions of the signals from single-scattering paths (left) and multiple-scattering paths (right) calculated from the crystal structure of **I** (plotted in the lower portion of the figure with a different color assigned to each path) demonstrate the differential contribution of the iron to oxygen, phosphorus and carbon neighbors. (Distances are not corrected for phase shift.)

**Table 3-4.** Fitting results of **I**, including coordination number (CN, fixed), interatomic distance (R), and Debye-Waller Factors ( $S^2$ ). Amplitude reduction factor ( $So^2$ ) and  $delE^\circ$  apply to all paths.  $So^2$  is fixed at 0.84.

Path	CN	R		$\delta^2$	
Fe-O <sub>p</sub> *	4.67	1.9572	(0.0007)	0.005	(0.001)
Fe-O <sub>c</sub> *	1.33	2.0926	(0.0007)	0.003	(0.001)
Fe-C	2	2.858	(0.005)	0.002	(0.001)
Fe-C-O	4	3.066	(0.002)	0.004	(0.009)
Fe-P	3	3.211	(0.001)	0.004	(0.001)
Fe-P-O	8	3.439	(0.005)	0.01	(0.005)
Fe-P	1	3.375	(0.002)	0.004	(0.002)
Fe-O-P-O	1	3.56	(0.02)	0.010	(0.003)
Fe-O	2	3.661	(0.002)	0.001	(0.002)
Fe-O-O	6	3.956	(0.002)	0.002	(0.009)
Fe-O + Fe-O	6	3.961	(0.002)	0.002	(0.009)
Fe-O-C	4	4.053	(0.002)	0.006	(0.006)
Fe-C-O-C	2	4.061	(0.002)	0.006	(0.006)
Fe-C-O-O	4	4.177	(0.002)	0.006	(0.006)
Fe-O-O	4	4.286	(0.002)	0.013	(0.010)
$delE^\circ$		-0.72 (0.09)			
$So^2$		0.84 (fixed)			

\* subscripts denote O atoms from  $PO_4^{3-}$  or  $C_2O_4^{2-}$  group, respectively.

## Conclusions

A new iron phosphate/oxalate material has been prepared and characterized such that it provides a useful molecular level model to advance understanding of phosphate binding in complex environmental systems. The reaction conditions necessary to form this mixed anion species demonstrate the significant role that the ligands and reaction medium have on controlling the redox state of the iron. Specifically in this system it is demonstrated that the alkylamine can prevent the organic acid from reducing the metal center and serve as a structure directing template. Structurally, this new iron oxalate phosphate [DAP]<sub>2</sub>[Fe<sub>5</sub>(C<sub>2</sub>O<sub>4</sub>)<sub>2</sub>(H<sub>2</sub>PO<sub>4</sub>)<sub>2</sub>(H<sub>1.5</sub>PO<sub>4</sub>)<sub>2</sub>(HPO<sub>4</sub>)<sub>2</sub>(PO<sub>4</sub>)<sub>2</sub>], **I**, can conveniently be viewed as a hybrid structure of an alkylammonium templated organic layer, representative of carboxylic acid structural network in natural OM, and an iron phosphate inorganic layer representative of a mineral phosphate. Atomic structural parameters determined for **I**, as well as those from other ferric iron oxalato-phosphate species,<sup>11-16</sup> indicate measurable difference between Fe--P and Fe--C second coordination shell distances. Characterization of **I** by both single crystal X-ray diffraction and X-ray absorption spectroscopy, we clearly demonstrate that EXAFS effectively can differentiate these. While real environmental systems are anticipated to be significantly more complex than this pure material, if ferric iron in a natural system is bound to both carboxyl groups from organic matter and phosphate, it should exhibit both Fe--C and Fe--P second neighbour contacts in the Fe R-space EXAFS spectrum.

## Experimental Section

**Synthesis and General Characterization.**  $[\text{DAP}]_2[\text{Fe}_5(\text{C}_2\text{O}_4)_2(\text{H}_x\text{PO}_4)_8]$ , **I**, was prepared using hydrothermal techniques starting from 1,3-diaminopropane (DAP),  $\text{FeCl}_3 \cdot 6\text{H}_2\text{O}$ ,  $\text{H}_2\text{C}_2\text{O}_4$  and 85% (weight percent) ortho phosphoric acid. Starting materials were used as purchased from Sigma-Aldrich without further purification. To avoid photo-reduction of Fe(III) by oxalate, the reaction was conducted in a dark room, with only a red-filtered light. In a typical synthesis 3.55 g of 85%  $\text{H}_3\text{PO}_4$  (30 mmol) was diluted with 18 mL of deionized water, followed by the rapid addition of 0.763 g of 97 % DAP (10 mmol). Addition of 1.35 g (5 mmol) of  $\text{FeCl}_3 \cdot 6\text{H}_2\text{O}$  results in an amber colored solution which then turns to a pale green color upon addition of 0.630 g (5 mmol) of  $\text{H}_2\text{C}_2\text{O}_4 \cdot 2\text{H}_2\text{O}$ . The overall mole ratio of the reactants was 1:1:6:2:200 ( $\text{FeCl}_3 \cdot 6\text{H}_2\text{O}:\text{H}_2\text{C}_2\text{O}_4 \cdot 2\text{H}_2\text{O}:\text{H}_3\text{PO}_4:\text{DAP}:\text{H}_2\text{O}$ ). The mixture was stirred for approximately 30 minutes, then transferred to a Parr acid digestion bomb, which was placed in an oven at 150°C for 120 hours. Upon cooling, crystalline solid products were isolated by filtration following and characterized by X-ray diffraction and, by thermogravimetric analysis.

Powder X-ray diffraction measurements were performed on samples loaded into 0.5 mm Pyrex capillaries affixed to a rotating goniometer on an INEL diffractometer using monochromatic Co radiation ( $K_{\alpha 1} = 1.7890\text{\AA}$ ) with a CPS-120 detector.

Thermogravimetric analysis (TGA) of **I** was carried out using a TA Instruments 2950 Thermogravimetric Analyzer in the temperature range of 22-800 °C under a nitrogen atmosphere.

**Single Crystal Structure.** A single crystal of  $[\text{DAP}]_2[\text{Fe}_5(\text{C}_2\text{O}_4)_2(\text{H}_x\text{PO}_4)_8]$ , **I**, was mounted on a nylon loop with a small amount of NVH immersion oil and affixed to a goniometer on a Bruker-Nonius X8 Apex2 diffractometer at a temperature of 173 K. Unit cell dimensions were determined from a symmetry constrained fit of 9933 reflections with  $5.12^\circ < 2\theta < 57.62^\circ$ . Reflections were collected from the entire Ewald sphere with 5002 unique reflections measured with a mixture of  $\phi$  and  $\omega$  scans collected up to  $57.98^\circ$  ( $2\theta$ ). The frame integration was performed using SAINT.<sup>25</sup> The resulting raw data were scaled and absorption corrected using a multi-scan averaging of symmetry equivalent data using SADABS.<sup>26</sup> The structure was solved by direct methods using the XS program.<sup>27</sup> All non-hydrogen atoms were obtained from the initial E-map. The hydrogen atoms for the 1,3-diammonium n-propyl cation were introduced at idealized positions and were allowed to ride on the parent atom. Attempts to find chemically reasonable atomic positions for hydrogen atoms bonded to the  $\text{PO}_4$  anions were unsuccessful and were therefore omitted from the final model. The structural model was fit to the data using full matrix least-squares based on F of 4456 unique reflections [ $I > 1.0\sigma(I)$ ]. The calculated structure factors included corrections for anomalous dispersion from the usual tabulation. The structure was refined using the LSTSQ program from NRCVAX.<sup>28</sup> The final R factors obtained were  $R_f = 0.037$  and  $R_w = 0.051$ .

**XAS.** X-ray absorption spectra were collected for standards and compound **I** on Beamline X-11B at the National Synchrotron Light Source (NSLS), Brookhaven National Laboratory. Iron foil, strengite ( $\text{FePO}_4 \cdot 2\text{H}_2\text{O}$ ), and vivianite ( $\text{Fe}_3(\text{PO}_4)_2 \cdot 8\text{H}_2\text{O}$ ) standards were purchased from a chemical supply company or synthesized according to literature procedures.<sup>29</sup> In a typical experiment, about 8 mg of sample was ground into fine powder and

mixed with about 90 mg of boron nitride (BN), then pressed into a 1.3 cm diameter plexiglass sample holder well of 1 mm depth. The storage ring was operating at a maximum current of 300 mA. Spectra were recorded in transmission mode using a channel-cut Si(111)-monochromator, which was detuned >30% to reject higher harmonics. The spectra were scanned in the range of 200 eV below to a wavevector ( $k$ ) of  $14 \text{ \AA}^{-1}$  above the Fe K-edge at 7112 eV. All XANES spectra were normalized such that the edge step is 1.<sup>30</sup> Iron K-edge EXAFS data were processed using IFEFFIT package.<sup>31</sup> Data were  $k^2$ -weighted after being normalized for background removal in a  $k$  range of 0-13  $\text{\AA}^{-1}$ . Interatomic distances from a representative Fe atom (Fe2 was selected, being bound to both phosphate and oxalate) were calculated from crystallographic data of **I** using the ATOMS program inside IFEFFIT package. Backscattering paths and phase corrections were calculated by the FEFF6 program. EXAFS data were Fourier transformed across a  $k$  range of 3.0-12.5  $\text{\AA}^{-1}$  for R-space fitting between 1.0 and 4.0  $\text{\AA}$ , which was conducted in the Artemis program. When fitting the data in Artemis,  $k=1$ ,  $k=2$ , and  $k=3$  were chosen to optimize the fits over all three weighting factors.<sup>30</sup> When constructing the model, all paths with computed amplitude <20% were discarded because these paths were not needed to fit spectral features across the chosen  $k$ -space and R-space fitting ranges. To simplify the model, paths that are composed of same atoms; and whose difference of  $R_{\text{eff}}$  (from FEFF 6 calculation based on the crystal structure) is within 0.1  $\text{\AA}$ , are grouped together. Normally, for each group of paths, the path whose  $R_{\text{eff}}$  is the closest to the  $R_{\text{eff}}$  average is included in the structure model to represent other paths. If all paths in that group have the same difference to the  $R_{\text{eff}}$  average, then the path with higher amplitude is chosen. For each chosen path, the parameter coordination number (CN) is fixed

as the combination of the degeneracy of all paths in that group, except for the Fe-O paths in the first coordination shell, due to its most dominant contribution to the overall EXAFS spectrum. In the structure of **I**, 2/3 Fe has both PO<sub>4</sub> and C<sub>2</sub>O<sub>4</sub> coordinated, while 1/3 of Fe is only ligated to PO<sub>4</sub> such that out of the total of eighteen Fe-O bonds to the three Fe metal centers, there are 4 Fe-O<sub>C</sub> bonds, and 14 Fe-O<sub>P</sub> bonds. Thus the CN for Fe-O<sub>P</sub> path is fixed as 4.67, while it is 1.33 for the Fe-O<sub>C</sub> path. An amplitude reduction factor ( $S_0^2$ ) of 0.84 was determined from EXAFS analysis of scorodite (FeAsO<sub>4</sub>·2H<sub>2</sub>O) and was fixed in the theoretical model. When fitting the parameter “delR”, an isotropic structural expansion factor “alpha” was introduced to all paths to allow a proportional (percentage) change in “delR” relative to “Reff” values that were calculated by FEFF6 program.

#### **ACKNOWLEDGMENT**

This work was supported by the USDA-CSREES NRI Grant No. 2005-35107-16253 and NSF Grant No. DMR-0705190 Beamline X-11B (National Synchrotron Light Source—Brookhaven National Laboratory) is supported by DOE’s Divisions of Materials Science and Chemical Sciences.

#### **Supporting Information Available.**

Single crystal crystallographic information for [DAP]<sub>2</sub>[Fe<sub>5</sub>(C<sub>2</sub>O<sub>4</sub>)<sub>2</sub>(H<sub>x</sub>PO<sub>4</sub>)<sub>8</sub>], **I**, is available in .cif format. A figure of the TGA analysis of **I** is also provided in a supplemental figure. This material is available free of charge via the Internet at <http://pubs.acs.org>.

## REFERENCES

- (1) Brown, G. E.; Sturchio, N. C. *Applications of Synchrotron Radiation in Low-Temperature Geochemistry and Environmental Sciences* **2002**, *49*, 1.
- (2) Banerjee, S. K.; Sengupta, M.; Gupta, S. K. *Journal of the Indian Chemical Society* **1980**, *57*, 188.
- (3) Skoog, A.; Arias-Esquivel, V. A. *Geochimica Et Cosmochimica Acta* **2008**, *72*, A874.
- (4) Violante, A.; Pigna, M. *Soil Science Society of America Journal* **2002**, *66*, 1788.
- (5) Khare, N.; Martin, J. D.; Hesterberg, D. *Geochimica Et Cosmochimica Acta* **2007**, *71*, 4405.
- (6) Bloom, P. R. *Soil Science Society of America Journal* **1981**, *45*, 267.
- (7) Gerke, J. *Geoderma* **1993**, *59*, 279.
- (8) Choudhury, A.; Natarajan, S.; Rao, C. N. R. *Chemistry of Materials* **1999**, *11*, 2316.
- (9) Lin, H. M.; Lii, K. H.; Jiang, Y. C.; Wang, S. L. *Chemistry of Materials* **1999**, *11*, 519.
- (10) Jiang, Y. C.; Wang, S. L.; Lii, K. H.; Nguyen, N.; Ducouret, A. *Chemistry of Materials* **2003**, *15*, 1633.
- (11) Choudhury, A.; Natarajan, S.; Rao, C. N. R. *Chemistry-a European Journal* **2000**, *6*, 1168.
- (12) Beauchemin, S.; Hesterberg, D.; Chou, J.; Beauchemin, M.; Simard, R. R.; Sayers, D. E. *Journal of Environmental Quality* **2003**, *32*, 1809.
- (13) Seiter, J. M.; Staats-Borda, K. E.; Ginder-Vogel, M.; Sparks, D. L. *Journal of Environmental Quality* **2008**, *37*, 477.

- (14) Khare, N.; Hesterberg, D.; Beauchemin, S.; Wang, S. L. *Soil Science Society of America Journal* **2004**, *68*, 460.
- (15) Khare, N.; Hesterberg, D.; Martin, J. D. *Environmental Science & Technology* **2005**, *39*, 2152.
- (16) Vilge-Ritter, A.; Rose, J.; Masion, A.; Bottero, J. Y.; Laine, J. M. *Colloids and Surfaces a-Physicochemical and Engineering Aspects* **1999**, *147*, 297.
- (17) van Schaik, J. W. J.; Persson, I.; Kleja, D. B.; Gustafsson, J. P. *Environmental Science & Technology* **2008**, *42*, 2367.
- (18) Karlsson, T.; Persson, P.; Skyllberg, U.; Morth, C. M.; Giesler, R. *Environmental Science & Technology* **2008**, *42*, 5449.
- (19) Grunes, L. A. *Physical Review B* **1983**, *27*, 2111.
- (20) Siffert, C.; Sulzberger, B. *Langmuir* **1991**, *7*, 1627.
- (21) Goldberg, M. C.; Cunningham, K. M.; Weiner, E. R. *Journal of Photochemistry and Photobiology a-Chemistry* **1993**, *73*, 105.
- (22) Taxer, K.; Bard, H. *Crystal Research and Technology* **2004**, *39*, 1080.
- (23) Baies, R.; Pralong, V.; Caignaert, V.; Raveau, B. *Materials Research Bulletin* **2006**, *41*, 1170.
- (24) Vencato, I.; Mascarenhas, Y. P.; Mattievich, E. *American Mineralogist* **1986**, *71*, 222.
- (25) Bruker-Nonius In *version 7.34A*; Bruker-Nonius: Madison, WI 53711, USA, 2006.
- (26) Bruker-Nonius In *version 2.10*; Bruker-Nonius: Madison, WI 53711, USA, 2004.
- (27) Bruker-AXS In *version 6.12*; Bruker-AXS: Madsion, WI 53711, USA.

- (28) Gabe, E. J.; Lepage, Y.; Charland, J. P.; Lee, F. L.; White, P. S. *Journal of Applied Crystallography* **1989**, 22, 384.
- (29) Hesterberg, D.; Zhou, W. Q.; Hutchison, K. J.; Beauchemin, S.; Sayers, D. E.; Munksgaard Int Publ Ltd: 1999; Vol. 6, p 636.
- (30) Kelly, S.; Hesterberg, D.; Ravel, B. *Methods of Soil Analysis*; Soil Science Society of America: Madison, WI, 2008.
- (31) Newville, M. *Journal of Synchrotron Radiation* **2001**, 8, 322.

**Chapter 4: Phosphate sorption to organic  
matter/ferrhydrite mixtures as affected by aging time**

## Abstract

It has been hypothesized that Fe from an oxide mineral migrates to organic matter (OM) forming new Fe-OM complexes as the Fe-oxide ages with OM. These new Fe-OM complexes are believed to provide new sorption sites for phosphate ( $\text{PO}_4$ ) via the formation of  $\text{PO}_4$ -Fe-OM ternary complexes. However, direct evidence for such OM/Fe-oxide interaction is lacking. In order to determine whether OM complexes Fe from an Fe-oxide and evaluate the impact on  $\text{PO}_4$  sorption, mixtures (pH 6.8) of ferrihydrite (FH) and Pahokee peat or Pahokee peat humic acid (HA) aged for 55 days during which  $\text{PO}_4$  sorption capacities of these mixtures were monitored. After aging for 55 days all OM/FH mixtures exhibited 20% to 50% decrease in  $\text{PO}_4$  sorption capacity.  $\text{PO}_4$  sorption to any peat/ $\text{FeCl}_3$ /FH mixtures is always higher than to a peat/FH mixture when all the systems were controlled for constant total Fe and peat but differed in the ratio of  $\text{FeCl}_3$  and ferrihydrite. Extended X-ray absorption fine structure (EXAFS) analyses on selected aged peat/ferrihydrite samples showed no evidence of Fe(III)-peat complexation. The decreased  $\text{PO}_4$  sorption to ferrihydrite as the OM/FH mixtures aged was attributed to ferrihydrite crystallization, competition of phosphate and organic matter, and Fe dissolution by dissolved organic carbon.

## 4.1. Introduction

Soil organic matter and oxide minerals are both important components regarding nutrient retention and phyto-availability.<sup>1</sup> Organic matter possesses high affinity for Fe or Al-oxide surface.<sup>2,3</sup> The sorptive interaction between OM to mineral surface first takes place through a rapid step during which OM binds to mineral surface.<sup>4,5</sup> Spectroscopic data suggest that OM binds to mineral surface via ligand exchange between the carboxyl and phenol-OH groups from OM and  $H^+$  or  $OH^-$  from the mineral.<sup>6,7</sup> Organic matter sorption to oxide minerals effectively decreases the mineral's small pores and surface area.<sup>7,8</sup> Fe or Al-oxides are also major sinks for soil phosphate ( $PO_4$ ).<sup>9-11</sup> Thus, the competition between OM and  $PO_4$  for sorption sites on mineral surface is considered the primary mechanism for the inhibited sorption of  $PO_4$  to minerals.<sup>12-17</sup>

Following the initial rapid sorption of OM to mineral surface is a much slower, diffusion-controlled process during which OM penetrates the meso or even micro-pores inside the mineral.<sup>4</sup> This process might take days or even longer, e.g. months. During this slow process, the influence of OM on  $PO_4$  sorption appears to be different from the initial inhibitory effect. According to Borggaard et al.,<sup>18</sup> when  $PO_4$  was first mixed with humic acid (HA) and a Al- or Fe-oxide, less  $PO_4$  was sorbed to the oxide/HA mixture than to the control system (no HA). As the mixture of  $PO_4$ /oxide/HA equilibrated for a longer time (up to 28 days), eventually the amount of  $PO_4$  adsorbed to the oxide/HA mixture is the same as to the mineral itself. While the increase of  $PO_4$  sorption in a  $PO_4$ /oxide/HA mixture might be a kinetic issue of the  $PO_4$  sorption process, a 15% increase of  $PO_4$  sorption capacity was observed in aged (56 days) Fe-oxide/humic mixtures compared to fresh mixtures.<sup>19</sup> The

interaction between humic substances and the Fe-oxide during aging might have rendered an enhancing effect on PO<sub>4</sub> sorption to the oxide/HA system.

It has been found that Al- or Fe-OM complexes provide sorption sites for PO<sub>4</sub> in organic matter, presumably via the formation of PO<sub>4</sub>-Al/Fe-OM ternary complexes.<sup>20-23</sup> The increased PO<sub>4</sub> sorption in the aged Fe-oxide/HA mixtures described above was parallel with increased pyrophosphate extractable Fe from the mixtures,<sup>19</sup> which indicates an increase of humic complexed Fe in the system. Therefore, it has been proposed that iron atoms from the bulk oxide migrate to organic matter forming new Fe-OM complexes during aging. These new Fe-OM complexes are believed to provide new sorption sites for PO<sub>4</sub> via the formation of PO<sub>4</sub>-Fe-OM ternary complexes.

Although existing research results support the metal migration and ternary complexation model, a detailed understanding of such mechanism has yet to be achieved. During the long, slow process of organic matter sorption to an oxide mineral, the impact imparted from such a process on mineral structure remains unclear; and direct evidence for the formation of new Al- or Fe-OM complexes is still lacking. In this regard, probing the change of metal coordination structure in an oxide mineral as it ages with organic matter is a key factor to elucidating any impact that aging of an oxide/OM mixture would have on PO<sub>4</sub> sorption.

The technique of EXAFS (extended X-ray absorption fine structure) spectroscopy is an element specific tool to probe the coordination structure of the element of interest, even in complex environmental matrices. It has been applied to determine the coordination structure of Fe in organic matter or soils,<sup>24-26</sup> in oxide minerals,<sup>27,28</sup> in phosphate/oxalate mixed anion

material.<sup>29</sup> EXAFS analyses has showed that the spectral signals from Fe-C coordination can be isolated from those from longer Fe-Fe or Fe-P bonding.<sup>30,31</sup> Thus, if organic matter is able to complex Fe from the bulk mineral forming new Fe-C bonds, these new Fe-C bonds will be revealed by corresponding spectral features in the EXAFS spectrum.

Applying the technique of EXAFS and other analytical methods, the study presented here attempts to elucidate how aging of Fe-oxide/OM mixtures impacts the structure of Fe-oxide and PO<sub>4</sub> sorption. The specific objectives were: (1) determine any change of PO<sub>4</sub> sorption capacity of ferrihydrite as it ages with organic matter; (2) determine if Fe(III) from ferrihydrite is complexed by organic matter and, if so, how the Fe-OM complexation contributes to the change in the systems' PO<sub>4</sub> sorption capacity. The findings of this study add to the very much needed understanding of the longitudinal influence of organic matter on phosphate sorption to oxide minerals.

## 4.2. Materials and Methods

### *Organic matter preparation and ferrihydrite synthesis*

Pahokee peat and Pahokee peat humic acid (HA) were purchased from International Humic Substance Society (IHSS). Both peat and humic acid were hydrated before usage. In a typical peat hydration process, ~100 mL of deionized water was mixed with ~5g peat. The mixture was shaken for 1 hour. KOH (1 M) was then added to the peat suspension to raise the pH to 11 and the suspension was again shaken for 1. The suspension was adjusted to pH 7.5 using HCl (1 M) and shaken for additional 4 to 5 days during which time the pH was adjusted twice per day. The peat suspension was adjusted to pH 2.5 and the solid peat was separated from supernatant by centrifugation (10000 rpm, 15 min). The solid peat was washed with 0.1 M HCl three times, then 0.05 M KCl three times. A final peat stock suspension was prepared by mixing the solid peat with ~200 mL 0.05 M KCl; its pH was adjusted to 2.5 with 0.05 M HCl. The dry mass of peat suspension was determined by drying triplicate samples (~1 g) at 70°C overnight. To hydrate peat humic acid, solid HA (~0.5 g) was first mixed with ~20 mL of 0.05 M KCl and the mixture was shaken for 30 min. The pH was then raised to 11 with 0.05 M KOH and the mixture was shaken for 1 hour. HCl (0.05 M) was then added to the mixture to reduce the pH to 7.5. To insure homogeneity, the HA suspension was shaken for 1 hour and pH adjusted to 7.5 prior to measurement of dissolved organic carbon (DOC) concentration.

Ferrihydrite (FH) was synthesized as described in Murray and Hesterberg,<sup>32</sup> with pH of the stock suspension adjusted to 6.8. The dry mass of FH stock suspension was determined by drying triplicate samples (~1 g) at 110°C overnight. For XRD analysis, a subsample (~10

g) was washed with deionized water for three times and freeze dried. The powder diffraction pattern confirmed that the synthesized material was 2-line ferrihydrite. To avoid crystallization, FH stock suspensions were always used within two weeks of synthesis.

### ***Preparation of peat/FH and HA/FH mixtures***

A total of six OM/FH mixtures containing ferrihydrite (1 g) and various amounts of peat or HA were prepared for the aging experiments. Our past experiment found that ferrihydrite possesses a HA sorption capacity of 400 mg HA g<sup>-1</sup> FH. Hence HA to FH input was chosen to be 80 and 160 mg g<sup>-1</sup> FH. Peat input ranges from 1 to 16 g g<sup>-1</sup> FH in peat/FH systems. In a typical preparation, an aliquot of peat suspension or HA solution for desired amount of OM was weighed into a 1-L HDPE bottle along with ~300 mL of 0.05 M KCl solution and the pH was adjusted to ~5 with 0.05 M KOH or HCl. An aliquot of FH suspension (equivalent to 1 g dry mass) was then added to the organic matter and the mixture pH was adjusted to 6.8. KCl (0.05 M) was then added to the suspension to yield a total mass of 1 kg. These OM/FH suspensions were aged with shaking at the speed of 0.5 s<sup>-1</sup> in a water-bath shaker at 25°C.

### ***PO<sub>4</sub> sorption to peat/FH and HA/FH mixtures***

At various time points throughout the aging process, three samples of 30 g suspension each were removed from the entire mixture and placed in 30-mL HDPE centrifuge tubes for 1-point PO<sub>4</sub> sorption measurement. In a typical experiment, 1.32 mL of 0.05 M KH<sub>2</sub>PO<sub>4</sub> solution was added to an OM/FH sample so that P to Fe loading was equal to 235 mmol P/mole Fe. The samples equilibrated for 42 hours, during which pH was adjusted to 6.8 three

times. The reported  $\text{PO}_4$  sorption data of the OM/FH mixtures are averages of triplicate measurements.

### ***$\text{PO}_4$ sorption to peat/ $\text{FeCl}_3$ /FH mixtures***

In order to evaluate the influence of Fe-peat complexation on  $\text{PO}_4$  sorption,  $\text{PO}_4$  sorption isotherm experiments were conducted to a total of nine peat/ $\text{FeCl}_3$ /FH mixtures (no aging). These mixtures were controlled for constant total Fe and peat, which are equal to those in the system of 1 g peat  $\text{g}^{-1}$  FH. In these systems 0 to 50% of total Fe was added as  $\text{FeCl}_3$ ; the rest of Fe was added as ferrihydrite. For each system, eight peat/ $\text{FeCl}_3$ /FH samples were prepared for  $\text{PO}_4$  adsorption experiment. In a typical 8-point sorption isotherm experiment, designated amount of  $\text{FeCl}_3$  solution (0.0167 M) was added to each of the eight peat suspensions that each contains 0.03 g peat. The peat/ $\text{FeCl}_3$  mixtures were adjusted to pH 5 slowly and shaken for 1 hour. Eight aliquots of FH suspension that each yields a designated amount of FH dry mass were added to the peat/ $\text{FeCl}_3$  mixtures. The mixtures were then shaken for 1 hour. Solution of  $\text{KH}_2\text{PO}_4$  (0.05 M) was added to each sample so that P inputs were equal to 0~225 mmol P  $\text{mole}^{-1}$  Fe. All mixtures were adjusted to pH 6.8, and the mass was brought to 25 g with 0.05 M KCl. At 24 and 42 hours after  $\text{PO}_4$  addition, pH was adjusted to 6.8 again and mass was brought to 29 and 30g, respectively. The solid materials in each sample were separated from supernatant by centrifugation. The supernatants were collected for total P concentration measurements. The amount of adsorbed P in each sample was taken as the difference between added P and P remaining in solution. For each system adsorbed and dissolved P data were fitted with a Langmuir model and the calculated sorption maximum from the fitting model is reported in this chapter.

### ***Preparation for peat/FH systems for EXAFS data collection***

To evaluate if Fe-peat complexation takes place as FH ages with peat, separate peat/FH systems that have aged for 1, 7, or 55 days were prepared for EXAFS data collection. Based on our base titration data, Pahokee peat has acidity of 2400 mmol kg<sup>-1</sup> at pH 7. To insure enough complexation sites in peat for Fe, total Fe (from FH) to peat inputs were chosen to be 300, 600, and 1200 mmol Fe kg<sup>-1</sup>. In a typical preparation, an aliquot of peat suspension (equivalent to 0.288 g dry mass) was placed in a 250-mL HDPE and the pH was raised to ~5 with KOH (0.05 M). Designated amount of FH suspension was then added to peat suspension and the suspension pH adjusted to 6.8. In the following two days pH was adjusted twice a day and the final mass was brought to 240 g with 0.05 M KCl. No more pH adjustment was done during the aging process. The peat/FH suspension was placed in a water-bath shaker for aging at 25°C.

### ***Preparation for peat/FeCl<sub>3</sub>/FH mixtures for EXAFS data collection***

To illustrate the spectral difference of Fe due to difference coordination environment in Fe(III)-peat complexes and ferrihydrite, EXAFS data were also collected for three peat/FeCl<sub>3</sub>/FH systems. These systems were controlled for constant total Fe and peat which are equal to those in the system of 1200 mmol Fe kg<sup>-1</sup> peat. Zero to 100% of total Fe was added as FeCl<sub>3</sub>; the rest of Fe was added as ferrihydrite. In a typical preparation, an aliquot of peat suspension (equivalent to 0.288 g dry mass) was placed in a 250-mL HDPE and designated amount of FeCl<sub>3</sub> solution (0.0167 M) was added to the peat suspension. The mixture was shaken for one hour then the pH adjusted to ~5. Designated amount of FH suspension was then added to the peat/FeCl<sub>3</sub> mixture and the pH adjusted to 6.8. The

peat/FeCl<sub>3</sub>/FH suspension was placed in a water-bath shaker and shaken for 24 hours during which two more pH adjustments were made. Then the final suspension mass was brought to 240 g with 0.05 M KCl.

### ***EXAFS data collection and processing***

When all peat/FH or peat/FeCl<sub>3</sub>/FH systems were ready for EXAFS data collection, the suspensions were centrifuged and the supernatants were decanted. The wet pasty mixtures were pressed into sample holders for EXAFS analysis. Iron K-edge EXAFS data were collected at beamline X-11B at the National Synchrotron Light Source (NSLS) of Brookhaven National Lab (Upton, NY). The storage ring was operating at a maximum current of 300 mA. Spectra were recorded in transmission mode using a channel-cut Si(111)-monochromator, which was detuned >30% to reject higher harmonics. The spectra were scanned from 200 eV below to a wavevector ( $k$ ) of 14 Å<sup>-1</sup> above the Fe K-edge at 7112 eV. All data were processed using IFEFFIT package which include the Athena and Artemis interface.<sup>33</sup> Data were  $k^2$ -weighted after being normalized for background removal in a  $k$  range of 0-13 Å<sup>-1</sup>, then were Fourier transferred across a  $k$  range of 2.5~11.5 Å<sup>-1</sup>.

For fitting the data of peat/ferrihydrite samples a structural model was built upon the structure of a nano-crystalline ferrihydrite.<sup>34</sup> The crystallographic data were fed to the ATOMS program inside the IFEFFIT package. Back scattering paths and phase corrections were calculated by the FEFF6 program. When constructing the model with Artemis, all paths with a computed amplitude <10% were discarded because these paths were not needed to fit spectral features across the chosen  $k$ -space and  $R$ -space. To simplify the model, two Fe-O paths ( $R_{\text{eff}}$ =1.932 and 2.011 Å) were chosen to fit the first-shell Fe-O data. For the second-

shell, single scattering Fe-Fe paths were grouped together if the difference of  $R_{\text{eff}}$  (interatomic distance between the central Fe atom and the surrounding atoms) was within 0.1 Å. Within each group of paths, if a path whose  $R_{\text{eff}}$  is the closest to the mean  $R_{\text{eff}}$ , it is then included in the structural model. If all paths in that group have the same difference to the mean  $R_{\text{eff}}$ , then the path with higher amplitude is chosen. Fourier transformed data were fitted in an  $R$  range of 1~4 Å, which was conducted in the Artemis program where  $k=1$ ,  $k=2$ , and  $k=3$  were all chosen to optimize the fits over all three weighting factors.<sup>35</sup> Amplitude reduction factor ( $S_0^2$ ) was fixed as 0.84 for all data based on past fitting results. When fitting the data of ferrihydrite only, the parameter of coordination number (CN) for each chosen path is fixed as the sum of the degeneracy of all paths in that group. Parameters of  $\delta^2$  (mean displacement of interatomic distance) and  $\Delta R$  (difference between the actual bond length and the calculated bond length) in each path were set as variables for fitting. The fitting results of  $\delta^2$  for ferrihydrite data were used as fixed values for the  $\delta^2$  parameters for the peat/FH data.

When fitting EXAFS data from peat/FeCl<sub>3</sub>/ferrihydrite samples, a structural model was constructed with representative Fe-O, Fe-Fe, and Fe-C paths calculated from the crystallographic data from the nano-crystalline ferrihydrite<sup>34</sup> and an Fe(III) oxalatophosphate compound.<sup>29</sup>

### ***Auxiliary analyses***

X-ray diffraction data of ferrihydrite samples were collected at beamline 01C at the National Synchrotron Radiation Research Center (Hsinchu Taiwan). Aged ferrihydrite samples were also analyzed for B.E.T. surface area with a Monosorb surface analyzer (Quantachrome Instruments, Boynton Beach Florida).

Ferrihydrite and the system of 80 mg HA/g and 1g peat/g were also measured for their 0.4 M HCl extractable Fe as index of change of crystallinity with aging following the procedures described in Cornell and Schneider.<sup>36</sup>

Dissolved P in the supernatants were measured with the molybdate blue method<sup>37</sup> with a Shimadzu spectrophotometer at  $\lambda=840$  nm. Dissolved Fe concentrations in the supernatants were measured with an ICP-OES spectrometer. Dissolved organic carbon concentrations were determined with a Shimadzu Total Organic Carbon Analyzer (Shimadzu 5400).

### 4.3. Results

#### *Change of PO<sub>4</sub> sorption to organic matter/ferrihydrite mixtures*

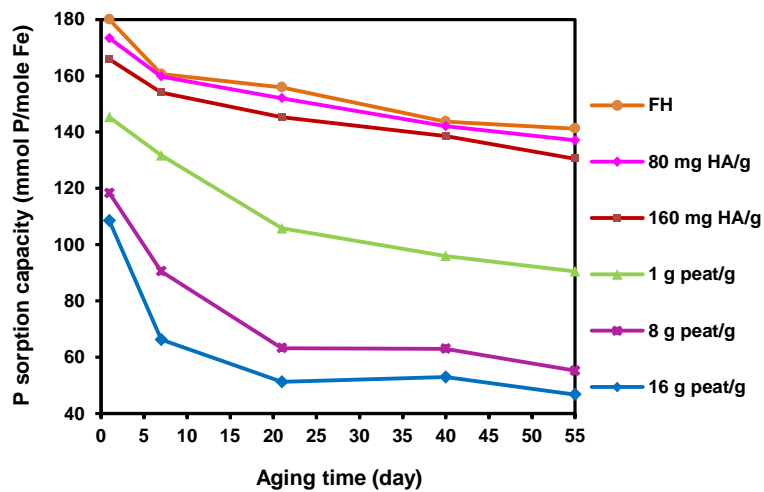


**Figure 4-1.** Change of PO<sub>4</sub> sorption to ferrihydrite and organic matter/ferrihydrite mixtures as a function of aging time at pH 6.0. All mixtures are described by the mass of organic matter per gram of ferrihydrite.

To determine the change of PO<sub>4</sub> sorption to organic matter/ferrihydrite mixtures as they aged, PO<sub>4</sub> sorption data were collected at different time points during aging and are displayed in

Figure 4-1. Systems that have aged for one day are considered fresh samples, and are regarded

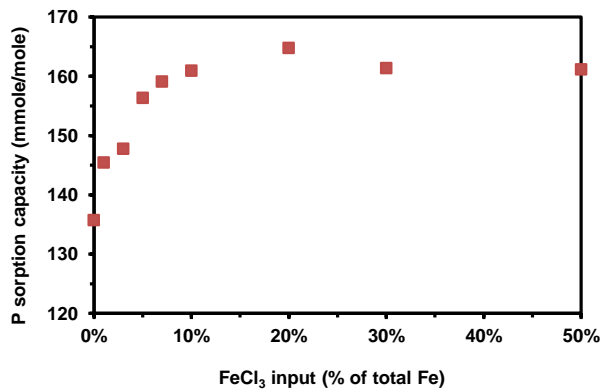
as points of reference for comparison with more aged samples hereafter. Fresh ferrihydrite sorbed up to 180 mmol P/mole Fe. With the same aging time, all OM/FH mixtures exhibited

lower PO<sub>4</sub> sorption capacities than ferrihydrite; and the mixture's PO<sub>4</sub> sorption capacity decreased with more organic matter. From a longitudinal perspective, all systems showed decreasing PO<sub>4</sub> sorption capacities with aging regardless of the amount of OM present. The decrease was the fastest during the first seven days. An approximate decrease of ~8% during the first seven days and ~20% decrease over 55 days was observed in ferrihydrite and two HA/FH systems (80 and 160 mg HA/g). The three peat/FH systems (1, 8, 16 g peat /g) demonstrated a decrease of 10%, 24%, or 39% in PO<sub>4</sub> sorption capacity, respectively, in the first seven days. The overall decreases for these three systems are 38%, 53%, and 57%. In all cases a higher amount of OM in a system results in a greater overall decrease in P sorption capacity.

### ***Phosphate sorption to FeCl<sub>3</sub>/ferrihydrite/peat systems***

In order to evaluate the influence of Fe-peat complexation on PO<sub>4</sub> sorption, PO<sub>4</sub> sorption isotherm experiments were conducted to a series of peat/FeCl<sub>3</sub>/FH systems. These

systems had different inputs of FeCl<sub>3</sub> and FH but were controlled for constant total Fe and peat. The sorption data for each mixture were fitted to the Langmuir model and the calculated sorption maxima are compared in Figure 4-2. With all Fe being



ferrihydrite, the system's PO<sub>4</sub> sorption capacity is 136 mmol P/mole Fe. As total Fe changed from 100% ferrihydrite to the

**Figure 4-2.** PO<sub>4</sub> sorption to peat/FeCl<sub>3</sub>/ferrihydrite mixtures as a function of FeCl<sub>3</sub> input at pH 6.8. Total Fe and peat in these systems were controlled to be constant.

combination of 1% FeCl<sub>3</sub> and 99% ferrihydrite, the system's PO<sub>4</sub> sorption capacity increased by 7% to 145 mmol P/mole Fe. Phosphate sorption to the peat/FeCl<sub>3</sub>/FH mixtures continued to increase with more FeCl<sub>3</sub> input, then reached the maximum of 165 mmol P/mole Fe in the system in which 20% of total Fe was added as FeCl<sub>3</sub>. For the systems with FeCl<sub>3</sub> input greater than 20%, the PO<sub>4</sub> sorption capacities appear to be lower than the maximum value. Karlsson and Persson<sup>31</sup> identified monomeric Fe-peat complexation and ferric oxide-like polymers in peat when Fe content was 879 mmol Fe kg<sup>-1</sup>. In the systems with 30% or 50% of total Fe added as FeCl<sub>3</sub> to peat, Fe(III) to peat loading is 2850 or 4750 mmol/kg, respectively, which has exceeded the maximum binding sites in peat (2400 mmol kg<sup>-1</sup>). Such high Fe(III) input in peat very likely led to the formation of polymeric Fe (hydr)oxide clusters which provide less sorption sites for PO<sub>4</sub> per unit Fe than monomeric Fe-peat complexes. Nonetheless, Fe-peat complexation mixed with peat and ferrihydrite are proven to be more effective for PO<sub>4</sub> sorption than peat/ferrihydrite mixture. The data described in Fig. 4-2 suggest that the PO<sub>4</sub> sorption capacity of a peat/FH system will increase with aging if Fe migration to peat takes place so that Fe-peat complexes in the system increase.

### ***EXAFS analysis of Fe structure in aged peat/FH mixtures***

Evaluation of the spectral difference as Fe coordination structure in ferrihydrite changes to Fe-peat complexation as in a peat/FeCl<sub>3</sub> system provides reference to assess any structural transformation for ferrihydrite as it ages with peat. In the peat/FeCl<sub>3</sub>/FH mixtures (total Fe equal to 1200 mmol kg<sup>-1</sup> peat), as FeCl<sub>3</sub> input changes from 100% to 0%, Fe coordination structure should change from Fe-peat complexation dominant to ferrihydrite dominant. The EXAFS data of all peat/FH and peat/FeCl<sub>3</sub>/FH mixtures cover a *k* range from

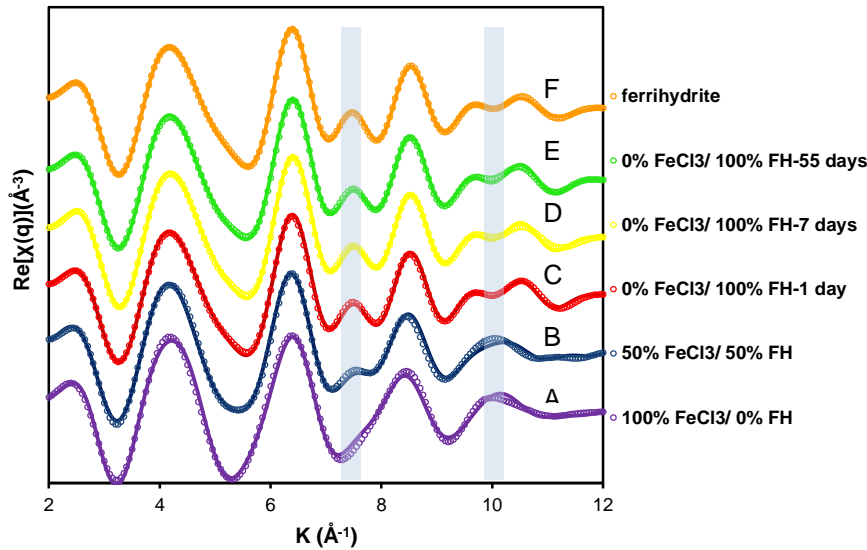


**Figure 4-3.** Fourier transform filtered ( $R+\Delta R=1-3.5 \text{ \AA}$ ) Fe K-edge EXAFS spectra of fresh ferrihydrite, peat/ $\text{FeCl}_3$ /FH mixtures, and peat/FH mixtures that have aged for 7 and 55 days. \*FH=ferrihydrite

system, EXAFS analysis reveals that spectral features from the second coordination shell are characteristic of Fe-C and Fe-Fe backscattering pairs at the distances of 2.848 and 3.076~3.375  $\text{\AA}$ , respectively (Table 4-1). Such results are confirming that the experimental EXAFS data are able to resolve the spectral difference between Fe-C and Fe-Fe coordination in the second shell. As  $\text{FeCl}_3$  input decreased to 50%, the modeled coordination number of Fe-C pair decreases while Fe-Fe pair increases. Full list of the fitting results of all peat/ $\text{FeCl}_3$ /FH mixtures are presented in Table 4-1. The Fourier transform (FT) filtered ( $R+\Delta R=1-3.5 \text{ \AA}$ ) EXAFS spectra of the three peat/ $\text{FeCl}_3$ /FH mixtures (Figure 4-3, spectrum A, B, and C) clearly demonstrates distinct spectral characteristics as Fe coordination structure changes from Fe-peat complexation dominant to ferrihydrite dominant.

For the peat/ $\text{FeCl}_3$ /FH mixture with  $\text{FeCl}_3$  input being 0% of total Fe, it is actually a peat/FH mixture. For this mixture, EXAFS data were collected for a fresh sample as well as

2.5 to 11.5  $\text{\AA}^{-1}$  after background removal.

Theoretically the experimental data can resolve any two interatomic distances whose difference is greater than 0.137

( $\Delta R \geq \frac{\pi}{2 * k_{\text{max}}}$ ).<sup>27</sup> For the 100%  $\text{FeCl}_3$  input

two aged samples (7 and 55 days). The spectra for these samples with various aging times resemble each other, and are almost identical to the spectrum of ferrihydrite (Figure 4-3, spectrum D, E, and F). Clearly the spectral features that belong to Fe-C pair (highlighted by vertical bars) are missing in any of the spectra of the aged peat/FH mixtures. The experimental data of ferrihydrite were successfully fit to the model constructed with the structural data of a nanocrystalline ferrihydrite.<sup>34</sup> Because of the similarity between the spectra of the peat/FH mixture samples and the spectrum of ferrihydrite, we did not attempt to model the peat/FH EXAFS data with any Fe-C path. Instead, these data were successfully fit to the structural model that was applied to model the ferrihydrite experimental data successfully, which confirms that there is no structural transformation for the Fe in ferrihydrite as it aged with peat. The same EXAFS analysis was also applied to another two aged peat/FH mixtures with Fe to peat input being 300 and 600 mmol Fe kg<sup>-1</sup> peat. Again, their EXAFS spectra resemble the spectrum of ferrihydrite and were successfully fit to the ferrihydrite structural model (data not shown). The collective results of EXAFS analyses indicate that Fe coordination structure remains being as in ferrihydrite regardless of aging with peat. That is to say no Fe migration forming new Fe-peat complexes was detected by EXAFS.

It is possible that the extent of structural transformation from Fe in ferrihydrite to Fe-peat complexes exceeds the detection limit of EXAFS. Thus, two peat/FH mixtures (1 and 8 g peat g<sup>-1</sup> FH) were monitored for their pyrophosphate extractable Fe during aging. In accordance with the results of EXAFS analyses, pyrophosphate extractable Fe from these

**Table 4-1.** Fitting parameters for the EXAFS data of the peat/FeCl<sub>3</sub>/FH mixtures and three peat/FH mixtures (0% FeCl<sub>3</sub>) that have aged for 1, 7, and 55 days. All systems were controlled for a constant total Fe to peat input which is equal to 1200 mmol Fe/kg peat. The interatomic distances of all paths for the three pea/FH (0% FeCl<sub>3</sub>) systems are the same. FH=ferrihydrite

System	Path	R (Å)		CN	$\delta^2$	$\Delta E_0$	R-factor		
100% FeCl <sub>3</sub> 0% FH	Fe-O1	1.948	(0.013)	3.0	fixed	0.006	1.43	0.0027	
	Fe-O2	2.027	(0.013)	3.0		0.006			(0.001)
	Fe-C	2.848	(0.045)	1.9	(0.6)	0.006			
	Fe-Fe1	3.076	(0.044)	1.7	(0.6)	0.013			fixed
	Fe-Fe2	3.375	(0.051)	1.1	(0.6)	0.009			
50% FeCl <sub>3</sub> 50% FH	Fe-O1	1.945	(0.013)	3.0	fixed	0.008	0.95	0.0027	
	Fe-O2	2.024	(0.013)	3.0		0.008			(0.001)
	Fe-C	2.766	(0.033)	1.7	(0.6)	0.006			
	Fe-Fe1	3.009	(0.023)	2.3	(0.7)	0.009			fixed
	Fe-Fe2	3.203	(0.043)	3.9	(0.8)	0.013			
0% FeCl <sub>3</sub> 100%-FH 1-day	Fe-O1					0.009	0.57	0.0010	
	Fe-O2					(0.001)			
	Fe-Fe1					0.018			(0.002)
	Fe-Fe2					0.008			(0.007)
	Fe-Fe4					0.004			(0.004)
	Fe-Fe5					0.004			(0.004)
	Fe-Fe6								
0% FeCl <sub>3</sub> 100% FH 7-day	Fe-O1	1.931	(0.001)	3	fixed	0.009	1.06	0.0010	
	Fe-O2	2.011	(0.001)	3		0.017			(0.004)
	Fe-Fe1	3.011	(0.020)	2		0.008			(0.006)
	Fe-Fe2	3.113	(0.020)	2		0.004			(0.003)
	Fe-Fe4	3.191	(0.096)	1		0.004			(0.003)
	Fe-Fe6	3.500	(0.020)	2					
0% FeCl <sub>3</sub> 100% FH 55-day	Fe-O1					0.009	0.54	0.0010	
	Fe-O2					(0.001)			
	Fe-Fe1					0.016			(0.003)
	Fe-Fe2					0.010			(0.005)
	Fe-Fe4					0.006			(0.003)
	Fe-Fe5					0.005			(0.003)

two mixtures remained constant during the whole aging process, which further supports that no Fe migration to peat took place during the aging of the peat/FH mixtures.

## 4.4. Discussion

### *Crystallization of ferrihydrite*

Ferrihydrite is not a thermodynamically stable mineral; its transformation to more crystalline species, e.g.

goethite ( $\alpha$ -FeOOH),

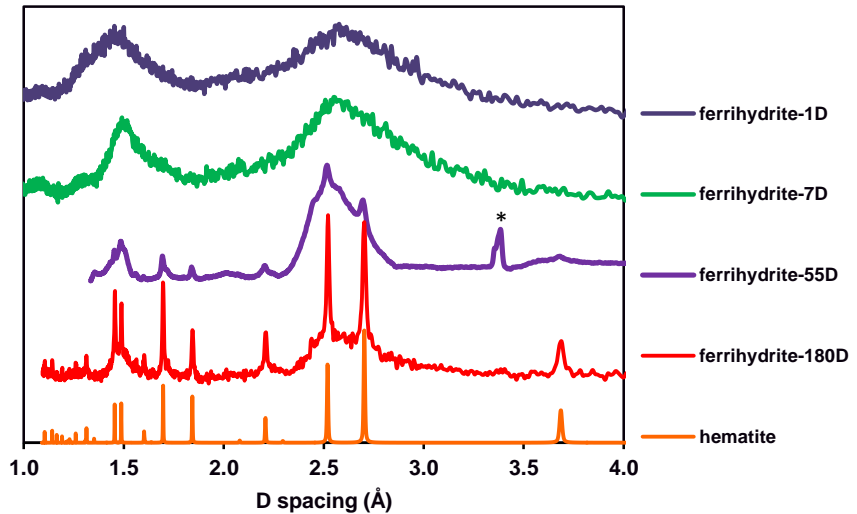
over time has been

widely observed.<sup>38-40</sup> In

this study, the

transformation of

ferrihydrite to hematite



at ambient temperature in a shaking condition was captured by XRD as

**Figure 4-4.** X-ray diffraction patterns of ferrihydrite that has aged for various time periods showing the transformation of ferrihydrite to hematite. \* This peak is possibly due to instrumental artifacts.

shown in Figure 4-4. The process of transformation from ferrihydrite to hematite was first signified by peak sharpening (seven days' aging), then by the appearance of peaks that belong to hematite on top of the original pattern as ferrihydrite had aged for 55 days. Parallel with the XRD data, the decrease of 0.4 M HCl extractable Fe, an indicator of non-crystalline Fe,<sup>41</sup> from aged ferrihydrite is in accordance with its crystallization with aging. Assuming Fe in fresh ferrihydrite is 100% acid extractable, a decrease of acid extractable Fe by 13% was

observed after ferrihydrite had aged for 55 days. A plot of acid extractable Fe from ferrihydrite versus its PO<sub>4</sub> sorption capacity during aging exhibits a linear relation as illustrated in Figure 4-5. As a result of crystallization, B.E.T. surface area of ferrihydrite dropped from 330 to 150 m<sup>2</sup> g<sup>-1</sup> after fresh ferrihydrite had aged for 55 days; and the surface area

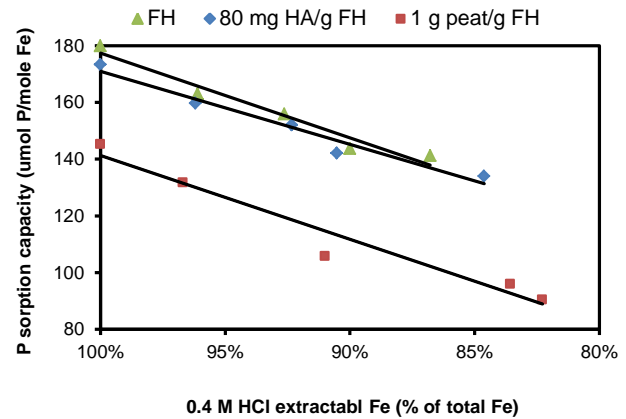


**Figure 4-5.** Phosphate sorption capacity as a function of 0.4 M HCl extractable Fe from three organic matter/ferrihydrite mixtures during aging for 55 days.

measurements also exhibit a linear relation with its PO<sub>4</sub> sorption capacities at different time points during aging (data not shown). In this study, ferrihydrite illustrated an approximate decrease of 20% in PO<sub>4</sub> sorption capacity over 55 days, which is lower than the decrease of 38% observed by Gerke<sup>19</sup> for a poorly crystalline Fe-oxide after aging for 56 days. Mobilization of sorbed Pb was observed as ferrihydrite transformed to goethite and hematite.<sup>42</sup> Multiple evidences obtained in this study confirm that the crystallization of ferrihydrite accounts for its decreased PO<sub>4</sub> sorption capacity with aging.

Decrease of 0.4 M HCl extractable Fe was also observed in the systems of 80 mg HA g<sup>-1</sup> and 1g peat g<sup>-1</sup>, by 14% and 18%, respectively. Linear relationship between acid extractable Fe and PO<sub>4</sub> sorption capacity at different time points during aging also exists for these two OM/FH mixtures (Fig. 4-5). Ferrihydrite appears to have crystallized during aging in the presence of OM, even to a greater extent based on the greater decrease of acid extractable Fe as shown in Fig. 4-5. Less acid extractable Fe from OM/FH mixtures could be

due to the acid/base buffering capacity of OM. We do not have XRD data for ferrihydrite that has aged with peat. However, the unchanged DOC concentrations (before PO<sub>4</sub> addition, see Fig. 4-6) in these two low OM mixtures suggest no ferrihydrite crystallization occurred during aging. In addition, it is well known that organic matter inhibits ferrihydrite crystallization.<sup>43-45</sup> Thus, ferrihydrite crystallization to more crystalline species is not considered in this discussion.

### ***Competition between organic matter and PO<sub>4</sub>***

As described in Fig. 4-1, the PO<sub>4</sub> sorption capacity of any OM/FH mixture is lower than that of ferrihydrite itself; and an OM/FH mixture with a greater amount of OM illustrates a smaller PO<sub>4</sub> sorption capacity. These results clearly show the inhibitory effect of Pahokee peat or peat HA on PO<sub>4</sub> sorption to ferrihydrite, which is consistent with the results from other similar studies.<sup>12-17</sup> Nevertheless certain organic matter was found to have no or insignificant effect on PO<sub>4</sub> sorption to oxides or soils.<sup>16,18,46,47</sup> The dividing results could be due to the inherent diversity of chemical characteristics, e.g. complexation ability, of different kinds of organic matter and experimental approaches.

Regarding the mechanism for OM inhibiting PO<sub>4</sub> sorption, competition between OM and PO<sub>4</sub> for sorption sites,<sup>13,17,48</sup> as well as Fe/Al dissolution by dissolved organic carbon (DOC)<sup>15,49</sup> have been recognized as the causes of PO<sub>4</sub> mobilization. For the low OM systems (80, 160 mg HA g<sup>-1</sup>, and 1 g peat g<sup>-1</sup>), after PO<sub>4</sub> addition DOC concentrations always increased each time of PO<sub>4</sub> sorption measurement. The increased DOC concentration is indicative of OM desorption by PO<sub>4</sub> (Figure 4-6). For instance, DOC concentration was 12.6 mg/L in the system of 1 g peat/g (1 day aging) before PO<sub>4</sub> addition. No dissolved Fe was

detected. After  $\text{PO}_4$  addition, DOC concentration increased to 64.8 mg/L, and dissolved Fe concentration became 41  $\mu\text{M}$  accounting for  $\sim 0.5\%$  of total Fe in the system. The dramatic increase of DOC after  $\text{PO}_4$  addition and the slight increase of dissolved Fe reveal that ligand exchange between  $\text{PO}_4$  and sorbed organic carbon took place during  $\text{PO}_4$  sorption process, which suggests that the competition between OM and  $\text{PO}_4$  should account for the inhibited  $\text{PO}_4$  sorption to ferrihydrite.

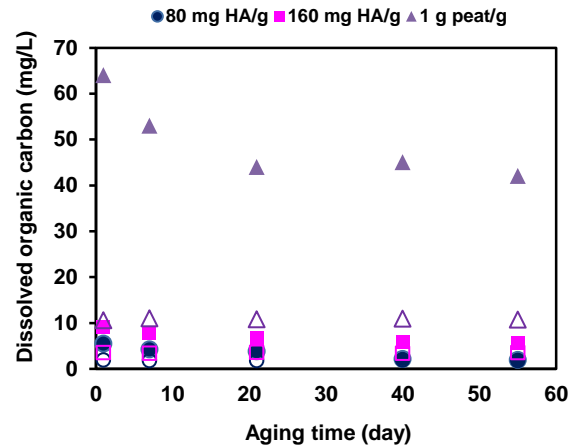


**Figure 4-6.** Dissolved organic carbon concentration before (hollow symbols) and after (solid symbols)  $\text{PO}_4$  addition to three organic matter/ferrihydrite mixtures during the aging of 55 days. HA=Pahokee peat humic acid

For each of the low OM systems (80, 160 mg HA  $\text{g}^{-1}$ , and 1 g peat  $\text{g}^{-1}$ ), the DOC concentration remains unchanged before  $\text{PO}_4$  addition (open symbols in Fig. 4-6). With longer aging time, however, the amount of released organic carbon after  $\text{PO}_4$  addition decreases in each mixture. This phenomenon is the most prominent in the system of 1 g peat  $\text{g}^{-1}$  FH for the post- $\text{PO}_4$  addition DOC concentration decreased from 64.8 to 32.5 mg  $\text{L}^{-1}$  as the mixture had aged for 55 days. It has been found that sorptive interaction between OM and oxide minerals makes OM more resistant to microbial degradation.<sup>7,50</sup> As organic matter aged with ferrihydrite or goethite, Kaiser et al.<sup>51</sup> found that the desorbable organic carbon decreased by up to 16%; and OM formed additional bonds with Fe on mineral surface. For the studied OM/FH mixtures, the fact that less organic carbon was desorbed by  $\text{PO}_4$  with aging suggests that peat or HA gained stability or stronger resistance against the competition

with  $\text{PO}_4$ , possibly by forming more or stronger bonds with Fe. As discussed above, the decrease of 0.4 M HCl extractable Fe from the two OM/FH mixtures upon aging is actually greater than that from ferrihydrite. Given the uncertainty of ferrihydrite crystallization in the presence of peat or HA, the greater decrease of acid extractable Fe at the end of aging also suggests Fe-OM bonding becomes stronger with aging.

In the high OM systems (8 or 16 peat/g), >30% of total organic carbon was detected in the supernatants. Change of DOC concentrations before and after  $\text{PO}_4$  addition was not noticeable. But the competition between OM and  $\text{PO}_4$  during aging appears to be stronger because the overall decrease of  $\text{PO}_4$  sorption capacity in these two systems is greater than 50% which is much greater than the decreases in the rest of systems studied.

### ***Dissolved Fe in high organic matter systems***

For the two high peat mixtures (8 and 16 g peat  $\text{g}^{-1}$  FH), more than a third of total organic carbon was detected in the supernatants. Change of DOC before and after  $\text{PO}_4$  addition is much less apparent than in the three low OM mixtures (discussed in previous section). Along with high DOC, 5.6% and 10.5% of total Fe was detected in the supernatants of the two fresh high peat systems, 8 and 16 g peat  $\text{g}^{-1}$ , respectively. In addition to the competition between OM and  $\text{PO}_4$ , Fe dissolution or dispersion by DOC further decreases the available sorption sites for  $\text{PO}_4$  on ferrihydrite surface, which exacerbates the inhibitory effect of peat on  $\text{PO}_4$  sorption. After aging for 55 days, dissolved Fe in these two mixtures increased to 9.8% and 13.5% of total Fe, respectively. For high OM mixtures, aging has dual effects: increase OM stability and increase Fe dissolution. Such dual effect intensifies the

aging effect on PO<sub>4</sub> sorption. Therefore, the greatest decrease of PO<sub>4</sub> sorption capacity (>50%) was observed in these two high peat mixtures.

## 4.5. Conclusions

Although organic matter has been extensively studied for its role on PO<sub>4</sub> sorption to oxide minerals, few studies focused on the effect from a longitudinal perspective. Aiming at filling this research gap, the study presented here focused on the interaction between ferrihydrite and two kinds of organic matter, Pahokee peat and Pahokee peat humic acid, and the impact on PO<sub>4</sub> sorption over a period of 55 days. Contrast to the results from earlier investigations, our batch experiments show that aging of OM/FH mixtures leads to decreased PO<sub>4</sub> sorption capacity. With constant total Fe and peat, peat/FeCl<sub>3</sub>/ferrihydrite mixtures illustrate higher PO<sub>4</sub> sorption capacity than peat/FH mixtures; and greater FeCl<sub>3</sub> input results in greater PO<sub>4</sub> sorption capacity. Moreover, Fe K-edge EXAFS analyses of selected aged peat/FH mixtures provides no evidence for Fe-peat complexation during aging, which is also supported by the unchanged pyrophosphate extractable Fe from the mixtures during aging. For ferrihydrite, structural transformation to more crystalline species, hematite is responsible for its decreased PO<sub>4</sub> sorption capacity. For OM/FH mixtures, we conclude that aging increases OM's stability, which imparts stronger resistance to organic matter against the competition with PO<sub>4</sub>. With high OM input, aging also increases Fe dissolution. These factors, individually or collectively, account for the decrease of PO<sub>4</sub> sorption to ferrihydrite as it ages with organic matter.

## 4.5. References

- (1) Bot, A.; Benites, J. *The importance of soil organic matter*; Food and Agriculture Organization of the United Nations: Rome Italy, 2005.
- (2) Gu, B. H.; Schmitt, J.; Chen, Z. H.; Liang, L. Y.; McCarthy, J. F.; Mp *Environmental Science & Technology* **1994**, 28, 38.
- (3) Schneider, M. P. W.; Scheel, T.; Mikutta, R.; van Hees, P.; Kaiser, K.; Kalbitz, K. *Geochimica Et Cosmochimica Acta* **2010**, 74, 1606.
- (4) Avena, M. J.; Koopal, L. K. *Environmental Science & Technology* **1999**, 33, 2739.
- (5) Kaiser, K.; Zech, W. *Soil Science* **1998**, 163, 714.
- (6) Fu, H. B.; Quan, X. *Chemosphere* **2006**, 63, 403.
- (7) Kaiser, K.; Guggenberger, G. *European Journal of Soil Science* **2007**, 58, 45.
- (8) Kaiser, K.; Guggenberger, G. *European Journal of Soil Science* **2003**, 54, 219.
- (9) Violante, A.; Colombo, C.; Buondonno, A. *Soil Science Society of America Journal* **1991**, 55, 65.
- (10) Violante, A.; Pigna, M. *Soil Science Society of America Journal* **2002**, 66, 1788.
- (11) Khare, N.; Hesterberg, D.; Beauchemin, S.; Wang, S. L. *Soil Science Society of America Journal* **2004**, 68, 460.
- (12) Bhatti, J. S.; Comerford, N. B.; Johnston, C. T.; Uf *Soil Science Society of America Journal* **1998**, 62, 1089.
- (13) Antelo, J.; Arce, F.; Avena, M.; Fiol, S.; Lopez, R.; Macias, F.; Kq *Geoderma* **2007**, 138, 12.

- (14) Hunt, J. F.; Ohno, T.; He, Z. Q.; Honeycutt, C. W.; Dail, D. B. *Biology and Fertility of Soils* **2007**, *44*, 277.
- (15) Ohno, T.; Erich, M. S. *Journal of Environmental Quality* **1997**, *26*, 889.
- (16) Ohno, T.; Crannell, B. S. *Journal of Environmental Quality* **1996**, *25*, 1137.
- (17) Guan, X. H.; Shang, C.; Chen, G. H. *Journal of Colloid and Interface Science* **2006**, *296*, 51.
- (18) Borggaard, O. K.; Raben-Lange, B.; Gimsing, A. L.; Strobel, B. W.; Bj *Geoderma* **2005**, *127*, 270.
- (19) Gerke, J.; Mt *Geoderma* **1993**, *59*, 279.
- (20) Bloom, P. R.; Lr *Soil Science Society of America Journal* **1981**, *45*, 267.
- (21) White, R. E.; Thomas, G. W. *Fertilizer Research* **1981**, *2*, 159.
- (22) Haynes, R. J.; Swift, R. S.; Cd *Journal of Soil Science* **1989**, *40*, 773.
- (23) Gerke, J.; Hermann, R. *Zeitschrift Fur Pflanzenernahrung Und Bodenkunde* **1992**, *155*, 233.
- (24) Vilge-Ritter, A.; Rose, J.; Masion, A.; Bottero, J. Y.; Laine, J. M. *Colloids and Surfaces a-Physicochemical and Engineering Aspects* **1999**, *147*, 297.
- (25) Gustafsson, J. P.; Persson, I.; Kleja, D. B.; Van Schaik, J. W. J. *Environmental Science & Technology* **2007**, *41*, 1232.
- (26) van Schaik, J. W. J.; Persson, I.; Kleja, D. B.; Gustafsson, J. P. *Environmental Science & Technology* **2008**, *42*, 2367.
- (27) Drits, V. A.; Sakharov, B. A.; Salyn, A. L.; Manceau, A. *Clay Minerals* **1993**, *28*, 185.

- (28) Toner, B. M.; Santelli, C. M.; Marcus, M. A.; Wirth, R.; Chan, C. S.; McCollom, T.; Bach, W.; Edwards, K. J. *Geochimica Et Cosmochimica Acta* **2009**, *73*, 388.
- (29) Kizewski, F. R.; Boyle, P.; Hesterberg, D.; Martin, J. D. *Journal of the American Chemical Society* **2010**, *132*, 2301.
- (30) Karlsson, T.; Persson, P.; Skyllberg, U.; Morth, C. M.; Giesler, R. *Environmental Science & Technology* **2008**, *42*, 5449.
- (31) Karlsson, T.; Persson, P. *Geochimica Et Cosmochimica Acta* **2010**, *74*, 30.
- (32) Murray, G. C.; Hesterberg, D. *Soil Science Society of America Journal* **2006**, *70*, 1318.
- (33) Newville, M. *Journal of Synchrotron Radiation* **2001**, *8*, 322.
- (34) Michel, F. M.; Ehm, L.; Antao, S. M.; Lee, P. L.; Chupas, P. J.; Liu, G.; Strongin, D. R.; Schoonen, M. A. A.; Phillips, B. L.; Parise, J. B. *Science* **2007**, *316*, 1726.
- (35) Kelly, S.; Hesterberg, D.; Ravel, B. *Methods of Soil Analysis*; Soil Science Society of America: Madison, WI, 2008.
- (36) Cornell, R. M.; Schneider, W. *Polyhedron* **1989**, *8*, 149.
- (37) Murphy, J.; Riley, J. P. *Analytica Chimica Acta* **1962**, *26*, 31.
- (38) Schwertmann, U.; Murad, E. *Clays and Clay Minerals* **1983**, *31*, 277.
- (39) Schwertmann, U.; Friedl, J.; Stanjek, H. *Journal of Colloid and Interface Science* **1999**, *209*, 215.
- (40) Schwertmann, U.; Stanjek, H.; Becher, H. H. *Clay Minerals* **2004**, *39*, 433.
- (41) Cornell, R. M.; Schneider, W.; Giovanoli, R. *Polyhedron* **1989**, *8*, 2829.

- (42) Martinez, C. E.; Sauve, S.; Jacobson, A.; McBride, M. B. *Environmental Science & Technology* **1999**, *33*, 2016.
- (43) Eusterhues, K.; Wagner, F. E.; Hausler, W.; Hanzlik, M.; Knicker, H.; Totsche, K. U.; Kogel-Knabner, I.; Schwertmann, U. *Environmental Science & Technology* **2008**, *42*, 7891.
- (44) Cornell, R. M.; Schwertmann, U. *Clays and Clay Minerals* **1979**, *27*, 402.
- (45) Schwertm.U *Nature* **1966**, *212*, 645.
- (46) Borggaard, O. K.; Jorgensen, S. S.; Moberg, J. P.; Rabenlange, B.; Eb *Journal of Soil Science* **1990**, *41*, 443.
- (47) Goyne, K. W.; Jun, H. J.; Anderson, S. H.; Motavalli, P. R. *Journal of Environmental Quality* **2008**, *37*, 154.
- (48) Violante, V.; Gianfreda, L. *Soil Science Society of America Journal* **1993**, *57*, 1235.
- (49) Gerke, J. *Zeitschrift Fur Pflanzenernahrung Und Bodenkunde* **1993**, *156*, 253.
- (50) Kalbitz, K.; Schwesig, D.; Rethemeyer, J.; Matzner, E. *Soil Biology & Biochemistry* **2005**, *37*, 1319.
- (51) Kaiser, K.; Mikutta, R.; Guggenberger, G. *Soil Science Society of America Journal* **2007**, *71*, 711.

**Chapter 5: Determining the redox capacity of Pahokee  
peat and the mechanism of its chemical reduction**

## Abstract

The mechanistic role of organic matter as a redox mediator for iron oxide reduction is investigated by measuring the relative reduction rate of Pahokee peat (PP) and the native Fe(III) in peat. Measurements of reduction of ferrihydrite (FH), FeCl<sub>3</sub>, and Fe(III)-citrate (Fe-Cit) by hydrogen reduced peat, along with measurement of the acid addition required to maintain a constant pH of 6, provide a measure of the reducing capacity, the mechanism of reduction, and identification of the redox active functional groups in peat. The kinetics of peat chemical reduction is well fit by a model of a diffusion-limited reaction proceeding in spherical particles. These data demonstrate the existence of two distinct redox reservoirs: one assigned to quinone functional groups and the other to reducible acid and neutral carbonyl functional groups. The iron(III) native to peat is reduced at more than three times the rate that the organic matter is reduced. Chemical reduction of a peat/FH mixture clearly demonstrates that FH and peat are reduced independently. While peat can act as a remote electron-shuttle, it does not act as an active electron shuttle between the H<sub>2</sub> electron source and FH. Microbial reduction data are most consistent with a model in which peat transports biogenic Fe(II) by complexation to mitigate the inhibitory impact of Fe(II) accumulation on microbial ferric oxide reduction.

## 5.1. Introduction

Soils are complex materials of which numerous components are redox active. The various redox processes in soils, both naturally occurring and a result of human activity are critically important for nutrient and/or pollutant mobility, retention and remediation.<sup>1-3</sup> In particular iron(III) oxides are important sinks for oxyanions (e.g.  $\text{PO}_4^{3-}$ ,  $\text{AsO}_4^{3-}$ ,  $\text{SeO}_4^{2-}$ )<sup>4-7</sup> and trace metals.<sup>8,9</sup> These species tend to be more immobilized by ferric minerals and mobilized upon reduction to ferrous iron.<sup>10-12</sup> Numerous reports have implicated soil organic matter (OM) as a mediator of the reduction of iron(III) oxides.<sup>13-19</sup> The reversible redox processes of OM have been attributed primarily to their significant quinone functional groups, whereby one electron processes interconvert quinones to semiquinones to hydroquinones.<sup>20,21</sup> Other components of the OM such as carboxylic acids, ketones, and sulfide moieties also exhibit reducing capacity.<sup>22-24</sup>

Lovley et al.<sup>13</sup> first demonstrated that humic substances (HS) facilitated microbial reduction of Fe(III) oxide both with respect to the rate and extent of reduction. Experiments in which microbially reduced HS was isolated from the microorganisms demonstrated that HS has the capacity for significant electron storage. The humic substances were shown to accept electrons from microorganisms then transfer the electrons to Fe(III) oxides. This, combined with the observation of an enhanced rate of Fe(III) oxide microbial reduction in presence of OM, has been explained as the result of an electron shuttle mechanism. Importantly, this electron shuttle mechanism allows reduction to occur with no direct contact between the microbes and minerals.

However, we observed that under equivalent reducing conditions, chemical reduction of ferrihydrite (FH) by  $H_2$  in the presence of only a Pt/C catalyst is faster than either chemical or microbial reduction of FH in the presence of peat. This would suggest that organic matter may also have an inhibitory effect on the rate of iron(III) oxide reduction. Thus while organic matter unquestionably can act as a remote shuttle of electrons to iron(III)-oxide minerals, the objective of this research was to perform a more sophisticated mechanistic investigation of the reduction of organic matter and its ability to facilitate or inhibit the reduction of ferric oxides. Several investigators have established that microbial reduction and chemical reduction with  $H_2$  or  $H_2S$  reduce humic substances to the same extent.<sup>13,25,26</sup> This implies that the same functional groups in the OM act as electron acceptors, independent of the method of reduction. Therefore a mechanistic investigation focused on the more readily controlled chemical reduction is likely valid for understanding both chemical and microbial processes.

While a majority of studies probing OM/iron-oxide systems utilize humic acid solutions, OM in soils and sediments is normally in particulate form. Therefore in this study we chose to investigate solid phase OM, Pahokee peat and an ubiquitous iron(III) oxide, ferrihydrite (FH) to represent soil OM and Fe(III) oxides, respectively. To accomplish our objectives, we have measured the rate of chemical reduction of the HCl extractible iron native to peat; measured the rate of reduction of peat using FH, Fe-Cit and  $FeCl_3$  as external oxidants; and measured the post-reduction reducing capacity of peat/FH mixtures after both chemical and microbial reduction. The acid consumption data to maintain a constant pH at 6 were also utilized to understand the chemical reduction mechanism. All kinetic data were analyzed with established kinetic models for gas-solid reactions.<sup>27</sup> These findings

significantly refine the understanding of the redox properties of organic matter and its role in ferric oxide chemical reduction.

## **5.2. Materials and methods**

### ***Pahokee peat hydration*** Pahokee

peat purchased from International Humic Substances Society (IHSS) was hydrated prior to usage. Detailed hydration procedure can be found in the Materials and Method section of Chapter 4.

### ***Iron(III) probe species***

Details for ferrihydrite synthesis and characterization can be found in the Materials and Method section of Chapter 4.

FeCl<sub>3</sub> and Fe-Citrate (Fe-Cit) solutions (0.0125 M) were prepared with FeCl<sub>3</sub>·2H<sub>2</sub>O and by mixing FeCl<sub>3</sub>·2H<sub>2</sub>O and Na-citrate (1:1 molar ratio), respectively. All chemicals were purchased from Sigma Aldrich.

### ***Reduction experiments***

Reduction experiments were performed using a 2-L water jacketed glass reactor vessel (Wilmad-Labglass Corp., Buena, NJ), wrapped with Al foil to avoid photochemical reactions and maintained at 25 °C with a circulating water bath. The reactions were maintained at a constant pH of 6.0 using a Radiometer Analytical Model TM850 Autotitrator (Radiometer Analytical Corp., Lyon, France) with 0.05 M HCl or KOH. The electrical potential of each reaction was measured against a Ag/AgCl standard electrode with a Pt working electrode, and reported with respect to S.H.E.

***Reducing capacity of peat*** Peat suspensions were prepared by mixing an aliquot of stock suspension (1 g dry mass) with 0.05 M KCl solution at pH 6 sufficient to yield a total suspension mass of 1 kg. The suspension was equilibrated for 24 h under N<sub>2</sub>. A powder of 10% Pt on activated C (Pt/C, Sigma Aldrich Co., Milwaukee, WI) (0.25 g) was added to the suspension and the system purged with H<sub>2</sub> (1.7% or 0.5% in N<sub>2</sub>, 65 mL/min) for 48 hours. In experiments 1-3, the catalyst was added immediately before initiation of the H<sub>2</sub> purge. In experiment 4, the catalyst was added to the peat suspension prior to the 24 h N<sub>2</sub> equilibration. Periodically 15 mL fractions were withdrawn into sealed brown serum bottles, purged with N<sub>2</sub> for 15 min to remove residual H<sub>2</sub>. The hydrogen-free suspension was then transferred to a N<sub>2</sub> flushed glove box. A 2 mL aliquot of each suspension fraction was mixed with 2 mL FH suspension and the mixture shaken for 15 minutes. In a sealed serum bottle, 2 mL of the peat/FH mixture and 2 mL 1 M HCl were added and mixed for 24 h to measure 0.5 M HCl extractable Fe(II). Separate experiments demonstrated that equivalent amounts of HCl extractable Fe(II) were obtained from 15 min, 1 h, 4 h and 24 h reactions of the chemically reduced peat and FH (Figure 5-1). The reducing capacity of H<sub>2</sub> reduced peat with respect to FeCl<sub>3</sub> and Fe-Cit solutions was analyzed following the same procedure described for FH.

***Peat/ferrhydrite mixtures*** In a typical experiment, an aliquot of peat suspension (0.62 g dry mass equivalent) was weighed into a 1-L HDPE bottle along with 300 mL of 0.05 M KCl solution and the pH was raised to ~5 with 0.05 M KOH. An aliquot of FH suspension (equivalent to 0.4 g dry mass) was then added to peat suspension and adjusted to pH = 6. KCl (0.05 M) was then added to the suspension to yield a total mass of 0.8 kg. The peat/FH suspension was then transferred to the glass reactor and purged with N<sub>2</sub> for 24 hours prior to

initiation of reduction. For chemical reduction experiment, a powder of 10% Pt on activated carbon (0.100 g) was added to the reaction system prior to H<sub>2</sub> purging. For microbial reduction, *Shewanella putrefaciens* (strain CN32) was inoculated to the reaction mixture at a concentration of 10<sup>8</sup> cells mL<sup>-1</sup> prior to H<sub>2</sub> purging. The initial culture of CN32 was provided by Dr. Edward O'Loughlin, Bioscience Division, Argonne National Laboratory. CN32 was grown aerobically in tryptic soy broth at ambient temperature. Cells were harvested by centrifugation (15,680×g at 20 °C for 7 min) from a 16 h-old culture (late log-phase) and washed three times with sterile 0.05 M KCl. Cell pellets were resuspended in sterile 0.05 M KCl. Cell density was determined by absorbance at 420 nm.

For both chemical and microbial reduction, hydrogen gas (1.7% with N<sub>2</sub>, 65 mL min<sup>-1</sup> flow rate) was purged for 24 hours. Suspension fractions, 15 mL, were collected after 8 (or 11) and 24 h and purged with N<sub>2</sub> for 15 min. The Hydrogen-free peat fractions were then placed in a N<sub>2</sub> flushed glove box. Three 2 mL aliquots of each fraction were mixed with 2 mL H<sub>2</sub>O, ferrihydrite, and FeCl<sub>3</sub>, respectively; and the mixtures were shaken for 15 min. 2 mL of each peat/Fe(III) compound mixture was then mixed with 2 mL 1 M HCl in a sealed amber serum bottle and allowed to equilibrate for 24 hours. The resulting mixture was filtered, and the 0.5 M HCl extractable Fe(II) in the supernatant measured using the ferrozine method.<sup>28</sup> The remaining suspension fraction was filtered using a 0.2 µm membrane for analyses of dissolved Fe(II) and organic carbon (DOC). DOC was measured with a Schumadzu TOC-5400 total organic carbon analyzer.

### **5.3. Results and discussion**

#### ***Reducing capacity of Pahokee peat***

Numerous investigators have probed the reducing capacity of natural organic matter with respect to iron oxides. Previous work recognized that the measured reducing capacity of dissolved organic matter is dependent on the nature of the reduction potential of the oxidant used for the measurements.<sup>29,30</sup> Bauer et al.<sup>30</sup> also described a clear dependence of the morphology of iron oxides with more highly crystalline oxides acting as poorer oxidizing agents. For this reason, to investigate the reducing capacity of particulate Pahokee peat, oxidants with notably different reduction potentials were employed ( $\text{FeCl}_3$ ,  $E_h = 770 \text{ mV}$ ,<sup>31</sup>  $\text{Fe-Cit}$ ,  $E_h = 433 \text{ mV}$ <sup>32</sup> and  $\text{FH}$ ,  $E_h = 59 \text{ mV}$ <sup>32</sup>). These three oxidizing agents thus probe three redox domains of peat. Oxidation by  $\text{FH}$  probes the most reducing domain(s), identified as  $\text{PP}_1$ . The stronger oxidizing agent  $\text{Fe-Cit}$  will oxidize all of  $\text{PP}_1$  in addition to the somewhat less reducing domain(s),  $\text{PP}_2$ . The strongest oxidizing agent of this series,  $\text{FeCl}_3$  will reduce all of  $\text{PP}_1$  and  $\text{PP}_2$  as well as additional weaker reducing domain(s),  $\text{PP}_3$ .

A summary of the reduction data for four peat reduction experiments is given in Table 5-1. The reduction of  $\text{Fe(III)}$  native to the peat is reported in units of  $\mu\text{mol Fe(II)} \text{ g}^{-1}$  peat and the reducing capacity of peat as measured by oxidation by various ferric sources is reported as  $\mu\text{mol}_c \text{ g}^{-1}$  peat. As expected, because of the molecular complexity of peat, there is variation between samples. Experiments 2 and 3, which were conducted with the same batch of peat from a recently purchased supply exhibit very similar reduction characteristics, and thus provide the primary basis for mechanistic considerations discussed below. Experiments 1 and 4 were conducted using peat from a supply that had been purchased two decades previously and stored under ambient laboratory conditions. As will be discussed below, experiment 4 is distinct from the other three; the primary experimental difference

**Table 5-1.** Summary of Pahokee peat reduction data. PP<sub>1</sub>, PP<sub>2</sub>, and PP<sub>3</sub> represent the redox domains probed by different oxidizing agents. PP<sub>Q</sub> = quinone functional groups; PP<sub>A</sub> = carboxylic acid groups. PP<sub>C</sub> = neutral carbonyl groups; natFe = Fe native to peat. All kinetic data were fit to a diffusion controlled model unless specified. PB refers to a phase boundary limited kinetic model.

	1.7% H <sub>2</sub>		0.5% H <sub>2</sub>	0.5% H <sub>2</sub> 24h Pt/C pretreat
	Exp. 1	Exp. 2	Exp. 3	Exp. 4
<b>Native Fe(II)</b>				
$t_0$ $\mu\text{mol g}^{-1}$	44	36	41	39
$t_\infty - t_0$ $\mu\text{mol g}^{-1}$	81	86	80	72
<b>PP<sub>1</sub> = 2PP<sub>Q</sub></b>				
$t_0$ $\mu\text{mol}_c \text{g}^{-1}$	185	203	174	114
$t_\infty - t_0$ $\mu\text{mol}_c \text{g}^{-1}$	162	264	292	280
<b>PP<sub>2</sub></b>				
$t_0$ $\mu\text{mol}_c \text{g}^{-1}$	30	15	23	15
$t_\infty - t_0$ $\mu\text{mol}_c \text{g}^{-1}$	100	36	24	~310
<b>PP<sub>3</sub></b>				
$t_0$ $\mu\text{mol}_c \text{g}^{-1}$	15	49	30	42
$t_\infty - t_0$ $\mu\text{mol}_c \text{g}^{-1}$	58	61	51	~220
<b>H<sup>+</sup> = PP<sub>A</sub></b>				
$t_\infty$ $\mu\text{mol g}^{-1}$	42	51	34	150
<b>Average H<sup>+</sup>/(PP<sub>2</sub>+PP<sub>3</sub>)</b>	0.26	0.52	0.45	0.43
<b>k<sub>nat Fe</sub></b>	$7.8 \times 10^{-6} \text{ s}^{-1}$	$1.2 \times 10^{-5} \text{ s}^{-1}$	$9.3 \times 10^{-6} \text{ s}^{-1}$	$2.5 \times 10^{-6} \text{ s}^{-1}$
<b>k<sub>PP1</sub></b>	$2.6 \times 10^{-6} \text{ s}^{-1}$	$1.0 \times 10^{-6} \text{ s}^{-1}$	$1.0 \times 10^{-6} \text{ s}^{-1}$	$2.0 \times 10^{-6} \text{ s}^{-1}$
<b>k<sub>PP2</sub></b>	$4.2 \times 10^{-6} \text{ s}^{-1}$	$3.2 \times 10^{-6} \text{ s}^{-1}$	$1.0 \times 10^{-5} \text{ s}^{-1}$	$(\text{PP}_2 + \text{PP}_3) - \text{H}^+$ $> 1 \times 10^{-5} \text{ s}^{-1}$
<b>k<sub>PP3</sub></b>	$5.0 \times 10^{-6} \text{ s}^{-1}$	$3.2 \times 10^{-6} \text{ s}^{-1}$	$1.3 \times 10^{-5} \text{ s}^{-1}$	
<b>k<sub>H+</sub></b>	--	$3.5 \times 10^{-6} \text{ s}^{-1}$	$9.7 \times 10^{-6} \text{ s}^{-1}$	$2.5 \times 10^{-6} \text{ s}^{-1}_{PB}$

being when the Pt/C catalyst was added to the suspension. While experiments 1 and 2, conducted under equivalent experimental conditions, exhibit similar amounts of native iron and a similar reduction capacity of PP<sub>3</sub>, experiment 1 exhibited a notably lesser reduction capacity of PP<sub>1</sub> and greater capacity of PP<sub>2</sub> than did experiment 2 suggesting a different

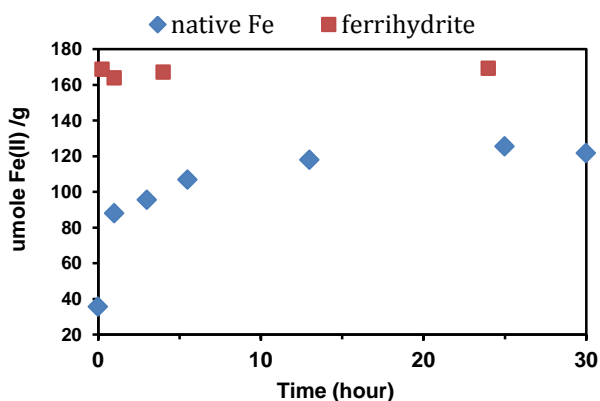


**Figure 5-1.** Comparison of the rate of reduction of iron(III) native to Pahokee peat under 1.7% H<sub>2</sub> and the rate of ferrihydrite reduction by H<sub>2</sub> reduced peat (24 h). The ferrihydrite data were obtained from reactions of ferrihydrite and reduced peat for 15 min, 1, 4, and 24 h, respectively.

components, which may also account for the native reducing capacity of OM that is not oxidized by O<sub>2</sub> but is readily oxidized by ferric iron.<sup>30</sup> In the present work we do not rigorously differentiate between the reversible and non-reversible reducing capacity in peat. Nevertheless we assume that the reducing capacity introduced in the hydrogen reduction and probed by the ferric species is largely reversible.

Upon initiation of the H<sub>2</sub> purge in the chemical reduction experiments, the measured electric potential, which started at ~ 300 mV, dropped to -290 mV (1.7% H<sub>2</sub>) and -240 mV (0.5 % H<sub>2</sub>), respectively, where it remained during the course of the reaction. The measured

distribution of functional groups between the two supplies of peat.

The zero time point, t<sub>0</sub> data in Table 5-1, demonstrates that peat exhibits a finite native reducing capacity, with a greater extent of reduction observed for

oxidants with the largest E<sub>h</sub>. This result is analogous to that observed in studies using soluble OM.<sup>29</sup> The native reducing capacity may include non-reversible redox

electric potentials in all reduction experiments does not vary with the reaction systems, other than with variation of the partial pressure (concentration) of H<sub>2</sub>. The H<sub>2</sub> Pourbaix diagram<sup>31</sup> indicates the H<sup>+</sup>/H<sub>2</sub> reduction potential is -360 mV at standard conditions (pH 6, 1 atm H<sub>2</sub>, 25 °C). The higher observed reduction potentials in these experiments are consistent with the assignment of the reduction potential as the H<sup>+</sup>/H<sub>2</sub> couple because of the significantly lower H<sub>2</sub> pressure.

The extent to which the various Fe(III) oxidizing agents react with fractions of peat

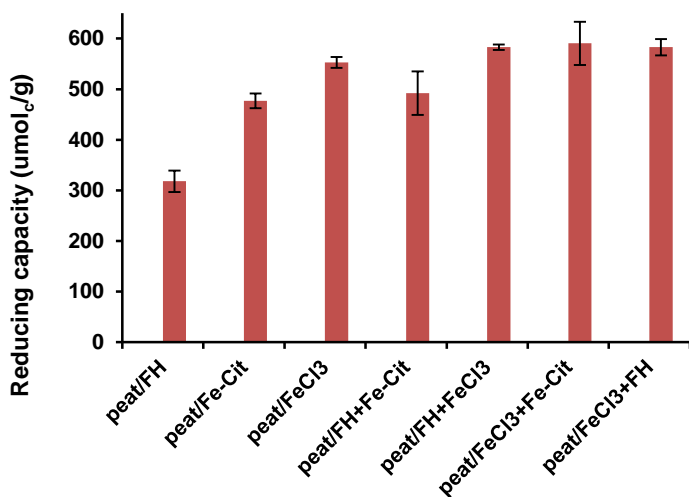


**Figure 5-2.** Reducing capacity of peat after 24 h reduction by 1.7% H<sub>2</sub>/N<sub>2</sub> as probed by different Fe(III) compounds and sequential mixtures of Fe(III) compounds. Error bars show standard deviation of three replicates.

suspensions provide indication of the enhanced reducing capacity imparted to the chemically reduced peat, (*t<sub>∞</sub>*-*t<sub>0</sub>*) data in Table 5-1 and Figures 5-2 and 5-5. The reducing capacity of native peat and chemically reduced peat probed by each of the oxidizing agents follows the trend FeCl<sub>3</sub>>Fe-Cit>FH. Oxidation of the reduced

peat was complete within 15 min of addition of the Fe(III) source as shown in Figure 5-1 for FH. This demonstrates that under the common set reaction conditions, differential reducing capacity is a function of the reduction potential of the Fe(III) source, and not a kinetic function related to changes in the morphology of the peat with time and shaking.<sup>33</sup> To confirm the path independent thermodynamic basis for the differential reduction capacities, a

series of sequential oxidation experiments was performed on samples of peat that had been reduced by H<sub>2</sub> (1.7% H<sub>2</sub> in N<sub>2</sub>) for 24 h (Figure 5-2). Addition of either Fe-Cit or FH to peat already oxidized by FeCl<sub>3</sub> results in no further oxidation. By contrast, if Fe-Cit or FeCl<sub>3</sub> is added to a sample previously oxidized only by FH, additional oxidation occurs. The sum of oxidation by Fe-Cit and FH or by FeCl<sub>3</sub> and FH is equivalent to the extent achieved by Fe-Cit or FeCl<sub>3</sub> independently. While oxidation of hydrogen-reduced peat by Fe(III) compounds is complete within ~15 min, it is interesting to note that, after exposure to air for 48 h the reduced peat retained 80% of its maximum reducing capacity towards FeCl<sub>3</sub>. This is consistent with previous observations of a kinetic barrier to oxidation of reduced organic matter by O<sub>2</sub>.<sup>30,34</sup>

These data cannot simply be explained by the respective differences in the reduction potential of the oxidizing agent. There must also be multiple redox states/domains in peat. This is consistent with reported E<sub>h</sub> values for humic substances at pH 7 that cover a range from -200 mV to +500 mV.<sup>35-38</sup> Two limiting models could account for the distinct redox environments probed by FH, Fe-Cit and FeCl<sub>3</sub>, respectively. In one model, the chemical moieties responsible for the peat's reducing capacity are clustered together in energy so as to exhibit "redox states." Alternatively, a continuum of redox states resulting from the complex assemblage of reducible functionalities in the macromolecular peat may exist for which the chosen oxidizing agents simply identify domains within the continuum. The states vs. domains models are schematically represented in Figure 5-4 as PP<sub>1</sub>, PP<sub>2</sub>, and PP<sub>3</sub>.

## *Kinetic modeling of Pahokee peat chemical reduction*

In an attempt to differentiate these respective models and to gain a better mechanistic understanding of the peat reduction, we examined the reaction kinetics corresponding to the various levels of reduction. The reduction kinetic data for experiments 2 and 3, reactions using the same batch of peat, are presented in Figure 5-3. To measure the reducing capacity of peat using the various Fe(III) redox probes, it was also necessary to measure the reduction of any Fe(III) native to the peat. The peat reduction data for each time point  $t_i$  presented in Figure 5-3 is determined by subtracting the amount of Fe(II) at  $t_0$  and the amount of reduced

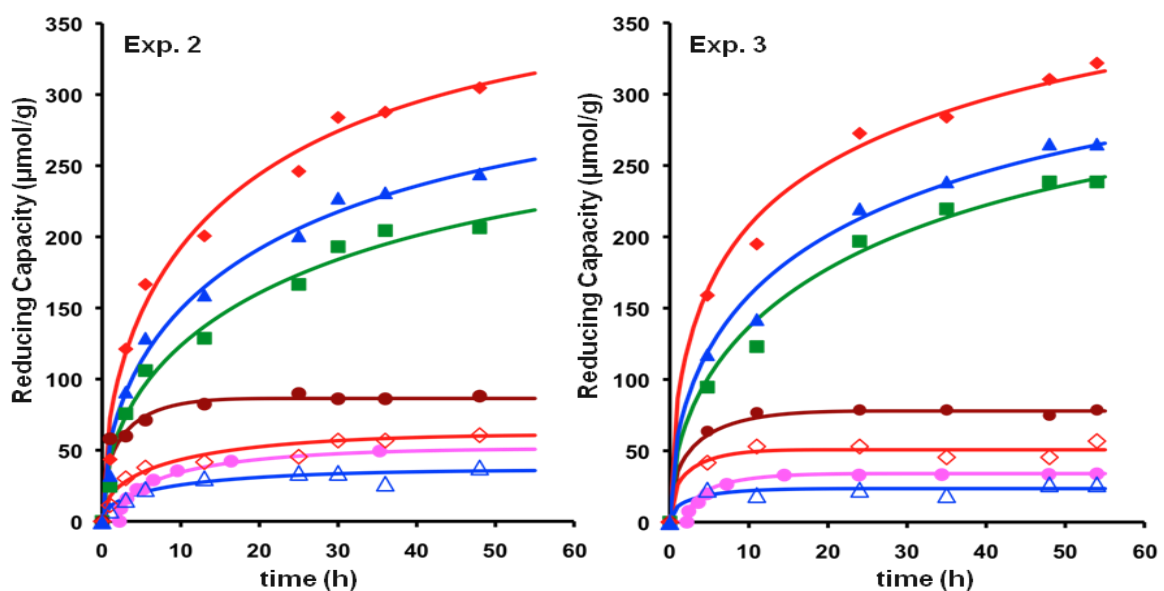


**Figure 5-3.** Reduction kinetics of samples of Pahokee peat (PP) for which the Pt/C catalyst was added immediately preceding reduction by 1.7% H<sub>2</sub>, Exp. 2, and 0.5% H<sub>2</sub>, Exp. 3. Reduction of Fe(III) native to peat (rust circles); the reduction of peat as probed by subsequent oxidation by FH (green squares, PP<sub>1</sub>), by Fe-Cit (blue triangles, PP<sub>1</sub>+PP<sub>2</sub>) and FeCl<sub>3</sub> (red diamonds, PP<sub>1</sub>+PP<sub>2</sub>+PP<sub>3</sub>), the acid consumed to maintain constant pH = 6 (pink circles, PP<sub>A</sub>); and Fe-Cit - FH (open blue triangles, PP<sub>2</sub>) and FeCl<sub>3</sub> - Fe-Cit (open red diamonds, PP<sub>3</sub>). The solid lines represent fits to the kinetic model. See Table 1 caption for denotations.

native iron at  $t_i$  and for each probe treatment from the total 0.5 M HCl extractable Fe(II). The rate of proton consumption required to maintain a constant pH = 6 was also measured.

A variety of factors must be taken into consideration to understand the kinetics of this complex, heterogeneous system. The reduction reaction(s) are catalyzed by Pt/C, thus hydrogen and/or substrate adsorption to the catalyst could be rate determining. Similarly a surface reaction between the hydrogen species and the peat could be rate determining. However, given that the peat itself is a solid phase, and the reducible species are distributed throughout the mass of organic matter, it is unlikely that the solid Pt/C catalyst particles will contact each reducible site of the solid peat. Thus, it is also reasonable to consider that diffusion of electrons, protons, and/or hydride into the solid peat could be rate determining.

The kinetic data for experiments 2-3 are well fit (Figure 5-3) using the model of a diffusion limited reaction proceeding in spherical particles (Eq. 5-1). This is confirmed by a Sharp-Hancock analysis.<sup>39</sup> The Jander equation,<sup>40,41</sup>

$$\left[ 1 - (1 - \alpha)^{\frac{1}{3}} \right]^2 = \frac{2Dk_0t}{r^2} \quad \text{Eq. 5-1}$$

where  $\alpha$  is the fraction of the reaction transformed,  $D$  is the diffusion coefficient, and  $r$  is the radius of the particle, describes this diffusion controlled reaction. Because the size of the peat particles was not explicitly determined but was assumed to be constant for all reactions with the same stock preparation, the data are fit to a particle normalized rate constant  $k = 2Dk_0/r^2$ . Given that  $\alpha$  is a unitless term, it must be multiplied by the amount of product formed at  $t_\infty$ ,  $C_\infty$ , to obtain the amount of reduced product at any given time. Thus the experimental curves are fit to Eq. 5-2.

$$C = C_{\infty} \left[ 1 - (1 - \sqrt{kt}) \right]^3 \quad \text{Eq. 5-2}$$

These fits are significantly superior to the next closest model of a shrinking-core phase boundary controlled reaction proceeding in a spherical particle, Eq. 5-3.<sup>41</sup> The latter will be shown to be important to understand the mechanism of experiment 4.

$$C = C_{\infty} \left[ 1 - (1 - kt)^3 \right] \quad \text{Eq. 5-3}$$

Care must be taken not to over interpret the particle normalized rate constants, as they are expected to vary with particle and sample size. This, in part, likely accounts for the variation in rate constants determined for experiments 1 and 2. Nevertheless, the particle normalized rate constants can provide invaluable mechanistic insight when sample consistency is controlled, such as was done for experiments 2 and 3.

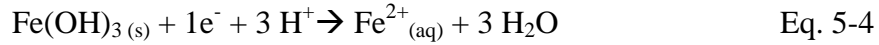
In the reactions 1-3, the rate of PP<sub>1</sub> reduction is significantly slower than reduction of all other species (Table 5-1). By contrast, reduction of Fe(III) native to peat is the fastest reaction observed. Reduction of PP<sub>2</sub> and PP<sub>3</sub> appear to proceed with a common rate constant. The rate constants for the consumption of acid required to keep the system at pH = 6 are equivalent to those observed for the reduction of PP<sub>2</sub> and PP<sub>3</sub>, albeit delayed by about two hours. It is not clear whether this delay is reflective of an actual delay in the reduction process, or the buffering capacity of peat, or an artifact of the auto-titrator. The latter two seem most likely. Of further interest, the rates of reduction of PP<sub>1</sub> and the Fe(III) native to peat are essentially unaffected by the partial pressure of H<sub>2</sub> in the reducing system. By contrast, the rate of reduction of PP<sub>2</sub> and PP<sub>3</sub> and the rate of acid consumption appear to be impeded by the increased H<sub>2</sub> partial pressure. These data suggest that there are two

mechanisms operative in the reduction of peat; likely the result of the reduction of distinct functional groups. Together the distinctive mechanisms, indicated by the comparative rate constants and response to H<sub>2</sub> partial pressure, suggest that peat consists of two redox reservoirs as probed by the chosen ferric species (Figure 5-4). The greater capacity of PP<sub>1</sub> in all cases suggests it to be the primary redox reservoir. PP<sub>2</sub> and PP<sub>3</sub>, by contrast appear to be a common reservoir with Fe-Cit and FeCl<sub>3</sub> probing different extents of a redox continuum.

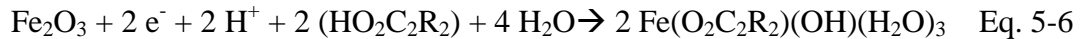
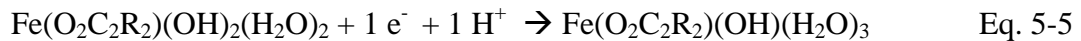
### ***Mechanistic Characterization of the Two Redox Reservoirs***

As described in the introduction a variety of functional groups in peat may be reduced. It has long been recognized that quinones are the primary functional groups, responsible for the reversible redox chemistry of OM.<sup>20,21,42</sup> The reduction of quinones to semiquinones and further to hydroquinones is further known to proceed in one-electron steps via a proton mediated electron transfer mechanism.<sup>21</sup> Though not as frequently invoked in the reversible redox chemistry of OM, carbonyl groups, such as ketones, and carboxylic acids, can be also be reduced by H<sub>2</sub> via hydride attack at the carbonyl carbon and protonation of the oxygen resulting in a secondary alcohol or aldehyde product, respectively.<sup>43</sup> These reduced products can subsequently be re-oxidized by Fe(III) oxidizing agents. These two reduction mechanisms can be differentiated as net 1 e<sup>-</sup>/1 H<sup>+</sup> and 2 e<sup>-</sup>/2 H<sup>+</sup> processes. Note that any 2e<sup>-</sup> processes will account for two equivalents of an Fe(III) redox probe. Given that upon reduction H<sub>2</sub> supplies an equivalent number of electrons and protons, no additional acid is required to balance such redox reactions. Nevertheless, a non-negligible amount of acid is required to maintain a constant pH = 6.

Reduction of native Fe(III) could be implicated as the reason for the acid requirement. The reduction of iron oxides is known to raise the pH as the Fe(III) oxide/hydroxides tend to be solids, and aqueous Fe(II) is often formed upon reduction, Eq. 5-4.<sup>31</sup> With hydrogen as the



reductant a net addition of two protons per aqueous Fe(II) would be required to maintain a constant pH. While not unreasonable, given the quantity of native Fe(III) and the amount of acid consumed, this picture is too simplistic. It has been well established that at the Fe concentrations in peat (~120 mmol Fe kg<sup>-1</sup> peat) and conditions utilized for these experiments, native Fe(III) will be coordinated to OM via a 5-membered oxalate-like Fe(O<sub>2</sub>C<sub>2</sub>R<sub>2</sub>) ring.<sup>44</sup> Furthermore, in our measurements, aqueous Fe(II) is only observed at much higher Fe/peat loadings, presumably after saturating peat iron-coordination capacity. Whether monomeric (Eq. 5-5), or oligomeric (ferrihydrite-like), Eq. 5-6, reduction of Fe(III) native to peat by H<sub>2</sub> should not require additional acid to maintain constant pH; the required protons simply being a byproduct of the hydrogen reduction. That the proton consumption is not attributable to the native Fe(III) reduction is further supported by the noted difference in rate constants  $k_{\text{H}^+}$  and  $k_{\text{nat Fe}}$  as well



as the inverse H<sub>2</sub> partial pressure dependence (Table 5-1).

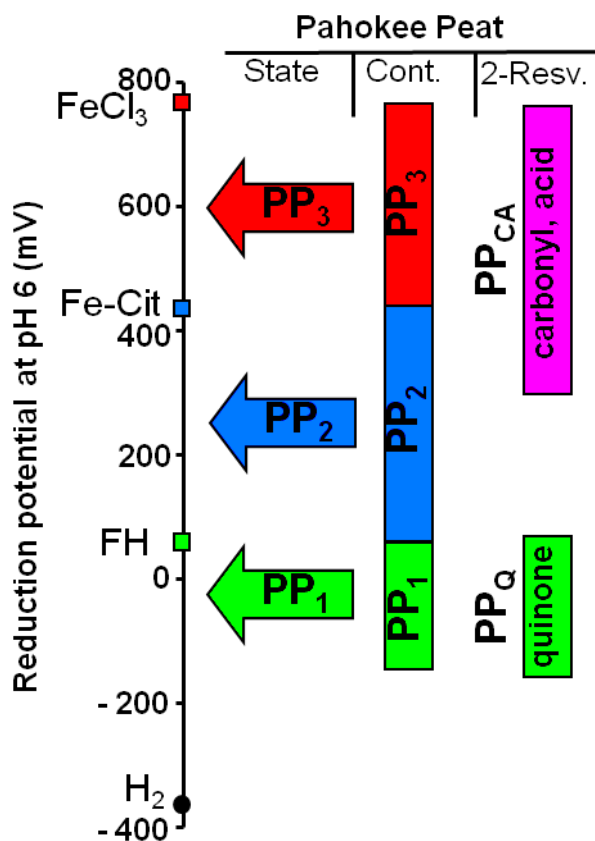


**Figure 5-4.** Schematic drawing showing the estimated reduction potentials in peat based on the redox state, continuum and two-reservoir models in relation to the reduction potentials of  $\text{FeCl}_3$ , Fe-citrate, ferrihydrite, and hydrogen at pH 6.  $\text{PP}_{\text{CA}}$  denotes the sum of neutral carbonyl groups ( $\text{PP}_{\text{C}}$ ) and acid groups ( $\text{PP}_{\text{A}}$ ). See Table 5-1 caption for the rest of denotations.

*The carbonyl reservoir.* Given the equivalence between the rate constants and dependence on  $\text{H}_2$  partial pressure of the ( $\text{PP}_2 + \text{PP}_3$ ) redox-reservoir and the proton consumption, we are left to conclude that the proton consumption is an indicator of the reduction of some fraction of the peat-functional groups within the second reservoir. Experiment 4 (Table 5-1 and Figure 5-5), in spite of its dramatically different reduction capacities and rates, provides strong support for this

assignment. In this experiment, three to five times as much acid was required to maintain a constant pH. Similarly, the reduced  $\text{PP}_2$  and  $\text{PP}_3$  capacity is three to five times greater than that observed for experiments 1-3, whereas the amount of

reducible native Fe(III) is essentially constant for all four reactions. When the  $\text{PP}_1$  capacity of reaction 4 is subtracted from the reduction probed by Fe-Cit and  $\text{FeCl}_3$ , the observed  $\text{PP}_2$  and  $\text{PP}_3$  capacity exhibits an immediate fast increase followed by a more linear rate of increase that tracks with a slope essentially twice that of the rate of proton consumption. Kinetic

analysis of the proton consumption rate in experiment 4 demonstrates that it no longer proceeds with diffusion-controlled kinetics. Rather, its rate is indicative of a shrinking-core phase boundary controlled mechanism, Eq. 5-3 (Figure 5-5). The difference of a factor of two is readily accounted for if this is a 2-electron process whereby two equivalents of the Fe(III) probe are required for each reduced functional group. If a carboxylic acid (denoted as  $PP_A$ ) is reduced to an aldehyde +  $H_2O$ , the loss of the acid functional group will require addition of an external proton to maintain a constant pH, after the OM buffering capacity is exhausted. Though proceeding via a diffusion controlled mechanism in experiments 1-3 and a phase boundary controlled mechanism in experiment 4, we are able to assign the amount of  $PP_A$  to be equivalent to the amount of protons consumed to maintain the constant pH = 6. The difference between the diffusion controlled reactions of experiments 1-3 and the phase boundary controlled reaction of experiment 4 can be accounted for by a different distribution of the Pt/C catalyst, discussed below.

We can subsequently assign the component of the  $PP_2$  and  $PP_3$  reducing capacity in experiment 4 that formed very fast but was not correlated to the added proton requirement, to the reduction of neutral carbonyl functional groups, e.g. ketone, (denoted as  $PP_C$ ) to alcohols. Conversion from a ketone to an alcohol would not have the same effect on the acidity of the system as the above noted reduction of carboxylic acid functional groups. The data for the reduction of  $PP_C$  in experiment 4 can be fit (Figure 5-5) using a model whereby a non-acid consuming  $2e^-$ -process proceeds with a diffusion limited mechanism, analogous to (or faster than) that observed for experiment 3 (equivalent  $H_2$  pressure). In all of the experiments, we

thus propose that the amount of  $PP_C$  in a sample of peat can then be determined from  $1/2(PP_2+PP_3) - H^+$ .

In summary, the sum of  $PP_C$  and  $PP_A$ ,  $PP_{CA}$ , represents the second, more weakly reducing reservoir in peat. The amount of  $PP_{CA}$ , number of acid and neutral carbonyl functional groups, should be equal to  $(PP_2 + PP_3)/2$ . In experiments 2 and 3, which both utilized equivalent

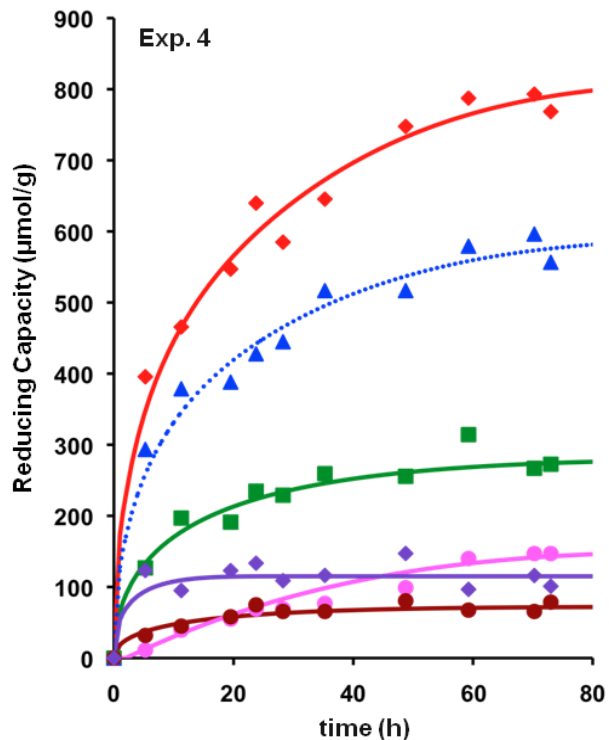


**Figure 5-5.** Kinetics of  $H_2$  reduction of a sample of peat that had been pre-treated with the Pt/C catalyst for 24 h, Exp. 4. Reduction of Fe(III) native to peat (rust circles,  $PP_{nat Fe}$ ); the reduction of peat as probed by subsequent oxidation by FH (green squares,  $PP_1 = PP_Q$ ), by Fe-Cit (blue triangles,  $PP_1 + PP_2$ ) and  $FeCl_3$  (red diamonds,  $PP_1 + PP_2 + PP_3$ ), the acid consumed to maintain constant pH = 6 (pink circles, equals  $PP_A$ ); and calculated neutral carbonyl group,  $PP_C$  (purple diamonds,  $PP_C = (PP_2+PP_3)/2 - H^+$ ). The solid lines represent fits to respective kinetic models; the fit of the Fe-Cit curve is based on an estimated ratio of  $PP_2/PP_3$  and thus represented as a dotted line. See Table 5-1 caption for denotations.

samples of peat,  $(PP_2 + PP_3)/2 \approx H^+ = PP_A$ . Therefore its secondary reservoir consists essentially entirely of reducible acid functional groups. By contrast, the sample of peat used in experiments 1 and 4, a supply purchased more than two decades ago, exhibits a significant amount of neutral carbonyl groups,  $PP_C$ .

Consideration of the mechanistic implications of the assignment of  $PP_2$  and  $PP_3$  reduction to the  $2e^-$  conversion of a  $C=O$  to  $C-O-H$  provides a possible explanation for the

observed inverse hydrogen dependence and dramatic difference between experiments 1-3 and 4. Formation of a  $[\text{H}^{\ominus}\text{--C=O--H}^{\oplus}]^{\ddagger}$  activated complex following hydride attack likely requires the association of both the  $\text{H}_2$  and the carbonyl functional group to be adsorbed to the Pt/C catalyst. In this regard, a higher  $\text{H}_2$  partial pressure may block access of the carbonyl functional groups to the catalyst's surface. This idea is further supported by comparison of experiments 1-3 with experiment 4. The data in experiments one and two most clearly fit a model of diffusion controlled kinetics. The faster rate of experiment three provides less data at the early stage of the reaction, thus mechanism differentiation is less clear. Nevertheless, it too is consistent with diffusion controlled kinetics. Presumably this requires diffusion of the  $\text{H}_2$  and Pt/C catalyst throughout the peat. Given the heterogeneous nature of the system, this is somewhat limited. By contrast, in experiment 4, the peat and Pt/C catalyst were equilibrated for 24 h prior to reduction. As seen in the  $t_0$  data, there was no significant change to the native reducing capacity by this incubation with the catalyst. However, the equilibration apparently distributed the catalyst throughout the peat particles such that more acid and neutral carbonyl sites were accessible for reduction in experiment 4. The very rapid reduction of  $\text{PP}_C$  and slower reduction of  $\text{PP}_A$  suggests that the Pt/C catalyst became associated with the neutral carbonyl functional groups of the peat during the 24 h incubation such that upon diffusion of hydrogen to the catalyst/organic functional group, the reduction proceeded. By contrast, reaction with the acid functional groups is now slowed, and proceeds via a shrinking-core phase boundary mechanism. A phase boundary controlled mechanism implies a structural/bonding change in the particle becomes rate limiting, rather than diffusion of hydride. That the phase-boundary controlled mechanism is not observed in

experiments 1-3 implies that in those reactions without the 24 h catalyst incubation, the catalyst and most of the reduced  $PP_{CA}$  functional groups were at or near the surface of the peat particle.

***The quinone reservoir.*** Having assigned the functional groups of the second redox reservoir to the two-electron reduction of carboxylic acid and neutral carbonyl functional groups ( $PP_{CA}$ ), it is most reasonable to assign the redox chemistry of the primary redox reservoir,  $PP_1$ , to the reversible reduction of quinone functional groups, designated as  $PP_Q$ . As noted above, under the slightly acidic conditions of these experiments, quinones are anticipated to undergo reduction via a proton coupled electron transfer mechanism whereby the quinone oxygen is protonated, followed by a one-electron reduction. These data cannot distinguish a single reduction to semiquinone and two reduction steps to hydroquinone. It is likely that both carbonyls of the quinone are reduced such that the total amount of reducible quinone in the peat,  $PP_Q$ , sample is equivalent to  $1/2PP_1$ . It is not anticipated that such a proton coupled electron transfer mechanism would be significantly impacted by the  $H_2$  partial pressure. A  $H_2$  pressure independence is in fact observed for the reduction of  $PP_1$ . By contrast the proton concentration, as well as the facility of proton diffusion is expected to influence the rate of proton mediated electron transfer. Consistent with this assignment, the rate constant for reduction of  $PP_Q$  in all four experiments is the same, within experimental error (Table 1). Furthermore, it is notable that the  $PP_Q$  reduction capacity is equivalent in all four experiments. It is reasonable to propose that unlike the  $H_2/Pt/C$  diffusion required for  $PP_{CA}$  reduction, proton diffusion throughout the entire peat particle is feasible. Thus the entire  $PP_Q$  capacity is accessible independent of catalyst pre-treatment.

**Native Iron.** Reduction of the native Fe(III) also is a one-electron process; likely proton coupled electron transfer. Here a Fe-OH ligand is likely protonated preceding electron transfer. Consistent with this model, the rate of native Fe(III) reduction is essentially equivalent for experiments 1-3, although almost an order of magnitude faster than that for PP<sub>Q</sub> reduction. We propose that the difference between the rate of reduction for PP<sub>Q</sub> and native Fe(III) may result from a more facile diffusion of H<sup>+</sup> to acid/anion sites, such as likely coordinated to the Fe(III), than to neutral quinone functional groups. This reasoning is consistent with the reduced rate of native Fe(III) reduction in experiments 1 and 4 for which the samples of peat are observed to have a greater ketone/neutral carbonyl content.

Based on the collective results from analyses discussed above, a more elaborate, two-reservoir model for the redox properties of Pahokee peat is presented in Fig. 5-4 (denoted as 2-Resv.). Most strongly reducing is the PP<sub>Q</sub> reservoir, capable of reducing FH. Quite distinct from this reservoir is a second reservoir PP<sub>CA</sub> consisting of neutral carbonyl and carboxylic acid functional groups. The latter is reasonably represented as a redox continuum that cannot be oxidized by FH, and for which the E<sub>h</sub> of Fe-Cit is in the middle of the continuum. FeCl<sub>3</sub> marks the upper bound of this continuum that we have measured, though it is reasonable to suspect there are additional functional groups that could be oxidized with a stronger oxidizing agent.

### ***Pahokee peat as a Redox Shuttle***

Finally we consider the implications of this reduction rate data on the generally accepted understanding of an electron shuttling role that OM is believed to play in the reduction of iron(III) oxides. As has been shown by various investigators, reduced OM

removed from the electron source, H<sub>2</sub> in these experiments, is capable of reducing a variety of Fe(III) substrates.<sup>13,25,26</sup> This confirms the ability of OM to act as what we describe as a remote electron shuttle. However, as seen in Figure 5-3 and Table 5-1, native Fe(III) is reduced at a faster rate than the organic functional groups. Therefore, the peat is not acting in a manner we describe as an active shuttle with respect to the reduction of native Fe(III). Instead, native Fe(III) is reduced via a mechanism independent of the peat. Of more relevance to OM mediation of redox chemistry in soils, it is instructive to consider the reduction of a mixture of peat and the non-crystalline iron(III) oxide, FH. Reactions to determine the amount of time the external oxidant must react with the reduced peat to measure its reducing capacity, Figure 5-1, indicate that pre-reduced peat is capable of

**Table 5-2.** Post-reduction reducing capacity of a peat/FH mixture with peat input of 1.55 g g<sup>-1</sup>FH reducing FH at a rate even faster than is observed for the H<sub>2</sub>, Pt/C reduction of

Reaction type	Time (hour)	% Fe(III) reduced	1.55 g PP/ g FH	
			PP <sub>Q</sub> μmol <sub>c</sub> g <sup>-1</sup> peat	PP <sub>CA</sub> μmol <sub>c</sub> g <sup>-1</sup> peat
microbial	11	8.6	0	93
	24	16.8	0	130
chemical	8	4.8	62	23
	24	8.0	82	41

native Fe(III) in peat. Thus to test the redox-shuttle mechanism we investigated the reduction of mixtures of peat with an excess of FH. Given the above rate data, if peat is acting as a

redox shuttle, then no residual peat reducing capacity with respect to FH should be observed until all the FH is reduced.

Reaction mixture with 1.55 g peat  $\text{g}^{-1}$  FH, about a four-fold excess based on the above measured reducing capacity of  $\text{PP}_Q$ , were examined. Equivalent peat/FH reaction mixture was reduced for 24 h chemically ( $\text{H}_2$ , Pt/C) and microbially ( $\text{H}_2$ , CN 32). The post-reduction reducing capacity of each reaction mixture was then probed with the oxidizing agents FH and  $\text{FeCl}_3$ ; data are given in Table 5-2. Interestingly, the post-reduction samples from the chemical reduction exhibited reducing capacity characteristic of both  $\text{PP}_Q$  and  $\text{PP}_{CA}$  reservoirs even though only 5% of the FH in the experimental mixture was reduced after 8 h and 8 % was reduced after 24 h. Given that an excess of FH was present in the initial reaction mixture, the observation that additional FH can be reduced by post-reduction  $\text{PP}_Q$  suggests that the original reactant FH was reduced to a less reactive intermediate mixed-valent phase, and/or that a blocking Fe(II) shell is created on the FH particle surface. Intermediates of magnetite and green rust have been reported in iron(III) oxide reduction in the presence of OM<sup>45</sup>. Nevertheless our data indicate that  $\text{PP}_Q$  cannot react with either the mixed-valent or Fe(II)-surface blocked FH. Based on these results it can be concluded that if  $\text{PP}_Q$  acts as an active shuttle, it only facilitates surface reactions and/or the partial reduction of FH to a mixed valent state. But we additionally observe that the extent of reduction of both  $\text{PP}_Q$  and  $\text{PP}_{CA}$  as a function of time in the peat/FH reaction mixture tracks almost identically to the extent of reduction of peat itself (compare Table 5-2 and Figure 5-3). Together all these data clearly indicate that there is no significant amount of active electron shuttling by the peat between the chemical reduction source and the ferrihydrite.

We have not yet examined the microbial reduction kinetics of peat as extensively as the above reported measurement of the chemical reduction kinetics. However, data from the microbial reduction of the 1.55 g peat g<sup>-1</sup> FH mixture indicate that under the conditions examined, the microbial reduction was much more effective at reducing the FH than was the chemical reduction, with twice the amount of Fe(II) produced (Table 5-2). Furthermore, the post-microbial reduction peat/FH mixture exhibits no PP<sub>Q</sub> reduction capacity (capacity with respect to FH), but more than three times the PP<sub>CA</sub> reducing capacity. Since there is no residual PP<sub>Q</sub> capacity in this experiment, it is possible that an active electron-shuttle between the microbes and the FH is operative. Nevertheless, while it is completely reasonable that different mechanism may be operative in the reduction of the OM depending on the reducing agent (H<sub>2</sub>, Pt/C vs. H<sub>2</sub>, microbes), it would be most unusual for the OM to act differently toward iron oxides depending on which species was responsible for its reduction. We submit that the Fe(II) complexation model suggested by Royer et al.<sup>46</sup> may more appropriately account for the role of peat in the microbial reduction of FH. Royer et al.<sup>33,46</sup> demonstrated that biological iron reduction is self-inhibited by the production of Fe(II) and enhanced by OM, and suggested the OM may complex the Fe(II), removing it from the microbes thus moderating the Fe(II) inhibition of further microbial reduction. The lack of any PP<sub>Q</sub> reducing capacity in the microbial reduction of this peat/FH mixture suggests that under the microbial reduction in the presence of peat, no blocking Fe(II) or mixed valent shell is formed on the surface of the FH particle. Instead, the microbes may reduce the FH directly or by OM-electron shuttle and then the OM complexes the reduced Fe(II), removing it from the microbes and preventing any further inhibition of the microbial reduction. Thus the primary

effect of the combination of microbes and peat may be to alter the reaction pathways assessable for FH reduction. This is reminiscent of the work of O'Loughlin et al.,<sup>45</sup> which demonstrated that microbial reduction of lepidocrocite in the absence of organic matter forms magnetite whereas in the presence of various humic acid species green rust is the more likely product.

In addition we note that the microbial reduction accessed a greater amount of the  $PP_{CA}$  reducing capacity than did chemical reduction. Nevertheless, it still did not achieve the  $PP_{CA}$  capacity achieved in experiment 4, in which the peat was incubated with the Pt/C catalyst for 24 h prior to chemical reduction. These data suggest that the interaction of the microbes and peat has the ability to restructure the peat such that a greater number of the acid and/or neutral carbonyl functional groups are accessible. While some of these functional groups are reduced, as evidenced by oxidation by the  $FeCl_3$  probe used to measure the  $PP_{CA}$  capacity, these functional groups also likely afford a greater capacity for the peat to complex any Fe(II) such that the microbial reduction is enhanced.

## 5.4. Conclusions

As recognized in the literature, multiple redox components exist in Pahokee peat. Kinetic data of the reduction of the redox components probed by  $FeCl_3$ , Fe-Cit, and ferrihydrite indicate that within the range of  $E_h$  probed with these oxidizing agents, there exist two redox reservoirs. The dominant reservoir exhibits kinetics consistent with a proton coupled electron transfer mechanism, limited by proton diffusion. This reservoir is assigned to quinone redox-active functional groups. The second reservoir exhibits kinetics consistent with a  $2e^-$ , hydride/proton transfer mechanism consistent with the reduction of carbonyl

functional groups. The requirement of acid addition to maintain a constant pH implies that a significant number of the reducible carbonyl groups are carboxylic acids. Thus, by measurement of the amount of acid required to maintain the constant pH = 6, and the amount of reduced peat that can be oxidized by FH and FeCl<sub>3</sub> it is possible to quantify amount quinone, carboxylic acid and neutral carbonyl functional groups that are involved in the redox chemistry of peat.

Chemical reduction of a peat/FH mixture demonstrates that while peat can act as a remote electron shuttle, neither the quinone (PP<sub>Q</sub>) nor the carbonyl (PP<sub>CA</sub>) reservoirs act as an active shuttle with respect to the reduction of iron oxides. Chemical reduction of FH in the presence of peat results in the reduction of both species independently. The analogous microbial reduction experiment of the peat/FH mixture does not similarly refute the ability of peat to function as an active electron shuttle. However, the data exhibiting an enhanced microbial reduction of FH in the presence of peat is equally consistent with a mechanism whereby peat complexes Fe(II), removing its inhibitory effect on the microbes. These data further suggest that microbial and chemical reduction of ferrihydrite may proceed via different mechanisms. Chemical reduction apparently proceeds with the formation of a blocking Fe(II) or mixed valent shell around the FH particles, which limits the extent of reduction. Microbial reduction does not appear to form this same kind of core/shell structure, and may directly reduce the FH. Blocking/limiting of microbial reduction may occur at the microbe, rather than the FH particle surface. Thus, the role of OM in the reduction of iron oxides may involve controlling which reaction mechanism(s) is operative more so than serving as an active electron shuttle.

## 5.5. Reference

- (1) Bennett, B.; Dudas, M. J. *Journal of Environmental Engineering and Science* **2003**, *2*, 265.
- (2) Mort, H. P.; Slomp, C. P.; Gustafsson, B. G.; Andersen, T. J. *Geochimica Et Cosmochimica Acta* **2010**, *74*, 1350.
- (3) Peretyazhko, T.; Sposito, G. *Geochimica Et Cosmochimica Acta* **2005**, *69*, 3643.
- (4) Violante, A.; Pigna, M. *Soil Science Society of America Journal* **2002**, *66*, 1788.
- (5) Asta, M. P.; Cama, J.; Martinez, M.; Gimenez, J. *Journal of Hazardous Materials* **2009**, *171*, 965.
- (6) Missana, T.; Alonso, U.; Scheinost, A. C.; Granizo, N.; Garcia-Gutierrez, M. *Geochimica Et Cosmochimica Acta* **2009**, *73*, 6205.
- (7) Sannino, F.; De Martino, A.; Pigna, M.; Violante, A.; Di Leo, P.; Mesto, E.; Capasso, R. *Journal of Hazardous Materials* **2009**, *166*, 1174.
- (8) Lee, G.; Faure, G. *Water Air and Soil Pollution* **2007**, *186*, 221.
- (9) Kumpiene, J.; Lagerkvist, A.; Maurice, C. *Waste Management* **2008**, *28*, 215.
- (10) Murray, G. C.; Hesterberg, D. *Soil Science Society of America Journal* **2006**, *70*, 1318.
- (11) Pedersen, H. D.; Postma, D.; Jakobsen, R. *Geochimica Et Cosmochimica Acta* **2006**, *70*, 4116.
- (12) Tufano, K. J.; Reyes, C.; Saltikov, C. W.; Fendorf, S. *Environmental Science & Technology* **2008**, *42*, 8283.

- (13) Lovley, D. R.; Coates, J. D.; BluntHarris, E. L.; Phillips, E. J. P.; Woodward, J. C. *Nature* **1996**, *382*, 445.
- (14) Kappler, A.; Benz, M.; Schink, B.; Brune, A. *Fems Microbiology Ecology* **2004**, *47*, 85.
- (15) Wolf, M.; Kappler, A.; Jiang, J.; Meckenstock, R. U. *Environmental Science & Technology* **2009**, *43*, 5679.
- (16) Amstaetter, K.; Kappler, A. *Geochimica Et Cosmochimica Acta* **2009**, *73*, A38.
- (17) Royer, R. A.; Burgos, W. D.; Fisher, A. S.; Jeon, B. H.; Unz, R. F.; Dempsey, B. A. *Environmental Science & Technology* **2002**, *36*, 2897.
- (18) Roden, E. E.; Kappler, A.; Bauer, I.; Jiang, J.; Paul, A.; Stoesser, R.; Konishi, H.; Xu, H. F. *Nature Geoscience* **2010**, *3*, 417.
- (19) Roden, E. E.; Wetzel, R. G. *Abstracts of the General Meeting of the American Society for Microbiology* **1999**, *99*, 452.
- (20) Klapper, L.; McKnight, D. M.; Fulton, J. R.; Blunt-Harris, E. L.; Nevin, K. P.; Lovley, D. R.; Hatcher, P. G. *Environmental Science & Technology* **2002**, *36*, 3170.
- (21) Scott, D. T.; McKnight, D. M.; Blunt-Harris, E. L.; Kolesar, S. E.; Lovley, D. R. *Environmental Science & Technology* **1998**, *32*, 2984.
- (22) Debnath, S.; Hausner, D. B.; Strongin, D. R.; Kubicki, J. *Journal of Colloid and Interface Science* **2010**, *341*, 215.
- (23) Suter, D.; Banwart, S.; Stumm, W. *Langmuir* **1991**, *7*, 809.
- (24) Afonso, M. D.; Stumm, W. *Langmuir* **1992**, *8*, 1671.
- (25) Jiang, J.; Kappler, A. *Environmental Science & Technology* **2008**, *42*, 3563.

- (26) Peretyazhko, T.; Sposito, G. *Geoderma* **2006**, *137*, 140.
- (27) Bamford, C. H., Tipper, C. F. H., Compton, R. G., Eds. 1984.
- (28) Kononets, M. Y.; Pakhomova, S. V.; Rozanov, A. G.; Proskurnin, M. A. *Journal of Analytical Chemistry* **2002**, *57*, 586.
- (29) Bauer, M.; Heitmann, T.; Macalady, D. L.; Blodau, C. *Environmental Science & Technology* **2007**, *41*, 139.
- (30) Bauer, I.; Kappler, A. *Environmental Science & Technology* **2009**, *43*, 4902.
- (31) Wulfberg, G. In *Inorganic Chemistry*; Wulfberg, G., Ed.; University Science Books: Sausalito, CA, 2000, p 243~314.
- (32) Thamdrup, B. In *Advances in Microbial Ecology*; B., S., Ed.; Kluwer Academic/Plenum Publishers: New York, 2000; Vol. 16, p 41~84.
- (33) Royer, R. A.; Dempsey, B. A.; Jeon, B. H.; Burgos, W. D. *Environmental Science & Technology* **2004**, *38*, 187.
- (34) Thieme, J.; McNulty, I.; Vogt, S.; Paterson, D. *Environmental Science & Technology* **2007**, *41*, 6885.
- (35) Visser, S. A. *Nature* **1964**, *204*, 581.
- (36) Matthiessen, A. In *Humic Substances in the Global Environment and Implication on Human Health*; Senesi, N., Miano, T. M., Eds.; Elsevier Science B.V.: Amsterdam, The Netherlands, 1994.
- (37) Osterberg, R.; Shirshova, L. *Geochimica Et Cosmochimica Acta* **1997**, *61*, 4599.
- (38) Straub, K. L.; Benz, M.; Schink, B. *Fems Microbiology Ecology* **2001**, *34*, 181.

- (39) Hancock, J. D.; Sharp, J. H. *Journal of the American Ceramic Society* **1972**, *55*, 74.
- (40) Jander, W. *Zeitschrift Fur Anorganische Und Allgemeine Chemie* **1927**, *163*, 1.
- (41) Koga, Y.; Harrison, L. G. In *Comprehensive Chemical Kinetics*; Bamford, C. H., Tipper, C. F. H., Compton, R. G., Eds.; Elsevier Science Publishers B.V.: Amsterdam, The Netherlands, 1984; Vol. 21, p 119~149.
- (42) Ratasuk, N.; Nanny, M. A. *Environmental Science & Technology* **2007**, *41*, 7844.
- (43) Noyori, R.; Ohkuma, T. *Angewandte Chemie-International Edition* **2001**, *40*, 40.
- (44) Karlsson, T.; Persson, P. *Geochimica Et Cosmochimica Acta* **2010**, *74*, 30.
- (45) O'Loughlin, E. J.; Gorski, C. A.; Scherer, M. M.; Boyanov, M. I.; Kemner, K. M. *Environmental Science & Technology* **2010**, *44*, 4570.
- (46) Royer, R. A.; Burgos, W. D.; Fisher, A. S.; Unz, R. F.; Dempsey, B. A. *Environmental Science & Technology* **2002**, *36*, 1939.

**Chapter 6: Influence of Pahokee peat on ferrihydrite  
chemical and microbial reduction**

## Abstract

Soil organic matter (OM) has been found to enhance Fe(III) oxide microbial reduction, which has been attributed to the electron shuttle mechanism. However, it is largely unknown whether OM exerts the same impact on ferric oxide chemical reduction. Aiming at elucidating the role of OM in ferric oxide reduction, ferrihydrite (FH) and particulate Pahokee peat were chosen to represent soil Fe(III) oxide minerals and OM in a series of reduction experiments that were conducted with  $H_{2(gas)}$  and a Pt catalyst or *Shewanella putrefaciens* (strain CN32). Ferrihydrite chemical reduction follows a 2-step reduction mechanism. The presence of peat alters the extent or rate of both steps. However, ferrihydrite chemical reduction is inhibited by peat. The impact of peat on ferrihydrite chemical reduction follows a 3-regime pattern depending on the peat loading. Kinetic modeling of all ferrihydrite chemical reduction data reveals that surface blocking and particle disaggregation by peat are two competing factors controlling the actual impact. Nevertheless, Pahokee peat does not act as an active electron shuttle in ferrihydrite chemical reduction. On the contrary, the combination of microorganisms and peat facilitates the operation of the electron shuttling mechanism and ferrihydrite microbial reduction is enhanced by peat. Dissolved Fe(II) data from the comparison between chemical and microbial reduction also suggest that peat facilitates the reduction by Fe(II) complexation.

## 6.1. Introduction

Iron oxide minerals, e.g. ferrihydrite or goethite, provide sorption media for oxyanions (e.g.  $\text{PO}_4^{3-}$ ,  $\text{AsO}_4^{3-}$ ,  $\text{SeO}_4^{2-}$ )<sup>1-4</sup> and trace metals<sup>5,6</sup> in soils or other environmental systems, which is critical to maintain environmental health. Iron is redox active in a broad range of reduction potentials that are consequential of change of oxic conditions in soils due to, e.g. water table fluctuation.<sup>7</sup> Increased dissolved phosphorus is normally observed as the soil reduction potential drops. Lab scale studies on Fe(III)-oxide minerals reduction have confirmed that Fe(III) reduction releases the adsorbed species concomitantly.<sup>8-11</sup> The close relation between Fe(III) reduction and sorbate release suggests it is important to understand the factors that affect Fe(III) oxide reductions, as it is these factors that control the rate and extent of reductive dissolution of the sorbates. Particularly, knowledge of the impact from other soil components on oxide mineral reduction is critical for controlling the dynamics of soil nutrients/pollutants.

Organic matter (OM) is an integral component in soils for it participates in many soil chemical and physical processes.<sup>12,13</sup> Moreover, research has shown that organic matter plays an important role in ferric oxide reduction. It has been found that OM can store electrons through biological reduction process; then transfer the electrons to electron acceptors, e.g. Fe(III).<sup>14-16</sup> In combination with the observed enhanced rate of Fe(III)-oxide microbial reduction in the presence of OM,<sup>14,17-22</sup> it is believed that OM enhances ferric oxide microbial reduction via an electron shuttle mechanism. Several investigators have established that microbial and chemical reduction reduce humic substances to the same extent,<sup>14,16,23</sup> which implies that the same functional groups are acting as the electron acceptors independent of

the method of reduction. Thus, it is reasonable to expect that OM also enhances ferric oxide chemical reduction. In our previous investigation on the redox properties of particulate Pahokee peat,<sup>24</sup> however, it clearly shows that solid peat acts as an active shuttle only in ferrihydrite (FH) microbial reduction, not in the chemical reduction. Thus, organic matter might not always enhance ferric oxide reduction, particularly chemical reduction.

According to the literature, various factors can affect ferric oxide chemical reduction. Murray and Hesterberg<sup>25</sup> reported that ferrihydrite hydrogen reduction rate was reduced by ~75% with a boehmite input of 0.002 g g<sup>-1</sup> FH, which was attributed to the adsorbed Al from boehmite dissolution. Similarly, ferrihydrite reduction by ascorbic acid was suppressed by exposure to an organic lipid which formed a 7 nm thick layer on the minerals surface.<sup>26</sup> Hence, adsorbed species appear to impede the chemical reduction of ferric oxides via surface blocking. By contrast, oxalate was shown to enhance hematite reduction by ascorbic acid.<sup>27</sup> It has been hypothesized that oxalate facilitates Fe(II) transport by forming soluble Fe(II)-oxalate complexes.

For ferric oxide microbial reduction, Fe(II) accumulation was found to greatly inhibit the reduction.<sup>28,29</sup> Thus, addition of an Fe(II) complexation agent, e.g. ferrozine or continuous-flow greatly enhances microbial ferric oxide reduction because the reduction passivating factor, Fe(II) is removed.<sup>20,30,31</sup> Particle size of the mineral also exerts impact on ferric oxide microbial reduction. Bosch et al.<sup>32</sup> illustrated that nanosized ferrihydrite colloids were reduced at a rate that is two order of magnitude higher than that at which bulk ferrihydrite was reduced biologically.

Interconversion between Fe(II) and Fe(III) occurs along with the fluctuation of redox potentials in soils.<sup>33</sup> So ferric oxide chemical reduction is equally important as microbial reduction in soils and other environmental systems. However, research attention mainly focuses on ferric oxide microbial reduction in the presence of organic matter. While it is well established that OM enhances ferric oxide microbial reduction, it is still not clear whether OM enhances or impedes the chemical reduction. Because of its vicinity to oxide mineral and its redox activity in soils, organic matter merits a sophisticated mechanistic investigation on its role on ferric oxide chemical reduction.

The chemical reduction of ferric oxides has been proposed to proceed via a 2-step<sup>34-36</sup> or 3-step<sup>37-40</sup> mechanism. Either mechanism involves the formation of Fe<sub>3</sub>O<sub>4</sub> as an intermediate, which has been confirmed by in situ XRD (X-ray diffraction) or XANES (X-ray absorption near edge structure spectroscopy) analyses in Fe(III)-oxide reduction.<sup>40-42</sup> The multiple steps in Fe(III)-oxide reduction could involve multiple kinetic functions controlling the reduction process. However, most of the studies of ferric oxide reduction under the influence of organic matter omit a rigorous kinetic analysis so that a true mechanistic understanding of the influence of OM on ferric oxide reduction is difficult to achieve.

Aiming at a better understanding of the role of organic matter on ferric oxide reduction, the investigation presented in this paper chose ferrihydrite, the most ubiquitous ferric oxide mineral in terrestrial systems and particulate Pahokee peat to represent soil Fe(III)-oxide and organic matter. The focus of this work is ferrihydrite chemical reduction in comparison to microbial reduction. The specific objectives are: 1) delineate the role of Pahokee peat in ferrihydrite chemical and microbial reduction; 2) apply kinetic modeling to

analyze ferrihydrite chemical reduction kinetic data; 3) elucidate the underlying mechanisms of peat influence on ferrihydrite chemical reduction in comparison with microbial reduction. The findings of this investigation are expected to shorten the gap between organic matter influence and ferric oxide chemical reduction.

## **6.2. Materials and methods**

***Pahokee peat hydration*** Pahokee peat purchased from International Humic Substances Society (IHSS) was hydrated prior to usage. Detailed hydration procedure can be found in the Material and method section of Chapter 4.

***Ferrihydrite synthesis and characterization*** Details for ferrihydrite synthesis and characterization can be found in the Materials and Method section of Chapter 4.

***Reduction experiments*** Reduction experiments were performed using a 2-L water jacketed glass reactor vessel (Wilmad-Labglass Corp., Buena, NJ), wrapped with Al foil to avoid photochemical reactions and maintained at 25 °C with a circulating water bath. The reactions were maintained at a constant pH of 6.0 using a Radiometer Analytical Model TM850 Autotitrator (Radiometer Analytical Corp., Lyon, France) with 0.05 M HCl or KOH. The electrical potential of each reaction was measured against a Ag/AgCl reference electrode via a Pt working electrode and reported with respect to S.H.E.

***Chemical and microbial reduction of Peat/FH mixtures*** All reaction systems contained 0.5 g FH kg<sup>-1</sup> suspension. The total mass of a suspension was 0.8 kg. In a typical experiment, an aliquot of peat suspension (0~0.88 g dry mass equivalent) was weighed into a 1-L HDPE bottle along with 300 mL of 0.05 M KCl solution and the pH was raised to ~5

with 0.05 M KOH. An aliquot of FH suspension (equivalent to 0.4 g dry mass) was then added to the peat suspension and the pH adjusted to 6. KCl (0.05 M) was then added to the suspension to yield a total mass of 800 g. In the follow section for results and discussion, individual experiments are identified by the respective g peat per g ferrihydrite (ranging from 0 to 2.2 g g<sup>-1</sup>). Based on our calculation, the molar mass of the synthesized ferrihydrite is 95.03 g mole<sup>-1</sup> Fe. In all reaction systems, total Fe concentration was equal to 5262 mM.

The peat/FH suspension was then transferred to the glass reactor and purged with N<sub>2</sub> for 24 hours prior to initiation of reduction. To expedite electron transfer between H<sub>2</sub> and the electron acceptor(s), a powder of 10% Pt on activated carbon (Pt/C, Sigma Aldrich Co., Milwaukee, WI) was added to the suspensions as a catalyst at a rate of 0.25 g g<sup>-1</sup> FH in all chemical reduction reactions prior to H<sub>2</sub> purge.

For microbial reduction, *Shewanella putrefaciens* (strain CN32) was inoculated to the reaction mixtures at a concentration of 10<sup>8</sup> cells mL<sup>-1</sup> suspension prior to H<sub>2</sub> purging. The initial culture of CN32 was provided by Dr. Edward O'Loughlin, Bioscience Division, Argonne National Laboratory. CN32 was grown aerobically in tryptic soy broth at ambient temperature. Cells were harvested by centrifugation (15,680×g at 20 °C for 7 min) from a 16 h-old culture (late log-phase) and washed three times with sterile 0.05 M KCl. Cell pellets were resuspended in sterile 0.05 M KCl. Cell density was determined by absorbance at 420 nm.<sup>21</sup>

Both chemical and microbial reduction of ferrihydrite of peat/FH mixtures was achieved by purge of H<sub>2</sub> gas at a concentration of 1.7% in N<sub>2</sub> (65 mL/min flow rate) for 48 hours. For a more complete understanding of ferrihydrite chemical reduction, ferrihydrite

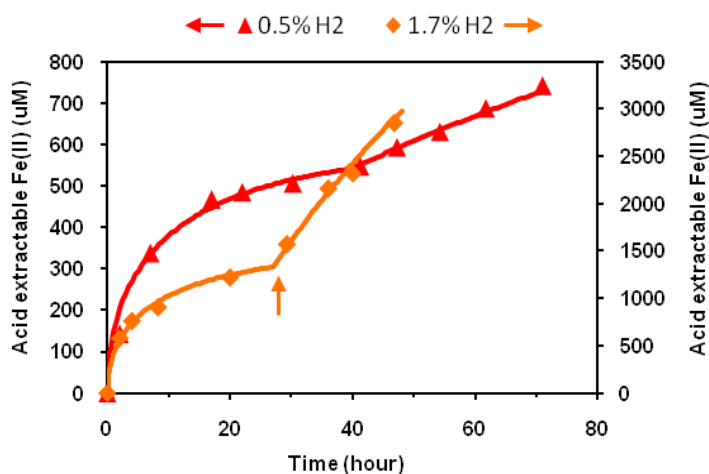
was also reduced by H<sub>2</sub> gas at a lower concentration 0.5%. Periodically 10 mL suspension fractions were collected and placed in a N<sub>2</sub> flushed glove box. 2 mL of each fraction was mixed with 2 mL 1 M HCl in a sealed amber serum bottle and allowed to equilibrate for 24 hours. The resultant mixture was filtered, and the 0.5 M HCl extractable Fe(II) in the supernatant measured using the ferrozine method.<sup>43</sup> The remaining suspension fraction was filtered using a 0.2 μM membrane for analyses of dissolved Fe(II) and organic carbon (DOC). DOC was measured with a Schumadzu TOC-5400 total organic carbon analyzer.

### 6.3. Results

#### *Ferrihydrite chemical reduction by H<sub>2</sub> (Pt/C catalyzed)*

It is important to understand the mechanism of ferrihydrite chemical reduction before attempting to understand any impact peat might have on FH reduction. Production of acid extractable Fe(II) as a function of

time is presented in Figure 6-1. Clearly there are two distinct portions of the reduction reaction. With 1.7% H<sub>2</sub>, approximately 40% of the reaction first takes place in



the first step in which the data are well fit using the model of a diffusion limited reaction proceeding in spherical particles (Eq. 6-1).

**Figure 6-1.** Production of 0.5 M HCl extractable Fe(II) during ferrihydrite reduction by 1.7% and 0.5% H<sub>2</sub> with a Pt/C catalyst at pH 6. Each suspension contained 0.5 g FH kg<sup>-1</sup>. Symbols represent experimental data, solid lines are the fits.

Discussion of Eq. 1 can be found in the results and discussion section of Chapter 5. The calculated diffusion curve exhibits a rate constant of  $3.0 \times 10^{-6} \text{ sec}^{-1}$ . The rest of the reaction then is well fit by a shrinking-core phase boundary controlled reaction

$$C = C_{\infty} \left[ 1 - \left( 1 - \sqrt{kt} \right) \right]^3 \quad \text{Eq. 6-1}$$

proceeding in a spherical particle as described by Eq. 2, where  $t = t_i - t_0$ , the time at which the apparent break in mechanisms is observed. The calculated rate constant and mechanism break time are  $k = 2.1 \times 10^{-6} \text{ sec}^{-1}$  and  $t_0 = 27 \text{ h}$ , respectively. (highlighted by the arrow under the curve in Fig. 6-2).

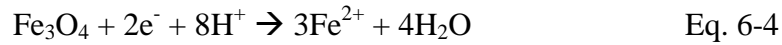
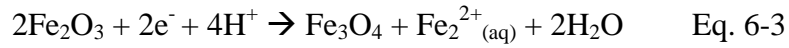
$$C = C_{\infty} \left[ 1 - (1 - kt)^3 \right] \quad \text{Eq. 6-2}$$

The sum of these two rate expressions remarkably fits the observed kinetics of FH chemical reduction. These two rate expressions also successfully fit the kinetic data of ferrihydrite reduction by 0.5%  $\text{H}_2$  (Fig. 6-2), with the rate constants being  $2.5 \times 10^{-6}$  and  $1.0 \times 10^{-7} \text{ s}^{-1}$  for the diffusion and phase boundary controlled reactions, respectively. The second mechanism breaks in at  $t_0 = 40 \text{ h}$ . Apparently, change of the reductant concentration does not affect the reduction mechanism, but the rate constants and extents of both steps, which are noticeably lower with lower  $\text{H}_2$  concentration.

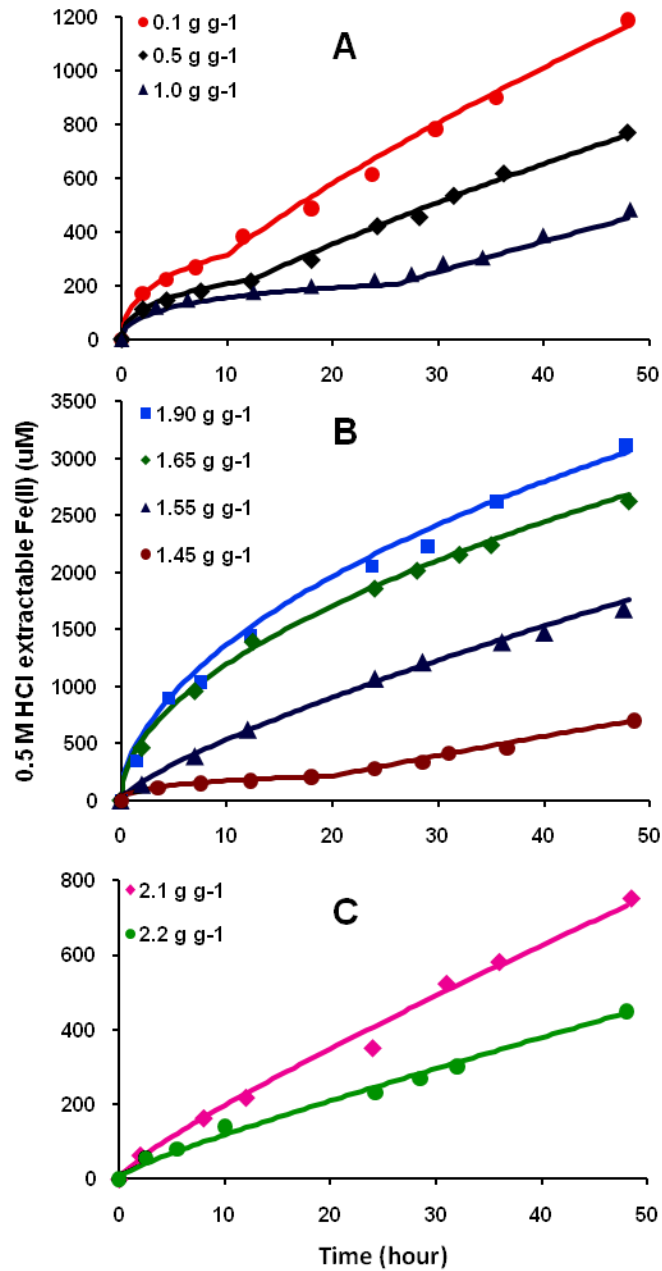
The term ferrihydrite is a general phrase for this naturally abundant ferric oxide. Its molecular formula has been proposed to be  $5\text{Fe}_2\text{O}_3 \cdot 9\text{H}_2\text{O}$ ,<sup>44</sup>  $\text{Fe}_5\text{O}_7(\text{OH}) \cdot 4\text{H}_2\text{O}$  or  $\text{Fe}_5\text{O}_3(\text{OH})_9$ ,<sup>45</sup> and  $\text{Fe}_4\text{O}_5(\text{OH})_2 \cdot 2.6\text{H}_2\text{O}$ .<sup>46</sup> The measured molar mass of the lab synthesized 2-line FH is  $95.03 \text{ g mole}^{-1} \text{ Fe}$  which fits any of the proposed molecular formula. For

discussion purpose,  $5\text{Fe}_2\text{O}_3 \cdot 9\text{H}_2\text{O}$  is adopted as the molecular formula of the synthesized ferrihydrite.

For ferric oxide reduction, a 3-step mechanism has been proposed as  $3\text{Fe}_2\text{O}_3 \rightarrow 2\text{Fe}_3\text{O}_4 \rightarrow 6\text{FeO} \rightarrow 6\text{Fe}$ , which is normally achieved under programmed temperature conditions up to  $\sim 600$  °C.<sup>34,40,47</sup> Obviously, the experimental conditions in those reports are distinct from the conditions described in this study in which reduction was conducted in solid/liquid interface at ambient temperature. Thus the formation of metallic Fe is not considered in this report. Kinetic analyses as discussed above suggest that ferrihydrite chemical reduction by  $\text{H}_2/\text{Pt}$  takes place via a 2-step model: FH is first reduced to a mixed-valent, magnetite ( $\text{Fe}_3\text{O}_4$ )-like phase via a diffusion controlled reduction as described by the half reaction in Eq. 6-3, followed by the reduction of  $\text{Fe}_3\text{O}_4$  to Fe(II) (Eq. 6-4) operated under a phase boundary controlled rate law.



## *Ferrihydrite chemical reduction as inhibited by peat*



In order to elucidate the impact of peat on ferrihydrite chemical reduction, peat/FH mixtures with peat input ranging from 0.1 to 2.2 g g<sup>-1</sup> FH were reduced by H<sub>2</sub> (1.7%) with a Pt/C catalyst at pH 6.0. The reduction kinetic data are presented in Figure 6-3. The diffusion controlled reduction is more noticeable in the mixtures with lower peat input (0.1~1.45 g g<sup>-1</sup>) than the rest mixtures suggesting that higher peat loading might have decreased or

**Figure 6-2.** Production of 0.5 M HCl extractable Fe(II) during the chemical reduction (1.7% H<sub>2</sub>) of peat/ferrihydrite mixtures at pH 6. Each suspension contained 0.5 g FH kg<sup>-1</sup>. Symbols represent experimental data, solid lines are the fits.

eliminated the extent of diffusion. The sum of the

two kinetic expressions also successfully fit all kinetic data presented in Fig. 6-2. The fitting results, including the extent of diffusion controlled reaction, rate constants and delay time for

the phase boundary controlled reaction, are listed in Table 6-1. Intriguingly, the presence of peat does not influence the rate constant of the diffusion controlled step for which the calculated rate constant is  $2.5 \times 10^{-6} \text{ s}^{-1}$  for all peat/FH reactions, which is slightly lower than

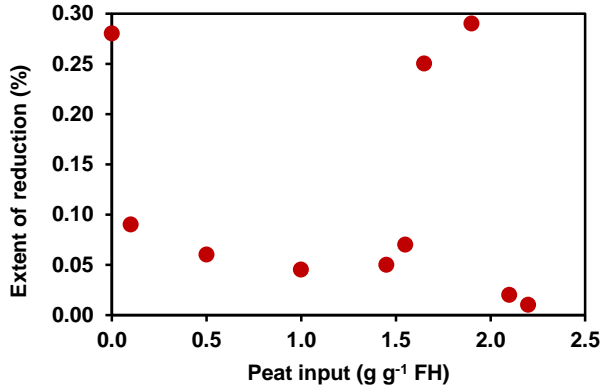


**Figure 6-3.** The extent of diffusion controlled reaction in the chemical reduction (1.7% H<sub>2</sub>) of ferrihydrite and peat/ferrihydrite mixtures as a function of peat input. The extent of diffusion is presented as the percentage of total Fe.

g<sup>-1</sup> FH. Throughout the whole peat input range (0.1~2.2 g g<sup>-1</sup> FH), the influence of peat on the extent of diffusion shows a three-regime pattern. Similarly, the influence of peat on the rate of the phase boundary controlled reaction also follows the 3-regime pattern, see Figure 6-4. Nevertheless, the experimental data and the fitting results both testify that

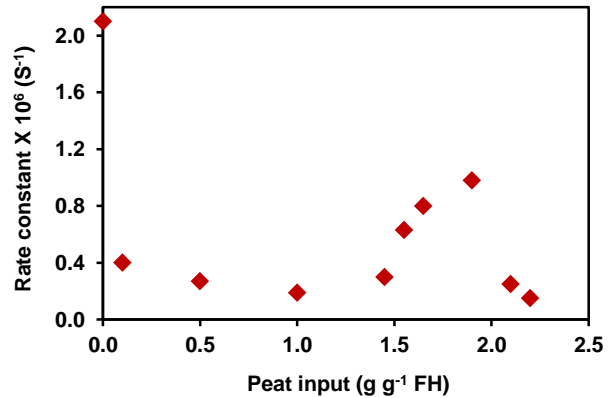


**Figure 6-4.** The calculated rate constants of the phase boundary controlled reaction in the chemical reduction (1.7% H<sub>2</sub>) of ferrihydrite and peat/ferrihydrite mixtures as a function of peat input.

the value calculated for ferrihydrite reduction ( $3.0 \times 10^{-6} \text{ s}^{-1}$ ). However, the presence of peat dramatically impacts the extent of diffusion, as presented in Figure 6-3. The extent of diffusion controlled reaction first drops with peat (0.1~1.0 g g<sup>-1</sup> FH), then increases as peat (1.0~1.9 g g<sup>-1</sup> FH). The diffusion controlled step is almost eliminated as peat input is  $\geq 2.1 \text{ g g}^{-1}$

ferrihydrite chemical reduction is inhibited by the presence of peat regarding the reduction rate and the extent. These findings are opposite to the expected results from the electron shuttle mechanism which is believed to enhance ferric oxide microbial reduction.

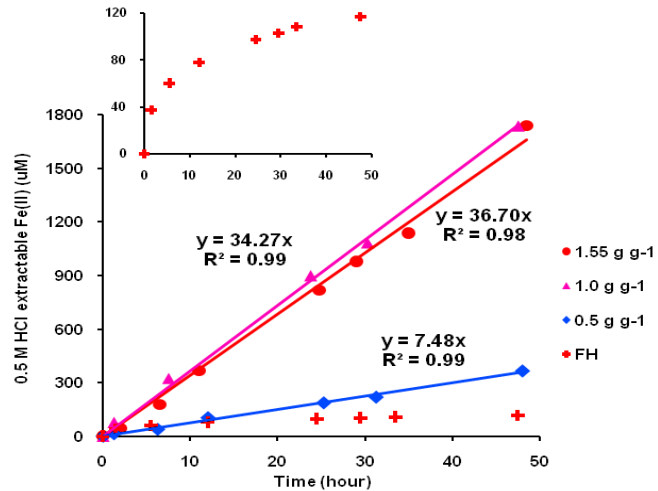
Due to the 3-regime pattern, for discussion purpose, the peat/FH mixtures are divided into three categories: low peat mixtures (0.1~1 g g<sup>-1</sup> FH), medium peat mixtures (1.45~1.9 g g<sup>-1</sup> FH), and high peat mixtures (2.1~2.2 g g<sup>-1</sup> FH)

**Table 6-1.** Fitting results for the extent of diffusion controlled reaction, rate constant of the phase boundary controlled reaction for the chemical reduction of peat/ferrihydrite mixtures with peat input ranging from 0 to 2.2 g g<sup>-1</sup> FH at pH 6. All reduction was conducted with 1.7% H<sub>2</sub>.

Peat input	Diffusion extent	Phase boundary rate (x 10 <sup>6</sup> )	Delay Time
g g <sup>-1</sup> FH	% of total Fe	S <sup>-1</sup>	H
0	0.280	2.10	27
0.1	0.090	0.40	10
0.5	0.060	0.27	12.5
1.0	0.045	0.19	26
1.45	0.050	0.30	20
1.55	0.070	0.63	1
1.65	0.250	0.80	1
1.9	0.290	0.98	1
2.1	0.020	0.25	0.7
2.2	0.010	0.15	0

## *Ferrihydrite microbial reduction enhanced by peat*

Aiming at a more thorough understanding of the role of Pahokee peat in ferrihydrite reduction, we also conducted ferrihydrite microbial reduction in the presence of peat. Figure 6-5 presents the production of acid extractable Fe(II) during the microbial reduction of ferrihydrite



and peat/FH mixtures with peat input ranging from 0.5 to 1.55 g g<sup>-1</sup> FH. Ferrihydrite and peat/FH mixtures were reduced with

**Figure 6-5.** Production of 0.5 M HCl extractable Fe(II) during the microbial reduction (1.7% H<sub>2</sub> with CN32) of ferrihydrite or peat/ferrihydrite mixtures. The inset figure shows the kinetic data of ferrihydrite microbial reduction data follow a non-linear pattern.

*Shewanella putrefaciens* (strain CN32) with H<sub>2</sub> (1.7%) being the electron source. Distinct from the peat/FH mixtures, ferrihydrite microbial reduction proceeds via non-linear, deceleratory path indicative of some sort of passivating factor(s) controlling the reduction. At the end of the 48-h experiment, only 2.2% of total Fe was reduced. The small extent of ferric oxide microbial reduction was also observed in other similar investigations.<sup>29,30</sup> The cessation of microbial ferric oxide reduction has been attributed to the accumulation of biogenic Fe(II) on the surface of mineral and microbes, which hinders electron transfer between the microorganisms and Fe(III). The presence of peat changes the kinetic function of ferrihydrite microbial reduction. As seen in Fig. 6-5, Fe(II) from microbial reduction of the peat/FH

mixtures increases linearly with time indicating that the presence of peat moderates the passivating stress that impedes FH microbial reduction. Linear regression was conducted to the kinetic data of microbial reduction of the peat/FH mixtures; and the slopes are treated as the reduction rates. The reduction rate increases with peat input up to 1 g g<sup>-1</sup>. Peat input greater than 1 g g<sup>-1</sup> doesn't seem to further enhance the reduction. On the contrary to ferrihydrite chemical reduction, the presences of particulate peat enhances ferrihydrite microbial reduction. These results are consistent with the findings from other similar investigations using dissolved organic matter.<sup>17,20-23,48</sup>

## 6.4. Discussion

### *Multiple mechanisms controlling the inhibition of peat in ferrihydrite chemical reduction*

As described above, the influence of peat on ferrihydrite chemical reduction illustrates a sophisticated pattern regarding the extent and rate of different reaction steps. The fact that the actual impact depends on the amount of peat present suggests that the mass ratio between peat and FH controls the OM/mineral interaction, which then determines the mechanism controlling the reduction process. In this section, the discussion will focus on how the interactions between peat and ferrihydrite affect the chemical reduction rate.

**Low peat input** With peat input being 0.1~1.0 g g<sup>-1</sup> FH, the initial (before reduction starts) dissolved Fe concentration in the mixtures, defined as the Fe detected in the supernatant that passes through a 0.2 μM membrane, ranges from non-detectable to 0.28% of total Fe. Only trace amounts of dissolved organic carbon (DOC) were detected. Organic matter has been shown to illustrate high affinity for oxide mineral surface.<sup>49-52</sup> The majority

organic carbon in these low peat mixtures is either in particulates or adsorbed to ferrihydrite surface. Adsorption of organic carbon to oxide minerals decreases the mineral's surface area and micropores.<sup>50,53,54</sup> The decreased phosphate sorption to ferrihydrite in the presence of humic acid or peat as discussed in Chapter 4 provides a manifestation of reduced surface area or sorption sites of ferrihydrite. According to the fitting results for the kinetic data from the chemical reduction of low peat mixtures, higher peat input decreases the extent of the diffusion controlled reduction and the rate of the phase boundary limited step (Table 1). These fitting results are the most consistent with a surface blocking model. By such model we conclude that higher peat input increases the amount of adsorbed organic carbon on ferrihydrite surface, which imparts a greater extent of surface blocking. The direct effect of surface blocking is the hindrance of hydrogen diffusion through the organic matter to Fe(III) making less hydrogen accessible to Fe(III). The model of surface blocking is also consistent with the decreased rate of phase boundary controlled step with a higher peat input as the adsorbed organic carbon hinders electron transfer from hydrogen to Fe(III).

**Medium peat input** The turning point of ferrihydrite chemical reduction kinetics is the peat input of 1.45 g g<sup>-1</sup> FH from which ferrihydrite reduction becomes faster with more peat. With peat input  $\geq 1.45$  g g<sup>-1</sup> FH, the initial dissolved Fe and DOC increases linearly with peat loading (data not shown). The detection of Fe in association with DOC in the supernatants is indicative of another kind of interaction between peat and ferrihydrite aggregates in addition to the sorptive interaction.

The B.E.T. surface area of the synthesized ferrihydrite is measured to be 330 m<sup>2</sup> g<sup>-1</sup>. Using Eq. 6-5 where  $D$  = particle diameter,  $S$  = surface area,  $\rho$  = density ( $3.8 \times 10^6$  m<sup>3</sup> g<sup>-1</sup>),<sup>55</sup>

the estimated particle diameter (assuming spherical particles) is calculated to be 4.8 nm, which is consistent with the measurement reported by Carta et al.<sup>55</sup> Based on the broadness

$$D = 6/(S \times \rho) \quad \text{Eq. 6-5}$$

of the diffraction lines, the calculated crystalline domain is ~0.6 nm using the Scherrer equation,<sup>56</sup> Eq. 6-6 where B = FWHM (full width half maximum),  $\lambda$  = wavelength  $\theta$  = Bragg angle of diffraction peak (diffraction pattern can be found in Chapter 4). Theoretically each ferrihydrite nano-particle is composed of 10 nano-crystallites. That fact that the crystalline domain of ferrihydrite is actually an order of magnitude smaller than its particle size probed by B.E.T. surface area indicates that ferrihydrite particles are aggregates of crystallites.

$$d = (0.9 \times \lambda)/(B \times \cos \theta) \quad \text{Eq. 6-6}$$

The observation of dissolved Fe in association with DOC increases with peat loading suggests that peat is breaking the nano-scale aggregates to even smaller ones, the process that we call disaggregation. As a result, the smaller aggregates provide more surface Fe, facilitating hydrogen diffusion and electron transfer, which are manifested by the increased calculated diffusion extent for the first step and rate constant for the phase boundary controlled step. Particularly, although the extent of diffusion increases with peat input, the medium peat input dramatically shortens the time needed to finish the diffusion controlled step.

**High peat input** Initial DOC and Fe in the supernatants continue to increase with peat input (data not shown), but the role of peat in ferrihydrite chemical reduction illustrates another turning point as more peat is mixed with ferrihydrite. With peat input being  $\geq 2.1 \text{ g g}^{-1}$

<sup>1</sup> FH, ferrihydrite reduction is greatly impeded with only ~10% of the total Fe(III) reduced. The time for the diffusion controlled step in the two high peat reduction reactions is even shorter than that in the medium peat reactions; and the extents of this step are drastically decreased. Therefore, high peat input almost eliminates the diffusion controlled reaction. According to our EXAFS analysis of a peat/FH mixture of 8 g g<sup>-1</sup> FH (such input equals Fe concentration being 1200 mmol/kg peat, see Chapter 4 for details of Fe EXAFS analysis), Fe-Fe coordination structure in the short range within 4 Å is essentially the same as in pure ferrihydrite. This result is showing that ferrihydrite aggregates can only be broken down by peat to a certain level beyond which increased peat input entails another peat/FH interaction mechanism so that ferrihydrite reduction is even more impeded. Our fitting results indicate that hydrogen diffusion through peat to Fe(III) almost disappears and the rate constants for the second, phase boundary controlled step are greatly reduced. The fitting results are suggesting that the positive impact from particle disaggregation is offset by the greater extent of surface blocking induced by high peat input, which explains the elimination of diffusion controlled reaction and the slow phase boundary controlled reaction.

### ***No electron shuttling between peat and ferrihydrite in chemical reduction***

Our previous investigation (Chapter 5) illustrated that peat possesses reducing capacity with respect to ferrihydrite after it has been reduced by H<sub>2</sub> in a peat/FH mixture. Electron storage in peat while it's being reduced by H<sub>2</sub> in the presence of ferrihydrite contradicts the expected role of a mediator in a redox reaction. The fact that chemical reduction of ferrihydrite is always inhibited in the presence of peat, regardless of the amount, provides sufficient evidence to show that Pahokee peat does not act as an active electron

shuttle in the chemical reduction of peat/FH mixtures. Instead, results of kinetic modeling of the reduction data suggest surface blocking and particle disaggregation are two competitive factors controlling the impact of peat on ferrihydrite chemical reduction.

Investigation on the reducing capacity of Pahokee peat with respect to ferrihydrite (Chapter 5) clearly shows that chemically reduced peat can quickly reduce ferrihydrite, which means both thermodynamics and kinetics favor the electron transfer from chemically reduced peat to ferrihydrite. A question must be asked: why are the stored electrons in peat kept from being transferred to ferrihydrite when peat and ferrihydrite are reduced simultaneously? A possible explanation is that electron path directly from hydrogen to ferrihydrite is more favored under the H<sub>2</sub> purging condition. However, this possibility is ruled out because H<sub>2</sub> is always removed from the peat/FH mixture before the reduced peat/FH is mixed with additional ferrihydrite. That is to say, hydrogen reduced peat can reduce added ferrihydrite, but not the coexisting “ferrihydrite”.

As discussed above, a 2-step reduction mechanism is operative in ferrihydrite chemical reduction with the Fe<sub>3</sub>O<sub>4</sub> or Fe<sub>3</sub>O<sub>4</sub>-like species being the intermediate. Because of that, it would most likely make sense that the hydrogen reduced “ferrihydrite” is not ferrihydrite anymore, but a mixture with the core being ferrihydrite coated by the secondary mineral; and the electron transfer from reduced peat to such secondary mineral is not either thermodynamically or kinetically favored. Nevertheless, the systematic investigation of ferrihydrite chemical reduction in the presence of peat in a wide input range clearly demonstrates that particulate organic matter, Pahokee peat inhibits ferrihydrite chemical reduction through multiple mechanisms.

### ***Mechanism for the enhancement of ferrihydrite microbial reduction***

Our data of ferrihydrite microbial reduction in the presence of peat show that peat facilitates ferrihydrite microbial reduction, which is consistent with the findings reported in the literature. A classic explanation for the enhancement of ferric oxide bioreduction by organic matter is the electron shuttle mechanism by which the electron transfer is expedited by the mediator, organic matter. Our investigation on the post-reduction reducing capacity of peat demonstrated that peat did not store electrons that can be transferred to ferrihydrite during the microbial reduction of a peat/FH mixture. The fact that ferrihydrite microbial reduction is enhanced by peat and peat does not store ferrihydrite-reducing electrons provides experimental grounds for the conclusion that peat as an active electron shuttle in the microbial reduction. However, ferric oxide microbial reduction can be enhanced by other factors, e.g. Fe(II) removal. Being an electron shuttle could be just one aspect of the multi-faceted role that organic matter plays in ferric oxide microbial reduction.

Several investigators have confirmed the formation of secondary minerals, e.g. Fe<sub>3</sub>O<sub>4</sub> or goethite in ferric oxide bioreduction.<sup>41,42,57-60</sup> The pathway of secondary mineralization can be altered by the carbon source for microbial respiration,<sup>61</sup> bacterial strain,<sup>62</sup> the present organic polymers,<sup>63</sup> and Fe(II) concentration.<sup>64</sup> The fact that peat mediates ferrihydrite microbial reduction implies that the combination of peat and microorganisms either retains the integrity of ferrihydrite by eliminating the formation of secondary mineral or directs the secondary mineralization pathway towards the formation of a secondary mineral that is reducible by microbially reduced peat.

A comparison between the chemical and microbial reduction of the system of 0.5 g g<sup>-1</sup> FH may provide some insight. Figure 6-6 presents the 0.5 M HCl extractable Fe(II) and dissolved Fe(II) data from the chemical and microbial reduction of the peat/FH mixture. Same amount of total Fe(II) was produced in both reactions. However, 67% of total Fe(II) is dissolved Fe(II) in the biological system while only ~8% of total Fe(II) is dissolved Fe(II) in the chemical system. Along with the difference of dissolved Fe(II), dissolved organic carbon concentrations are different too. Only a trace amount of DOC was detected in the system of 0.5 g g<sup>-1</sup> FH prior to the initiation of reduction. At the end of the reduction experiments, no DOC was detected in the chemical system but ~15 mg L<sup>-1</sup> DOC was detected in the biological system. High dissolved Fe(II) and the elevated DOC concentration in the biological system is indicative of Fe(II)-DOC complexation.

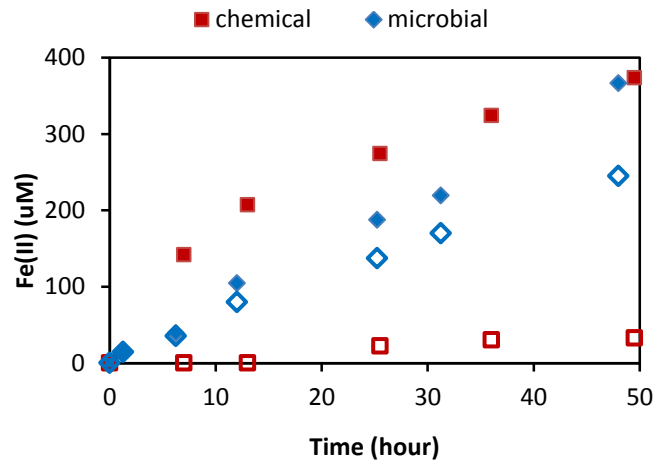


**Figure 6-6.** 0.5 M HCl extractable and dissolved Fe(II) from the chemical (1.7% H<sub>2</sub> + Pt/C) and microbial (1.7% H<sub>2</sub> + CN32) reduction of the peat/FH mixture of 0.5 g g<sup>-1</sup> FH at pH 6.0. Solid symbols are acid extractable Fe(II), hollow symbols are dissolved Fe(II).

The formation of soluble Fe(II)-DOC complexes facilitates biogenic Fe(II) transport, which can enhance the bioreduction on two

aspects. First, it eliminates solid biogenic Fe(II) accumulation on the mineral or microbe surface which has been shown to inhibit ferric oxide microbial reduction. Numerous studies have confirmed that removal of solid Fe(II) accelerate either chemical<sup>27,65</sup> or biological<sup>20,31,66</sup>

ferric oxide reduction. Secondly, with peat's finite Fe(II) retention capacity and 67% of total Fe(II) being dissolved, solid Fe(II) on ferrihydrite is minimal so that secondary mineralization is minimized. We do not have data to confirm whether secondary mineral(s) have formed and the mineral phase(s). The enhancement of ferrihydrite microbial reduction by peat and high dissolved Fe(II) concentration are the most consistent with no secondary mineral formation so that the integrity of ferrihydrite is maintained during the course of microbial reduction.

With the fact that ferrihydrite microbial reduction is mediated by peat, the measured kinetic data of Fe(II) production actually is a measure of peat microbial reduction. The enhancement of peat on ferrihydrite microbial reduction reaches the maximum extent when the input is  $1.0 \text{ g g}^{-1}$  FH. Higher peat input does not further enhance the reduction (Fig. 6-5). Jiang and Kappler.<sup>23</sup> also demonstrated that no further enhancement of ferric oxide microbial reduction was observed as the concentration of humic substances exceeded  $25 \text{ mg DOC L}^{-1}$ . These findings are suggesting that electron transfer from hydrogen to microorganisms or from microorganisms to organic matter is the rate limiting step.

## **6.5. Conclusions**

Aiming at elucidating the role of organic matter in Fe(III)-oxide chemical reduction, we conducted a sophisticated investigation of ferrihydrite chemical and microbial reduction in the presence of various amounts of Pahokee peat. The kinetic data of ferrihydrite chemical reduction reveal that ferrihydrite reduction follow a 2-step mechanism. The first step is diffusion controlled reaction followed by the phase boundary controlled second step. Kinetic modeling of all kinetic data from chemical reduction of peat/FH mixtures suggest that

particle surface blocking by peat and particle disaggregation by peat are two competitive factors controlling the impact of peat on ferrihydrite chemical reduction. However, the electron shuttle mechanism is not operative in peat/ferrihydrite chemical reduction, and ferrihydrite chemical reduction is inhibited by the presence of peat. By contrast, the presence of peat enhances ferrihydrite microbial reduction. Peat possibly enhances the microbial reduction by the electron shuttle mechanism and Fe(II)-complexation which eliminates the formation of secondary mineral.

## 6.6. References

- (1) Violante, A.; Pigna, M. *Soil Science Society of America Journal* 2002, 66, 1788.
- (2) Missana, T.; Alonso, U.; Scheinost, A. C.; Granizo, N.; Garcia-Gutierrez, M. *Geochimica Et Cosmochimica Acta* 2009, 73, 6205.
- (3) Asta, M. P.; Cama, J.; Martinez, M.; Gimenez, J. *Journal of Hazardous Materials* 2009, 171, 965.
- (4) Sannino, F.; De Martino, A.; Pigna, M.; Violante, A.; Di Leo, P.; Mesto, E.; Capasso, R. *Journal of Hazardous Materials* 2009, 166, 1174.
- (5) Lee, G.; Faure, G. *Water Air and Soil Pollution* 2007, 186, 221.
- (6) Tessier, A.; Fortin, D.; Belzile, N.; DeVitre, R. R.; Leppard, G. G. *Geochimica Et Cosmochimica Acta* 1996, 60, 387.
- (7) Fiedler, S.; Vepraskas, M. J.; Richardson, J. L. In *Advances in Agronomy, Vol 94* 2007; Vol. 94, p 1.
- (8) Peretyazhko, T.; Sposito, G. *Geochimica Et Cosmochimica Acta* 2005, 69, 3643.

- (9) Bennett, B.; Dudas, M. J. *Journal of Environmental Engineering and Science* 2003, 2, 265.
- (10) Sturm, A.; Crowe, S. A.; Fowle, D. A. *Chemical Geology* 2008, 249, 282.
- (11) Erbs, J. J.; Berquo, T. S.; Reinsch, B. C.; Lowry, G. V.; Banerjee, S. K.; Penn, R. L. *Geochimica Et Cosmochimica Acta* 2010, 74, 3382.
- (12) Bot, A.; Benites, J. *The importance of soil organic matter*; Food and Agriculture Organization of the United Nations: Rome Italy, 2005.
- (13) Stevenson, F. J. *Humus chemistry: genesis, composition, reactions*; Wiley & Sons, Inc.: New York NY USA, 1982.
- (14) Lovley, D. R.; Coates, J. D.; BluntHarris, E. L.; Phillips, E. J. P.; Woodward, J. C. *Nature* 1996, 382, 445.
- (15) Struyk, Z.; Sposito, G. *Geoderma* 2001, 102, 329.
- (16) Peretyazhko, T.; Sposito, G. *Geoderma* 2006, 137, 140.
- (17) Rakshit, S.; Uchimiya, M.; Sposito, G. *Soil Science Society of America Journal* 2009, 73, 65.
- (18) Lovley, D. R.; Fraga, J. L.; Blunt-Harris, E. L.; Hayes, L. A.; Phillips, E. J. P.; Coates, J. D. *Acta Hydrochimica Et Hydrobiologica* 1998, 26, 152.
- (19) Chen, J.; Gu, B. H.; Royer, R. A.; Burgos, W. D. *Science of the Total Environment* 2003, 307, 167.
- (20) Royer, R. A.; Burgos, W. D.; Fisher, A. S.; Unz, R. F.; Dempsey, B. A. *Environmental Science & Technology* 2002, 36, 1939.
- (21) Royer, R. A.; Burgos, W. D.; Fisher, A. S.; Jeon, B. H.; Unz, R. F.; Dempsey, B. A. *Environmental Science & Technology* 2002, 36, 2897.

- (22) Roden, E. E.; Wetzel, R. G. *Abstracts of the General Meeting of the American Society for Microbiology* 1999, 99, 452.
- (23) Jiang, J.; Kappler, A. *Environmental Science & Technology* 2008, 42, 3563.
- (24) Kizewski, F. R.; Martin, J. D.; Hesterberg, D. 2010 (paper in preparation).
- (25) Murray, G. C.; Hesterberg, D. *Soil Science Society of America Journal* 2006, 70, 1318.
- (26) Debnath, S.; Hausner, D. B.; Strongin, D. R.; Kubicki, J. *Journal of Colloid and Interface Science* 2010, 341, 215.
- (27) Afonso, M. D.; Morando, P. J.; Blesa, M. A.; Banwart, S.; Stumm, W. *Journal of Colloid and Interface Science* 1990, 138, 74.
- (28) Royer, R. A.; Dempsey, B. A.; Jeon, B. H.; Burgos, W. D. *Environmental Science & Technology* 2004, 38, 187.
- (29) Roden, E. E.; Urrutia, M. M. *Geomicrobiology Journal* 2002, 19, 209.
- (30) Roden, E. E.; Urrutia, M. M.; Mann, C. J. *Applied and Environmental Microbiology* 2000, 66, 1062.
- (31) Urrutia, M. M.; Roden, E. E.; Zachara, J. M. *Environmental Science & Technology* 1999, 33, 4022.
- (32) Bosch, J.; Heister, K.; Hofmann, T.; Meckenstock, R. U. *Applied and Environmental Microbiology* 2010, 76, 184.
- (33) Thomas, C. R.; Miao, S. L.; Sindhoj, E. *Wetlands* 2009, 29, 1133.
- (34) Munteanu, G.; Ilieva, L.; Andreeva, D. *Thermochimica Acta* 1997, 291, 171.

- (35) Wimmers, O. J.; Arnoldy, P.; Moulijn, J. A. *Journal of Physical Chemistry* 1986, 90, 1331.
- (36) Lebedeva, O. E.; Sachtler, W. M. H. *Journal of Catalysis* 2000, 191, 364.
- (37) Kissinger, H. E. *Analytical Chemistry* 1957, 29, 1702.
- (38) Spitzer, R. H.; Manning, F. S.; Philbroo, W. *Transactions of the Metallurgical Society of Aime* 1966, 236, 726.
- (39) Surman, J.; Kustrowski, P.; Chmielarz, L.; Dziembaj, R. *Przemysl Chemiczny* 2003, 82, 783.
- (40) Jozwiak, W. K.; Kaczmarek, E.; Maniecki, T. P.; Ignaczak, W.; Maniukiewicz, W. *Applied Catalysis a-General* 2007, 326, 17.
- (41) Hansel, C. M.; Benner, S. G.; Neiss, J.; Dohnalkova, A.; Kukkadapu, R. K.; Fendorf, S. *Geochimica Et Cosmochimica Acta* 2003, 67, 2977.
- (42) O'Loughlin, E. J.; Gorski, C. A.; Scherer, M. M.; Boyanov, M. I.; Kemner, K. M. *Environmental Science & Technology* 2010, 44, 4570.
- (43) Kononets, M. Y.; Pakhomova, S. V.; Rozanov, A. G.; Proskurnin, M. A. *Journal of Analytical Chemistry* 2002, 57, 586.
- (44) Loan, M.; Parkinson, G. M.; Richmond, W. R. *American Mineralogist* 2005, 90, 258.
- (45) Schwertmann, U.; Friedl, J.; Stanjek, H. *Journal of Colloid and Interface Science* 1999, 209, 215.
- (46) Bakardjieva, S.; Stengl, V.; Subrt, J.; Vecernikova, E. *Solid State Sciences* 2005, 7, 367.
- (47) Brown, R.; Cooper, M. E.; Whan, D. A. *Applied Catalysis* 1982, 3, 177.

- (48) Roden, E. E.; Kappler, A.; Bauer, I.; Jiang, J.; Paul, A.; Stoesser, R.; Konishi, H.; Xu, H. F. *Nature Geoscience* 2010, 3, 417.
- (49) Kaiser, K.; Guggenberger, G.; Zech, W. *Geoderma* 1996, 74, 281.
- (50) Kaiser, K.; Guggenberger, G. *European Journal of Soil Science* 2003, 54, 219.
- (51) Filius, J. D.; Lumsdon, D. G.; Meeussen, J. C. L.; Hiemstra, T.; Van Riemsdijk, W. H. *Geochimica Et Cosmochimica Acta* 2000, 64, 51.
- (52) Filius, J. D.; Meeussen, J. C. L.; Lumsdon, D. G.; Hiemstra, T.; Van Riemsdijk, W. H. *Geochimica Et Cosmochimica Acta* 2003, 67, 1463.
- (53) Kaiser, K.; Mikutta, R.; Guggenberger, G. *Soil Science Society of America Journal* 2007, 71, 711.
- (54) Mikutta, C.; Lang, F.; Kaupenjohann, M. *Soil Science Society of America Journal* 2004, 68, 1853.
- (55) Carta, D.; Casula, M. F.; Corrias, A.; Falqui, A.; Navarra, G.; Pinna, G. *Materials Chemistry and Physics* 2009, 113, 349.
- (56) Scherrer, P. *Göttinger Nachrichten Gesell.*, 1918.
- (57) Zegeye, A.; Ruby, C.; Jorand, F. *Geomicrobiology Journal* 2007, 24, 51.
- (58) Zegeye, A.; Mustin, C.; Jorand, F. *Geobiology* 2010, 8, 209.
- (59) Benner, S. G.; Hansel, C. M.; Wielinga, B. W.; Barber, T. M.; Fendorf, S. *Environmental Science & Technology* 2002, 36, 1705.
- (60) Tufano, K. J.; Benner, S. G.; Mayer, K. U.; Marcus, M. A.; Nico, P. S.; Fendorf, S. *Vadose Zone Journal* 2009, 8, 1004.

- (61) Salas, E. C.; Berelson, W. M.; Hammond, D. E.; Kampf, A. R.; Nealson, K. H. *Geomicrobiology Journal* 2009, 26, 451.
- (62) Salas, E. C.; Berelson, W. M.; Hammond, D. E.; Kampf, A. R.; Nealson, K. H. *Geochimica Et Cosmochimica Acta* 2010, 74, 574.
- (63) Jorand, F.; Zegeye, A.; Lartiges, B. *Geochimica Et Cosmochimica Acta* 2009, 73, A605.
- (64) Hansel, C. M.; Benner, S. G.; Fendorf, S. *Environmental Science & Technology* 2005, 39, 7147.
- (65) Banwart, S.; Davies, S.; Stumm, W. *Colloids and Surfaces* 1989, 39, 303.
- (66) Roden, E. E.; Urrutia, M. M. *Environmental Science & Technology* 1999, 33, 1847.

## **Chapter 7: Conclusions**

## 7.1. Ternary complexation between organic matter, iron, and phosphate

Ternary complexation between organic matter (OM), Fe/Al, and phosphate (PO<sub>4</sub>) requires both OM and PO<sub>4</sub> anions to be coordinated to the same metal center. From a thermodynamic perspective, coordination of mixed anions to one metal center demands comparable affinities, geometries, charges of both anions to the metal center. According to Eq. 7-1,<sup>1</sup> phosphate anion (PO<sub>4</sub><sup>3-</sup>) has a very high Fe(III) affinity (expressed as the logK of Fe(III)-PO<sub>4</sub><sup>3-</sup> complexation), much higher than the Fe(III) affinity of any organic acid (OA) anions listed in Table 2-1. Thermodynamics predicts that Fe-PO<sub>4</sub> complexation is favored against Fe-OA complexation.



\* aqueous complex

Although we do not know the equilibrium constant of Fe-OM complexation, it is the most likely that it is not the same to the PO<sub>4</sub> affinity for Fe(III). Thus, thermodynamics will lead to the equilibrium of either Fe-OM or Fe-PO<sub>4</sub> complexation, but not complexation of both anions to Fe.

In reality, reactions of Fe, PO<sub>4</sub>, and various organic acids at pH 5.5 under hydrothermal conditions only produced Fe-PO<sub>4</sub> solid species. None of the studied OA is incorporated in the solid products (Chapter 2). In addition, a search for iron ternary compounds with phosphate and another anion (excluding O<sup>2-</sup> and OH<sup>1-</sup>) in the Cambridge Crystallographic Database returned a limited number of results. In Chapter 3, we described the synthesis and analysis of a ternary Fe(III) oxalatophosphate ternary compound. The

synthesis of this compound was not successful until the application of an alkylammonium cation which was needed in all reported syntheses of similar compounds. Such cation plays an important role in the structural framework: it provides charge balance for Fe, oxalate, and phosphate and space for the second anion, oxalate. Thermodynamic theory and experimental data are showing that ternary complexation between  $\text{PO}_4$ , Fe and another anion is difficult to achieve.

Several studies found that OM or an organic soil exhibits a higher phosphate ( $\text{PO}_4$ ) sorption capacity with higher Fe or Al content.<sup>2-5</sup> Thus the concept of OM-Fe/Al- $\text{PO}_4$  ternary complexation has been proposed to explain the direct correlation between Fe/Al contents and  $\text{PO}_4$  sorption capacity. Yet, more conclusive and direct evidence has yet to be presented to support such hypothesis. Our research data of hydrothermal reactions of OA, Fe(III), and  $\text{PO}_4$  do not support OM/Fe/ $\text{PO}_4$  ternary complexation. As an alternative, phosphate sorption to organic matter or organic soil via precipitation with Fe or Al would make more chemical sense since  $\text{PO}_4$  has high affinity for Fe or Al. Giesler et al.,<sup>6</sup> observed IR (infrared spectroscopy) spectral features for hydrous Fe- $\text{PO}_4$  or Al- $\text{PO}_4$  like precipitates in a high Fe and Al humus soil via ATR-FTIR spectroscopy. The authors also reported that dissolved organic carbon (DOC) concentration increased after  $\text{PO}_4$  sorption indicating ligand exchange between organic carbon and  $\text{PO}_4$ , which should not have taken place if ternary complexation were the sorption mechanism.

## 7.2. Organic matter/Fe-oxide interactions

### *Impact on ferric oxide chemical reduction*

The redox properties of Pahokee peat as well as its impact on ferric oxide reduction were investigated in this research project (Chapter 5 and 6). Our ferrihydrite (FH) chemical reduction data show that OM affects ferric oxide chemical reduction via multiple mechanisms. Together with the data of DOC, dissolved Fe, and Fe EXAFS analysis for FH/peat mixtures with various peat inputs, we propose that the multiple mechanisms affecting ferric oxide chemical reduction are controlled by Fe-oxide/OM interactions and the interactions are determined by the relative amounts of OM and oxide mineral, as illustrated by Figure 7-1. Kinetic modeling for all chemical reduction data indicate that the reduction is a 2-step process controlled by first diffusion limited and then phase boundary limited rate laws. Low input of OM blocks oxide mineral surface resulting in lower reduction rate with increased amount of OM. As OM input increases, mineral particles are disaggregated by OM exposing more surface Fe. The chemical reduction rate is thus increased because more Fe is accessible to the reductant. Iron K-edge EXAFS analysis of ferrihydrite mixed with a high amount of peat (8 g g<sup>-1</sup> FH Chapter 4) confirms that short range iron hydroxide like structure remains. That is to say that oxide particle disaggregation by OM does not lead to the formation of monomeric Fe-OM complexes. With OM input being  $\geq 2.1$  g g<sup>-1</sup> FH, the smaller particles resulted from disaggregation are blocked again by OM, which dramatically inhibits the reduction rate. Regardless of the input of OM, ferric oxide chemical reduction is inhibited by OM.

## Aging effect

While the short range iron-hydroxide like structure remains in a fresh FH/peat mixture, our Fe EXAFS analyses of aged FH/peat mixtures indicate that aging does not change the short range Fe coordination structure. Our data do not support Fe atom migration to OM forming Fe-OM monomeric complexes as suggested by Gerke<sup>7</sup>. Opposite to the increased PO<sub>4</sub> sorption observed in aged oxide/humic mixtures,<sup>7</sup> we found that aging leads to

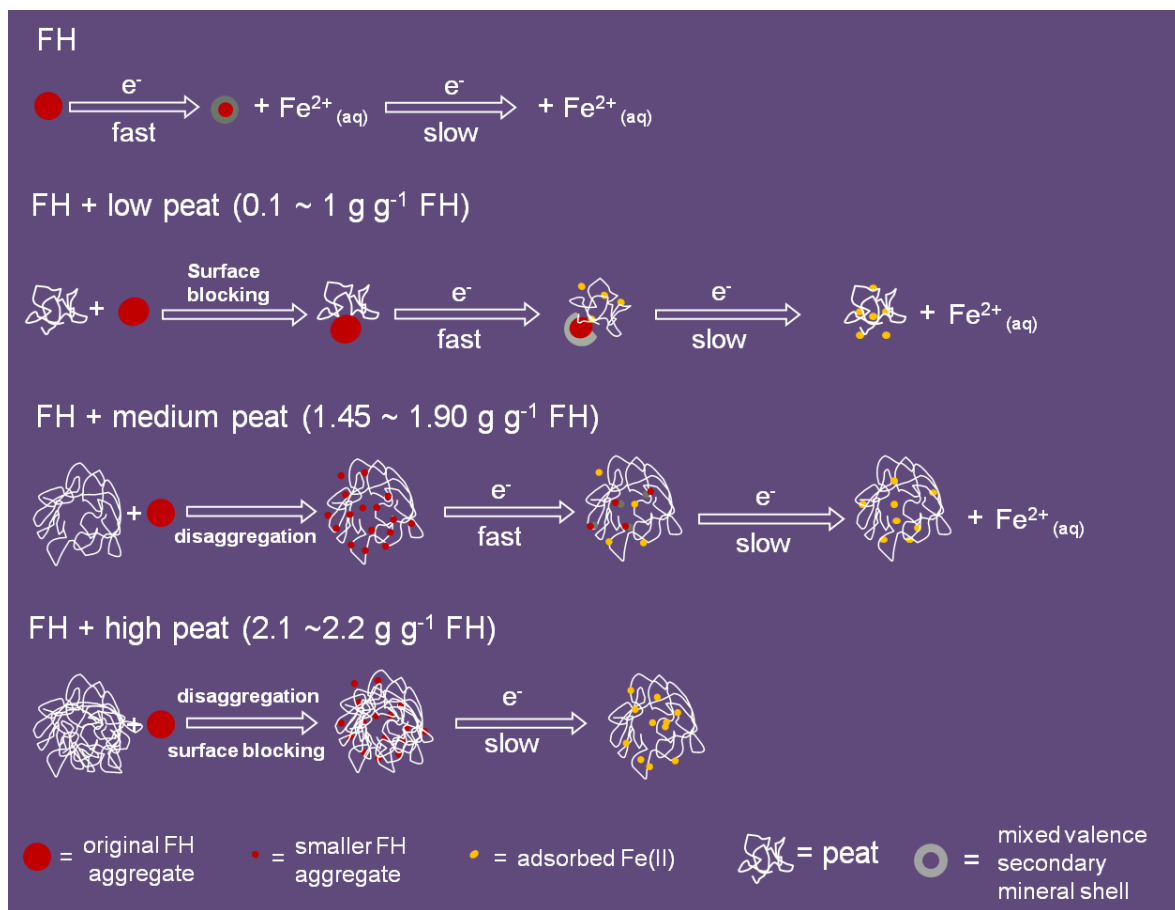


**Figure 7-1.** Schematic drawing showing the interactions between ferrihydrite and peat and the impact on ferrihydrite chemical reduction. All systems were reduced with hydrogen in the presence of a Pt/C catalyst. FH=ferrihydrite

decreased PO<sub>4</sub> sorption to Fe-oxide/OM mixtures, which is attributed to the competition between OM and PO<sub>4</sub>.

### 7.3. Multiple mechanisms contribute to the enhancement of organic matter in Fe(III)-oxide microbial reduction

Consistent with the results published in the literature, ferrihydrite microbial reduction is enhanced by particulate OM, peat (Chapter 6). Our data show that peat does not act as an active electron shuttle in ferrihydrite chemical reduction but in microbial reduction. While both reduction methods utilize hydrogen as the electron source, it is intriguing that the change of catalyst (microorganisms in microbial reduction vs. Pt/C in chemical reduction) alters the pathway of electron transfer to Fe(III).

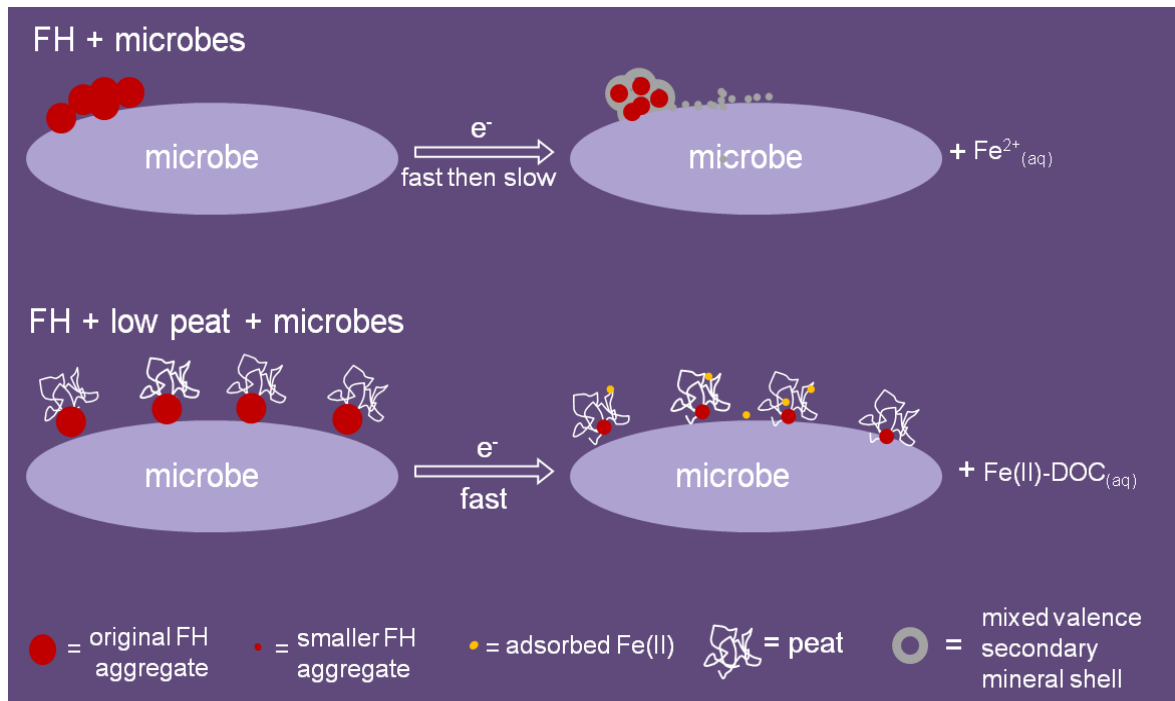


**Figure 7-2.** Schematic drawing showing the interactions between ferrihydrite and peat and the impact on ferrihydrite microbial reduction. The reduction was conducted with hydrogen gas. FH=ferrihydrite.

Electron shuttling has been the long held theory that explains the enhancement of OM on ferric oxide microbial reduction. Yet, our data of peat reducing capacity after it has been reduced with ferrihydrite chemically and biologically suggest that OM inhibits the formation of secondary mixed valence Fe mineral. On the other hand, data of dissolved Fe(II) and DOC in microbial reduction systems indicate that organic matter facilitates Fe(II) transport away from the microorganisms and oxide particles by forming Fe(II)-OM soluble complexes.

## 7.4. References

- (1) Lindsay, W. L. *Chemical Equilibria In Soils*; The Blackburn Press: Caldwell, New Jersey, USA, 2001.
- (2) Bloom, P. R.; *Soil Science Society of America Journal* **1981**, *45*, 267.
- (3) Richardson, C. J. *Science* **1985**, *228*, 1424.
- (4) Gerke, J.; Hermann, R. *Zeitschrift Fur Pflanzenernahrung Und Bodenkunde* **1992**, *155*, 233.
- (5) Nieminen, M.; Jarva, M. *Scandinavian Journal of Forest Research* **1996**, *11*, 321.
- (6) Giesler, R.; Andersson, T.; Lovgren, L.; Persson, P. *Soil Science Society of America Journal* **2005**, *69*, 77.
- (7) Gerke, J.; *Geoderma* **1993**, *59*, 279.